A METHODOLOGY FOR CONDUCTING DESIGN TRADES FOR A SMALL SATELLITE LAUNCH VEHICLE WITH HYBRID ROCKET PROPULSION

A Thesis
Presented to
The Academic Faculty

By

Havva İrem Çağlar

In Partial Fulfillment
of the Requirements for the Degree
Master of Science in the
School of Aerospace Engineering

Georgia Institute of Technology

August 2021

A METHODOLOGY FOR CONDUCTING DESIGN TRADES FOR A SMALL SATELLITE LAUNCH VEHICLE WITH HYBRID ROCKET PROPULSION

Thesis committee:

Professor Dimitri Mavris, Advisor
Aerospace Systems Design Laboratory
Georgia Institute of Technology

Dr. Michael J. Steffens
Aerospace Systems Design Laboratory
Georgia Institute of Technology

Dr. Bradford E. Robertson
Aerospace Systems Design Laboratory
Georgia Institute of Technology

Date approved:

to Mustafa Kemal Atatürk for his eternal ideas that inspired me to believe in women as equally as men and in scientific truths rather than dogmas

ACKNOWLEDGMENTS

A decade ago, I dreamed to pursue my graduate studies at Georgia Tech believing that its academical culture would help me develop new research and engineering skills. My dream came true when I moved to Atlanta for my graduate studies at the Aerospace Systems Design Laboratory (ASDL), following years of professional experience. During my studies, I was fascinated by the academic environment of Georgia Tech where I have learned so much about not only aerospace engineering but also about life and people.

I would like to express my sincere gratitude towards Dr. Dimitri Mavris, my advisor, especially for his leadership and helpfulness since the pandemic has started. From his lectures and feedback on my thesis research, I have learned so much which widened my perspective about engineering and scientific thinking. I always felt his passion towards aerospace engineering which made me fall in love with this profession even more.

I would like to express my appreciation to Dr. Michael J. Steffens and Dr. Bradford E. Robertson for providing helpful feedback on my thesis study. Their feedback was really useful and beneficial to me throughout the thesis research process.

I'd also like to express my sincere thanks to Roketsan, the company where my career began and continues, for sponsoring these studies. I am especially grateful to Dr. Ahmet Sofyalı for his support in brainstorming various thesis topics and providing valuable suggestions on my thesis, as well as Demet Küçük for her excellent coordination, especially during the difficult times of the pandemic.

Above all, I am very grateful to my mother who has been my best friend and the most enthusiastic supporter of my studies since I was a child. I would also like to thank my father who always motivated me to be courageous in the difficult tasks. The trust of my family has always encouraged me to go one step further.

TABLE OF CONTENTS

LIST OF TABLES

LIST OF FIGURES

LIST OF ACRONYMS

ANN Artifical Neural Networks

CDP Conceptual Design Phase

DOE Design of Experiments

DOF Degree of Freedom

DSE Design Space Exploration

GEO Geostationary Orbit

HEO High Elliptical Orbit

HTPB Hydroxyl-Terminated PolyButadiene

LEO Low Earth Orbit

LV Launch Vehicle

M&S Modeling and Simulation

MEO Medium Earth Orbit

PMF Propellant Mass Fraction

RSE Response Surface Equations

SLV Smallsat Launch Vehicles

SOA State of the Art

SUMMARY

The commercial space industry has recently seen a paradigm shift related to the launch of a small satellite into Low Earth Orbit. In the past, a small satellite was launched as a secondary payload with a medium or heavy launch vehicle where the primary payload placed a constraint on the orbit and schedule. Today, a dedicated launch of a small launch vehicle is the main operational concept to launch a small payload. Many Smallsat Launch Vehicles (SLV) have been under development by the commercial space industry to improve these launch services in recent years. Despite these efforts, the specific prices per launch are still high, and reducing these prices further remains a challenge.

One promising technology candidate to reduce costs for SLV is hybrid rocket propulsion which has matured recently with some cost and safety advantages. Although hybrid rocket propulsion faces a number of challenges, including a low regression rate and combustion instabilities, academia and commercial companies have invested significant resources in developing this technology. With this motivation, this thesis has focused on the conceptual design of SLV with hybrid rocket propulsion. Moreover, a cost reduction strategy currently used by the commercial space industry was observed to be the development of a unique engine and using multiple of them in a launch vehicle. Following this trend, the vehicle concept investigated in this thesis was an expendable ground-launched vehicle with some architectural variables such as the number of stages and the number of hybrid motors in each stage.

The design trade-off studies of such a small multistage launch vehicle with multiple hybrid motors in each stage require very long times especially when traditional point design approaches are used. As the number of design variables increase, the design space exploration becomes even more challenging. To provide a solution to this problem, a methodology for rapid conceptual design of such a vehicle was presented in this thesis.

A physics-based conceptual design approach was followed in this study since SLV are

relatively new concepts without much historical performance data. To conduct a multi-disciplinary analysis, a physics-based, integrated modeling and simulation environment was constructed with four core disciplines: trajectory analysis, aerodynamics, propulsion, and weight. Aerodynamics and propulsion analysis were conducted using a first-principles approach, which was based on fundamental theories. A 3 Degree of Freedom (DOF) industrial, transparent, physics-based trajectory analysis software was used in this study based on availability. However, any other trajectory analysis software that a system designer is familiar with can be used in its place. In other words, the methodology developed in this thesis would remain unchanged if another trajectory analysis software were used. The weight discipline was represented at a high level by using Propellant Mass Fraction (PMF) design variable.

A multidisciplinary modeling and simulation environment for launch vehicles may be computationally expensive depending on the fidelity levels of each discipline. Moreover, trajectory optimization is included in a launch vehicle design process conventionally which may be also computationally expensive depending on the optimization method. This expense poses a difficulty in performing a trade-off study for hundreds of vehicle design alternatives within the constraints of the schedule in the conceptual design phase. Because of this, trajectory optimization was removed from the design process to speed up the process by selecting a constant controller design.

The methodology developed in this thesis consisted of two sequential steps. In the first step, a surrogate modeling approach was followed to replace the Modeling and Simulation (M&S) environment. A DOE method and a surrogate modeling method suitable to this problem were searched in this part. To cover the design space, a hybrid DOE consisting of a Fast Flexible Filling DOE and a three-level Full Factorial DOE was chosen. Artificial Neural Networks method was selected to fit approximation models because of the type of design variables (both continuous and discrete variables) and nonlinearity of the problem. The first experiment was conducted to test this hypothesis. As a result, it was demonstrated

that this approach can provide accurate surrogate models for any desired response.

In the second step, the specific mechanical energy-based design trade-off method was developed using some statistical methods. This method estimates the lower bound of the vehicles' actual specific mechanical energy where the vehicles can be rapidly designed by using surrogate models. This lower bound was predicted with the help of the prediction interval of the specific mechanical energy's model fit error. To fit the surrogate models, the necessary data were gathered by running the DOE in the integrated M&S environment while imposing some terminal conditions on the altitude of the vehicles analyzed in this environment. Specifically, the surrogate models of specific mechanical energy and flight path angle were used to design the vehicles rapidly. The second experiment was conducted to test this hypothesis. As a result, the actual specific mechanical energies computed via trajectory optimization were found to be consistent with the predictions. Overall, it was demonstrated that the proposed method enables a system designer to rapidly design some feasible vehicles, which can then proceed to the next design phase for further comparison, analysis, and design.

CHAPTER 1
INTRODUCTION AND MOTIVATION

1.1 Introduction

Thousands of satellites have been operating around the earth where the earth's orbits can be categorized as High Elliptical Orbit (HEO), Low Earth Orbit (LEO), Geostationary Orbit (GEO), Medium Earth Orbit (MEO). When the orbital data of the currently operating satellites were analyzed, it was observed that 73 % of these satellites are operating in LEO (Satellite data, including launches up to and including 7/31/2020, was derived from [1]) as shown in Figure 1.1. This information demonstrates the space industry's intense interest in LEO since this orbit has been utilized for a variety of critical applications such as communications, military reconnaissance, earth observation, environmental monitoring, scientific and R&D.

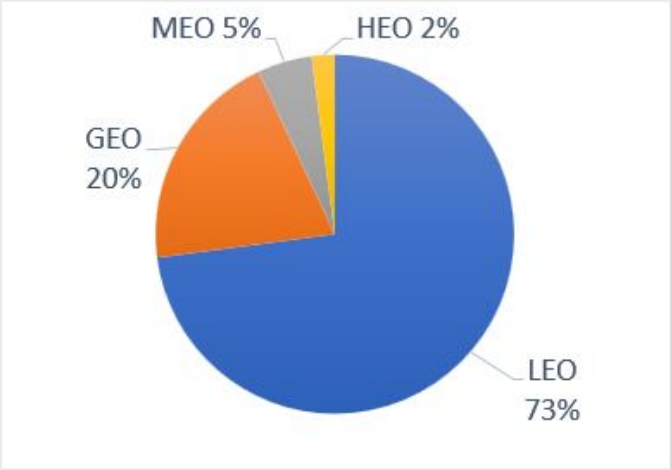

Figure 1.1: Orbits of the Operating Satellites

When the data were examined in greater depth, it was noted that the majority of these satellites fell into the category of small satellites, with a mass of less than 500 kg [1]. However, most of these small satellites have not been launched with SLV which have a

maximum payload capacity of 500 kg [2]. These satellites were generally delivered to ISS as secondary payloads on medium or heavy launch vehicles and then deployed from ISS to the target orbit. In this case, the primary payload has been posing a constraint to the orbit options for small satellites. This situation also causes small launch rates for small satellites where the primary payload dictates the schedule [3].

The commercial space industry has been interested in tackling problems with the current launch services of small satellites into LEO. There are so many SLV such as CAB-3A, Arion 2, Kuaizhou 1/1A, and Electron which are either under development or have been recently developed by commercial companies. These companies are interested in these vehicles because they are expected to offer a number of benefits, including orbital flexibility, increased launch frequency, on-demand launch capability, and the use of environmentally friendly propellants.

1.2 Motivation

The main motivation for developing the SLV is the growing demand for small satellite launches enabled by technological advancements. In this thesis, the term "small satellite" refers to minisatellites (101-500 kg), microsatellites (11-100 kg), and even nanosatellites (1-10 kg) [2].

The operations that SLV is expected to perform in the future can be broadly classified as follows:

1. Capability for a single small satellite launch

   Today, interest in small satellites such as CubeSats is significant, with academic institutions and numerous companies launching CubeSats into orbit. The SLV are projected to be able to launch these satellites at a lower cost.

2. Capability to launch constellations of nanosatellites

   Satellite constellations are groups of dozens or hundreds of satellites that cooperate

together. Satellite constellations can be used for a variety of applications, including broadband internet access and Earth observation.

The most frequently used measure in the economics of launch services is the specific pricing (price per launch/payload capacity), which typically increases as the payload mass decreases. Therefore, it is worth examining the specific prices of some state-of-the-art SLV as shown in Figure 1.3. Figure 1.2 shows the specific prices of some SLV based on the data provided by [4]. It was observed that for the nano and microsatellites, the specific prices are especially very high. Therefore, providing cost-effective launch services for small satellites to LEO remains a challenge.

NASA stated that the current cost of launching a 100 lb payload to LEO on a dedicated launcher is approximately $ 10 million. NASA is interested in lowering these prices to make access to space, particularly LEO, more affordable, as stated in the most recent technology roadmap, which includes two distinct goals regarding the costs of these launch services [3]:

1. Reduce launch costs by at least 50 % over the next two decades.

2. Reduce the cost of vehicles in the nano-launcher class to $ 1.5 million.

The first goal applies to all launch vehicles, whereas the second is unique to the nanolauncher class. The goal, in any case, is to reduce costs, which will benefit NASA, government agencies, and the commercial launch industry. These goals also serve as motivation for the development of new SLV in a variety of sizes.

Several influential technologies are emerging that have the potential to reduce the cost of launch vehicles in the future. A recently published comprehensive report by MIT identified the following technology areas for lowering the costs of launch services [5]:

- Propulsion

- Vehicle Manufacturing

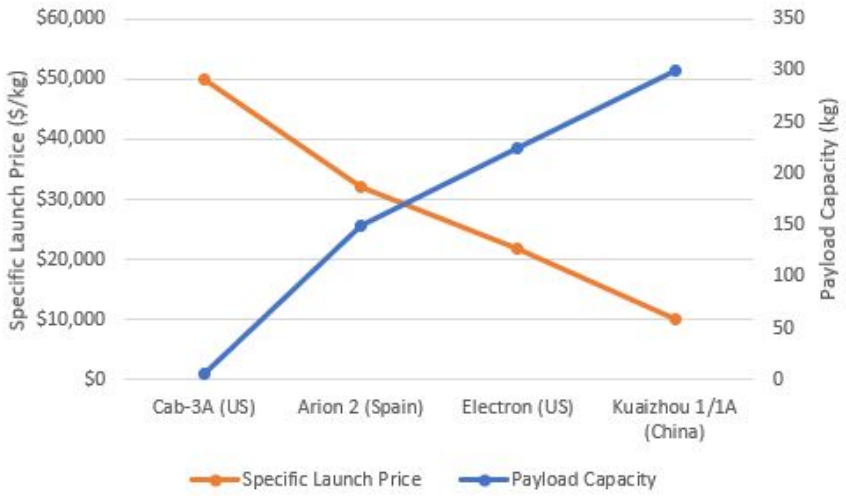

Figure 1.2: Specific Prices vs Payload Capacities

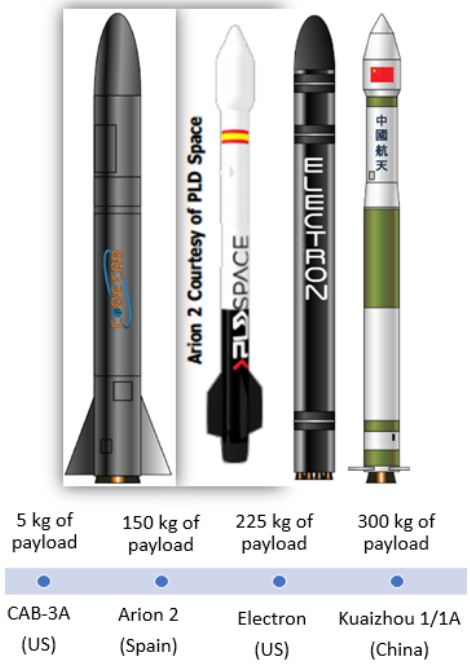

Figure 1.3: SOA Small Launch Vehicles

- Reusability
- Launch operations
- Ground support equipment
- Structures

Reusability has been a primary cost-cutting strategy for SpaceX and many other companies. Although it is projected that reusability will reduce costs, a significant cost decrease has yet to be demonstrated, because the development costs for reusable vehicles are higher [6]. Propulsion is another area where significant technological improvements have lately occurred, potentially lowering costs. The latest technology roadmap of NASA has outlined advanced capabilities of launch propulsion systems where some technology candidates were stated as follows [3]:

1. *Hybrid Motors*

   The hybrid motors that are now being developed are projected to lower the cost of launch services for nano and microsatellite services into LEO.

2. *Liquid Engines*

   The objective with liquid engines is to increase manufacturability in order to reduce costs while maintaining the engines' high performance.

3. *Solid Motors*

   The objective with solid engines is to increase performance and safety while reducing costs.

4. *Lightweight Engine Components*

   The goal of this technology is to reduce engine weight by using composite and hybrid metallic/composite components.

Hybrid rocket motor technology may be a key enabler of cost reductions in SLV. Hybrid motors typically combine a solid fuel with a liquid oxidizer. Hybrid rocket propulsion is very promising for small vehicles due to the advantages that these motors offer such as [7];

- Decreased cost
- Enhanced safety

- Mechanical simplicity
- Increased specific impulse
- Non-toxic propellants
- Start-stop-restart capability

In comparison to liquid engines, hybrid motors have a simpler mechanical design and simpler injection, feed, and control systems. Additionally, hybrid motors are safe. Another advantage is that hybrid motors outperform liquid engines powered by LOX/RP-1. Moreover, it is possible to improve performance of hybrid motors by the addition of metals. Finally, hybrid motors have a higher propellant density [8].

In comparison to solid motors, hybrid motors have been observed to be chemically simpler. Hybrid motors also outperform solid-state motors while requiring no toxic propellants. Another significant advantage of hybrid motors is their restart capability, which is comparable to that of liquid engines. Additionally, these motors are throttable. The explosion hazard is reduced, and hybrid motors have two safety-related advantages: zero TNT equivalence and the ability to stop [8].

Despite these benefits, hybrid motors have not been commercially viable due to technical difficulties. Hybrid motors that run on polymer fuels, in particular, face two significant challenges: a low regression rate and combustion instability. The low burning rate of solid fuel is a result of the combustion process's diffusive nature, which results in low thrust. Complex grain geometries with multiple ports and larger slivers are required for such motors. Additionally, as mentioned in [8], the combustion process produces rough pressure-time characteristics that can be classified as oxidizer feed system-induced instability (nonacoustic) and flame holding instability (acoustic).

Hybrid technology has matured recently with the solutions introduced by academia and the commercial companies towards the problems of these motors. To increase the low

regression rates, some methods were investigated to increase regression rate such as introducing additives in the fuel, swirl injection for liquid, using paraffin-based propellants [9]. The last one, hybrid motors using liquefying fuels was at the interest of Stanford University and Space Propulsion Group where higher regression rates were achieved by using a different combustion mechanism [10], [11]. A paraffin-based fuel with 3-4 times higher regression rates was developed and this improvement removed the need for a complex multiport grain. The scale-up tests were carried at NASA Ames Research Center. This advancement has been an important step to understand and make hybrid motors viable with simpler designs.

The second obstacle, combustion instability, can also be overcome. To begin, the instabilities caused by the oxidizer feed system can be resolved by stiffening the feed injection system. For instance, increasing its resistance to vibration can eliminate this type of oscillation. Second, flame holding instabilities can be eliminated in a variety of ways that contribute to the stabilization of the combustion process in boundary layers [7]. Certain companies have been able to resolve this issue through the use of advanced combustion chamber and injector design, as well as passive devices [12], [13].

Despite these advances, developing a predictive theory of combustion instability remains a key problem in the development of hybrid technology [7]. Some other drawbacks can also be listed as;

- Low combustion efficiency in large ports
- Slow response to throttling
- O/F shift

While certain issues remain with these motors, research is continuing to address them, particularly in academia and the commercial space sector. As the competition to develop cost-effective SLV increases, a new concept of small launch vehicles incorporating hybrid rocket propulsion technology could be one of the future solutions for lowering the launch

prices. Many commercial companies across the world have begun developing orbital vehicles using only hybrid rocket propulsion. HyImpulse (Germany), TiSpace (Taiwan), and Rocket Crafters (US) are a few of these companies [14].

1.3 Problem Identification

The phased approach to design divides the vehicle design process into three phases: conceptual design, preliminary design, and detail design phases [15]. A critical activity in the Conceptual Design Phase (CDP) is doing trade-off analyses in order to narrow the number of feasible vehicle designs to one or a few for further design and analysis. A similar phase, referred to as "Concept Studies" by NASA, was depicted as the first phase of a life cycle as illustrated in Figure 1.4. This is the phase where the feasibility of possible missions and concepts are evaluated among other activities such as cost, schedule, and risk evaluations [16]. The main outcome of this phase is a "Feasible Concept".

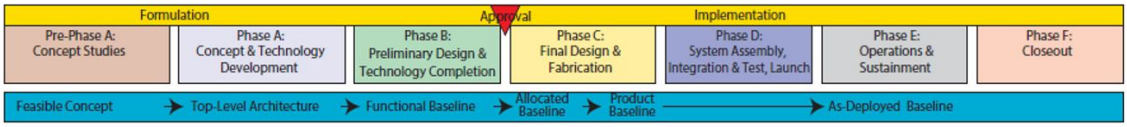

Figure 1.4: Life Cycle Phases

A small launch vehicle design process involving hybrid rocket propulsion should therefore begin with the CDP, which requires numerous trade-off analyses. Among the first considerations would be architectural options. There are so many different architectural variables even for a conventional expendable Launch Vehicle (LV) which is illustrated in Figure 1.5. Different architectures can be designed by varying the number of stages, the number of motors used in each stage, and the number of boosters as shown in this figure.

Some questions that a system designer of such a vehicle could ask in the CDP are listed below. These do not limit the questions, but they may serve as a starting point for initial investigations:

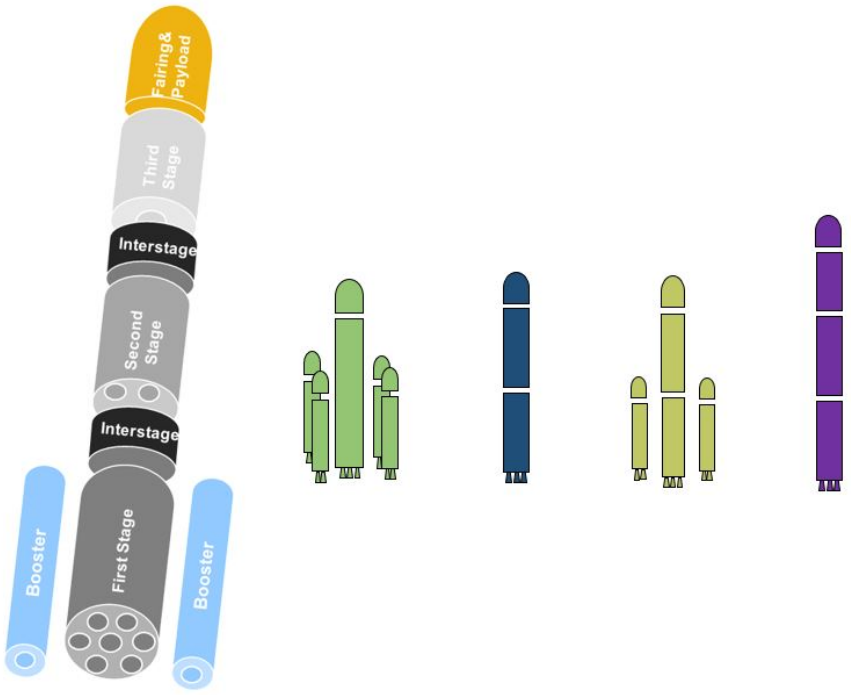

Figure 1.5: Architectural Alternatives for a Conventional Launch Vehicle

- What should the vehicle's approximate dimensions be (length, diameters of stages, etc.)?
- Which architectures can provide feasible design solutions?
- To reach the desired orbit, how many stages should be used?
- How many motors should be used in each stage to achieve the desired orbit?
- With the current limitations of this technology, can hybrid rocket propulsion technology enable a feasible orbital launch?
- What impact would any changes in subsystem design have on vehicle performance?

If one or more feasible vehicles can be designed in the CDP, these candidate designs may progress to the preliminary design phase. On the other hand, if any feasible design solution cannot be found in the CDP, then the requirements should be reviewed, or some technology integration studies should be conducted [17]. Because the concept definition is

developed at the end of this phase and has an impact on the subsequent phases of the design process, any decision made during this phase has a significant effect on the efficient use of project resources such as time and budget [17].

In addition to architectural design alternatives, subsystem design alternatives must be assessed during this phase. For example, various motor design options for a hybrid rocket propulsion system can be generated by altering some design variable candidates such as:

- Fuel
- Oxidizer
- Initial mixture ratio
- Nozzle inlet pressure
- Pressurization system to be used
- ISP
- Burn Time
- PMF of a motor or a stage

Table 1.1: Number and Type of Variables by Some Disciplines

Discipline	Number and Type of Variables
Aerodynamics	Few, Continuous
Trajectory	Many, Continuous
Weights and Sizing	Few to many, Continuous/Discrete
Structures	Many, Continuous/Discrete
Controls	Many, Continuous
Propulsion	Few, Continuous/Discrete

It is worth noting that some of these design variable candidates, such as ISP, are at higher levels, whilst others, such as initial mixture ratio or chamber pressure, are at lower levels. Furthermore, some design variables are discrete (e.g., fuel type, number of stages,

number of engines), whereas others are continuous (e.g. burn time, ISP). In Table 1.1, the types and number of design variables for some disciplines were provided [18]. As more disciplines and design variables are introduced to represent the design space, it may rapidly expand, resulting in a combinatorial explosion [19]. In this case, traditional approaches would require extremely long design cycle times to evaluate the system design space. However, within the constraints of a predefined schedule, the design space must be evaluated in order to select some feasible designs. The following research objective was stated and followed throughout the thesis as a result of this motivation.

Research Objective:

Develop a systematic methodology for conducting rapid conceptual design trade-off studies for an expendable small launch vehicle powered by hybrid rocket technology to determine the feasibility of an orbital launch from Earth to LEO.

1.4 Thesis Outline

The remaining chapters of this thesis were organized as follows. Chapter 2 introduced the literature search and some preliminary material related to this problem. The proposed methodology for carrying out design trades for the concept was presented in Chapter 3. Following that, Chapter 4 included the results of an extended design study. Chapter 5 concluded the thesis by stating the contributions and suggesting some future work.

CHAPTER 2
PRELIMINARY MATERIAL AND LITERATURE REVIEW

The previous chapter identified the problem and research objective that this thesis addresses. Because the objective of the thesis was to develop a rapid conceptual design methodology for a small launch vehicle powered by hybrid rockets, this chapter was broken into multiple subsections to review related material and literature. The first section examined multidisciplinary modeling and simulation approaches as well as some existing software. Following that, various advanced design methodologies were outlined as preliminary material to assist in the resolution of the problem stated in this thesis. Finally, an overview of recent studies on launch vehicle conceptual design was provided. The overarching hypothesis was given at the end of this chapter, which serves as the basis for establishing the methodology in the following chapter.

2.1 Launch Vehicle Conceptual Design Problem

In general, CDP produces the size, mass, cost, and risk associated with developing a vehicle within certain constraints such as cost and schedule. Additionally, this phase includes several objectives, including requirement definition, design evaluation, cost estimation, design and technology trade studies, and feasibility assessment [20].

The launch vehicle conceptual design is a highly complicated task requiring the synthesis of numerous disciplines. Historically, the disciplines of interest have varied from conceptual to detail design phases as illustrated in Figure 2.1 [21]. These disciplines were traditionally handled by separate teams within an organization.

For an aerospace system, these disciplines typically have competing objectives. Because a good vehicle design requires a compromise between these objectives, a trade-off analysis is used to aid in decision-making. To define, a trade-off analysis is a study in which

Figure 2.1: Disciplines Involved In Aerospace Vehicle Design

engineers define objectives, identify, and compare numerous design alternatives by weighing the benefits and disadvantages of various designs and architectures. Additionally, these investigations are used to detect the most sensitive parameters. Structural strength versus weight, aerodynamics versus structural strength, and structures versus control are some examples of competing disciplines in aerospace applications [20].

Traditionally, trade-off analysis and decision-making processes have relied heavily on the experience of engineers in the CDP [15]. However, a quantitative approach is also necessary, with M&S serving as an enabler throughout the conceptual design phase to enable quantitative evaluation [15]. The following section discusses several M&S approaches for launch vehicles.

2.2 Multidisciplinary Modeling & Simulation of Launch Vehicles

The majority of crucial decisions affecting the life-cycle costs of a program occur at the CDP [17]. Therefore, engineers are continually looking for ways to model complex and costly systems, such as a launch vehicle, without producing expensive prototypes. Applying M&S early in a project enables them to decide whether to continue with the project

without devoting more resources. The primary functions of M&S throughout the concept development phase are to evaluate alternatives, to visualize new concepts, and to evaluate effectiveness [20].

Some of the benefits of using M&S for conceptual design were summarized as follows [20];

- Reduce the time required to complete trade studies
- Eliminate some flawed solutions, thereby lowering quality costs
- Identify potential solutions
- Test concepts before putting them into operation
- Understand system behavior
- Enhance analysis
- Reduce development costs

There are also some challenges of using M&S. Some of these were listed as follows [20];

- The difficulty of implementing when the requirements are unknown in the early phases of a project
- Increasing development times
- Effects of hidden and significant assumptions
- The difficulty of collecting quality data
- Technological limitations
- Large resource requirements

For a launch vehicle conceptual design, the disciplines to model and simulate are selected depending on the problem and mission. NASA divided a launch vehicle conceptual design problem into smaller problems as shown in Figure 2.2 [18]. The primary disciplines for an ascent problem were outlined as trajectory, aerodynamics, propulsion, weight, and heating if an air-breather engine is included. The key disciplines in this thesis were trajectory, aerodynamics, propulsion, and weight because a hybrid rocket propulsion system was studied. The modeling approaches for each of these disciplines were discussed in the subsections that followed.

Ascent problem
Trajectory Weights and sizing Propulsion (Plus aerodynamics and heating if air-breathers)
Entry problem
Geometry Aerodynamics Trajectory Heating Structures Controls
Economics problem
Operations Hardware and software Safety Costs Business (Plus selected other disciplines)
On-orbit problem
Radiation Geometry/layout Weights and sizing Safety

Figure 2.2: Breakdown of the System Design Problem Into Smaller Problems for a Launch Vehicle

2.2.1 Launch Vehicle Performance Analysis

The objective of CDP is to generate a small number of candidate vehicles from a large number of options. To achieve this goal, the performances of many different vehicles must be evaluated and compared. However, there is no precise closed-form equation for analyzing launch vehicle performance [20]. Two most common approaches for evaluating launch vehicle performance were discussed in the subsections that follow.

The Tsiolkovsky Rocket Equation

The Tsiolkovsky equation, commonly known as the ideal rocket equation, is a simple model for determining the performance of space vehicles. This equation was provided in Equation 2.1 [22].

$$\triangle V_{ideal} = U_{eq} \ln \frac{m_{initial}}{m_{final}} \tag{2.1}$$

$$U_{eq} = I_{sp} g_e \tag{2.2}$$

where;

$\triangle V_{ideal}$: The ideal change in velocity that the vehicle could achieve

$m_{initial}$: Initial mass of the vehicle

m_{final}: Final mass of the vehicle

U_{eq}: Equivalent exhaust velocity

I_{sp}: Specific impulse

g_e: Gravitational acceleration of the Earth

This model provides a simple relationship between three important disciplines: vehicle performance, weight, and propulsion. However, it does not represent aerodynamics which is very crucial when comparing vehicle concepts with different architectures. This model cannot estimate the real performance of a launch vehicle since it neglects all velocity losses

occurring during launch. The ideal $\triangle V_{ideal}$ of a vehicle can be calculated with the model provided in Equation 2.3 correctly [23]:

$$\triangle V_{ideal} = \triangle V_{mission} + \triangle V_{thrustloss} + \triangle V_{dragloss} + V_{gravityloss} \tag{2.3}$$

In this equation, $\triangle V_{mission}$ is the required velocity change to insert the vehicle into an orbit. The three loss terms are dependent on the vehicle trajectory. $\triangle V_{thrustloss}$ contains two loss mechanisms related to thrust; a thrust loss due to the atmospheric pressure at the nozzle exit, and a thrust loss due to steering. $\triangle V_{dragloss}$ represents the velocity loss spent for opposing drag forces. $\triangle V_{gravityloss}$ is the velocity loss that is spent to fight gravity. If these losses can somehow be calculated, then the actual performance of a vehicle can be calculated correctly as well. However, one of the difficulties inherent in launch vehicle design is accurately and rapidly computing these path-dependent terms.

Review of Empirical Performance Data for Launch Vehicles

Using historical data to evaluate a vehicle's performance is one approach if there is any reliable data available. There is some historical $\triangle V_{ideal}$ data accessible in the literature for certain launch vehicles. For the class of medium and heavy launch vehicles, such data were compiled and summarized in [23]. Additionally, some useful empirical relationships for evaluating the performance of launch vehicles were developed using historical data in this study. The majority of the $\triangle V_{ideal}$ data was found to be distributed between 10000 and 14000 m/s. It was worthwhile to consider whether utilizing empirical relationships derived from these data to evaluate small vehicle performance is a good approach.

Empirical relationships are not usually suitable for extrapolation, but they are used for interpolation to ensure accuracy. Therefore, relying on these relationships may result in an erroneous assessment of the performance of SLV. Any empirical relationship to estimate performance should be obtained using data from this class of vehicles. SLV, on the other

hand, are relatively new concepts, with only a handful operating vehicles to date. Several companies are currently developing some SLV, however no performance data for these vehicles has been disclosed due to confidentially. Due to a lack of historical data, it is not possible to derive new empirical relationships for these vehicles.

2.2.2 Trajectory Analysis

Because the preceding approaches were insufficient for this problem, this section examined a physics-based approach. The trajectory is defined as the time-dependent path followed by a launch vehicle. The equations of motion that define the trajectory of a vehicle are fundamentally nonlinear ordinary differential equations that require numerical integration. A trajectory simulation establishes a parametric framework for simulating the vehicle's configuration, forces, atmospheric properties, basic control laws, and mission profile [20]. After establishing this framework, the optimal orbital trajectory can be identified by trajectory optimization, which is performed by incorporating an optimization algorithm into the simulation. The analysis performed with the integrated simulation and optimizer is known as "trajectory analysis". Trajectory analysis is the most effective method of quantifying launch vehicle performance, and it is crucial because it serves as a link between vehicle concept and performance [24].

The following are the basic applications of trajectory analysis [20]:

- Calculating the maximum payload mass that can be carried to the desired orbit
- Analyzing the impact of a design change to a subsystem on the overall performance of the vehicle
- Optimizing the performance of an upper stage
- Choosing a launch window
- Examining how the atmosphere influences the performance of the launch vehicle

The trajectory analysis approaches were discussed in the following subsections. [23] classified trajectory performance modeling methodologies into five broad categories:

Numeric

Numerical modeling integrates the equations of motion subject to some control laws. Because a trajectory simulation solves equations of motion, a numerical integration is required, with numerical integration methods classified as shooting and collocation. Shooting is used at each time step to update the state vector based on derivative information from previous time steps. The Euler and Runge Kutta methods are two well-known shooting methods. Collocation, on the other hand, computes the system's state using an interpolating function. [23].

Algorithms for trajectory optimization are often classified into two categories: global and local methods. The benefit of a global method is that it can calculate the global near-optimal, but the main disadvantage is the time required to run such algorithms. Some of the global methods are the genetic algorithm, particle swarm, ant colony optimization, and simulated annealing. Local methods, on the other hand, are relatively computationally inexpensive, but they may get stuck in local optima. Line search, Thrust Region, Simplex, and SQP methods are examples of direct methods [25].

There are two types of local methods: direct and indirect. The direct method converts an optimal control problem into a nonlinear programming problem. These methods are simple to implement. The key disadvantage is that solutions may be sub-optimal. The indirect approaches, on the other hand, use the Calculus of Variations to solve the optimal control problem. While indirect approaches are difficult to implement, they can yield accurate results [23].

The advantage of numerical modeling is the high fidelity it offers; yet, numerical models can be computationally expensive [23].

Analytic

Analytic models are composed of equations in closed form. The Ideal Rocket Equation is an example of a closed-form analytic model. At times, analytical models can be extremely accurate. For example, in exoatmospheric applications, the Ideal Rocket Equation can be accurate. However, the assumptions used to develop the Ideal Rocket Equation are invalid for atmospheric flight. Indeed, there is no closed-form equation that accurately describes the performance of a launch vehicle in atmospheric flight [20].

Empiric

Empiric models are basically statistical regression equations. These models are derived using some historical data. They have the advantage of being able to perform rapid performance evaluations. The disadvantage is that these models are erroneous when used for extrapolation.

Heuristic

A heuristic model is a simplified or rough calculation found in the literature. These models are used to quickly assess performance, although they are insufficiently precise [23]. Furthermore, such rough estimations for advanced vehicles may not be found in the literature.

Hybrid

Hybrid models are a mix of the models that have already been defined. In launch vehicle ascent performance modeling, for example, a combination of analytic and numerical models is typically utilized.

Objective Functions and Constraints in Launch Vehicle Trajectory Optimization

Similar to any other constrained optimization problem, trajectory optimization necessitates the determination of objective functions, inequality constraints, and equality constraints

based on the space mission requirements. Because these functions typically incorporate some parameters of a vehicle's or mission's performance such as target orbit's parameters and Gross Take-Off Mass, this section covered the most frequently used objective functions and constraints. [26] categorized objective functions based on the type and quantity as shown in Figure 2.3.

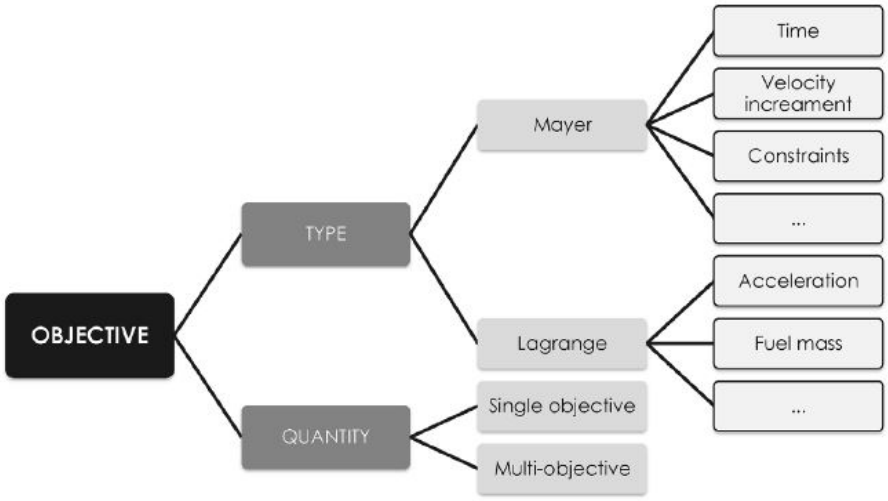

Figure 2.3: Objectives for Trajectory Optimization

The first type of objectives was Mayer which are functions of state variables at the end of a trajectory [26]:

1. Time

   In trajectory optimization problems, time refers to the amount of time a vehicle spends in space. Minimization of time is sometimes used as the objective.

2. Velocity increment

   The objective can be the minimization of the velocity increment or the sum of the velocity increments in multiple phases.

3. Initial and terminal conditions

The terminal and initial conditions are generally defined as constraints. Nevertheless, certain studies define constraints as objectives. The remainder of this thesis study addressed initial and terminal conditions as constraints rather than objectives.

The second type of objective was Lagrange. These are integrals of inputs or state variables in the trajectory.

1. Acceleration

   Occasionally, the cost function to be minimized is the integration of the square of the spacecraft acceleration within the transfer trajectory.

2. Fuel mass

   Along with velocity and acceleration, fuel mass is also used as a proxy for energy.

Scalarization:

Scalarization combines multiple objectives into a single function by multiplying each of them with weights. Weights are assigned in accordance with the relative importance of each objective. Several cost function models developed by scalarization were shared in Table 2.1 [26]:

Table 2.1: Modified Cost Functions

Scalarization	Modified Cost Function
Sum method	$J = \sum_{i=1}^{n} J_i$
Weighted sum method	$J = \sum_{i=1}^{n} \alpha_i J_i$
Normalized method	$J = \sum_{i=1}^{n} \frac{J_i}{\alpha_i}$
Global criterion method	$J = \sum_{i=1}^{n} J_i^2$

Next, several recent studies on multistage launch vehicle trajectory optimization were reviewed to identify various often used objective functions and constraints.

In [14], with gravity turn, maximum dynamic pressure, and orbital parameters constraints, the propellant consumption was minimized as an objective. In [27], the maximum

mass of the payload injected into the target orbit was included in the single objective function. Maximum dynamic pressure, maximum axial overload, and maximum attack angle were used as inequality constraints in this study, while orbital altitude, orbital inclination, orbital eccentricity, and flight path angle were used as equality constraints at the injection positions.

In [28], the objective was to obtain the maximum amount of orbital energy possible. Afterwards, the final time was adjusted to achieve the desired orbital energy. This adjustment was equivalent to maximizing the mass (while decreasing the amount of fuel consumed) in a particular orbit for free terminal time. At perigee, terminal constraints were specified in terms of inclination, perigee radius, and flight path angle.

In [29], the objective was to maximize the final mass. The terminal constraints were specified in terms of desired inclination, perigee radius, and apogee radius at the final orbit perigee point. Constraints on apogee radius were quantified in terms of desired orbital energy for a given perigee radius. Additionally, because the constraints were expressed in terms of perigee conditions, an additional constraint requiring a zero flight path angle was imposed.

In [30], the minimization of the gross launch mass was the objective. Orbital insertion velocity, final altitude, axial overload, normal overload, maximum dynamic pressure, upper stage burning time, nozzle exit diameter, thrust to weight ratio, grain fineness, rocket motor mass, rocket motor diameter, and total launch vehicle length were all inequality constraints. Zero angle of attack and zero flight path angle were the equality constraints.

[31] which was a survey of launch vehicle MDO methods, included several examples of common constraints used in trajectory optimization problems. Some mission specifications, such as desired orbit, payload mass, and gross lift-off weight (GLOW), were examples of equality constraints, while some of the inequality constraints were maximum chamber pressure, maximum load factor, or minimum nozzle exit pressure. The objective used in this study was to minimize the dry weight.

In [32], the objective was to maximize payload mass while meeting the inequality constraints of dynamic pressure, bending load, heat flux at fairing jettisoning, axial acceleration, and pitch-over rate. The assigned orbital radius (perigee and apogee) and assigned orbital inclination were both equality constraints.

In [33], for a fixed payload and a given launch vehicle configuration, the objective was to maximize orbit altitude. Orbit insertion velocity, axial overload, normal overload, maximum dynamic pressure, and maximum angle of attack were the inequality constraints, while zero angle of attack and zero orbit insertion angle were the equality constraints.

In [34], both single-objective and multi-objective optimization problems were solved. The objective was to minimize the gross mass in the single-objective problem. The multi-objective function was constructed using the weighted sum of the standard deviations of the height, velocity, and flight path angle at the injection point. The inequality constraints included orbital height deviation from the desired value, orbital velocity deviation from the desired value, path angle deviation from the desired value, angle of attack during maneuvering phase, angle of attack in the first stage separation, maximum dynamic pressure, aerodynamic load indicator (the multiplication of dynamic pressure and angle of attack).

Finally, in [35], the objective function of the optimization was to minimize the launch weight. The inequality constraints included dynamic pressure, normal overload, angle of attack.

Challenges of Trajectory Optimization

The performance analysis of a vehicle is the primary focus during the conceptual design phase, despite the fact that trajectory optimization is an intermediate step in calculating performance. In fact, the problem of trajectory analysis in the context of launch vehicle design is one difficulty of launch vehicle conceptual design [24].

One challenge with trajectory optimization is that it is a computationally expensive analysis. Traditionally, subject experts perform trajectory optimization one at a time for

each vehicle concept, limiting the number of vehicles evaluated in a limited amount of time. If hundreds of vehicles must be traded-off during the conceptual design phase, the schedule may not allow for such extensive trajectory optimization.

Another problem is that a high fidelity trajectory analysis (e.g., with a 6 DOF trajectory simulation) generates a large number of outputs, some of which may be unnecessary during the conceptual design phase. Because the primary concern is only basic performance estimates, the use of project resources for this type of costly analysis may be questionable in the early design phases.

Trajectory optimization becomes extremely expensive, especially when global optimization methods such as genetic algorithms are involved, despite the fact that global optimizers yield near-optimal solutions. If a gradient-based optimization approach is utilized, the solution may get stuck in a local optima for non-convex problems. In this case, the calculated local optimum may not provide a reliable estimate of vehicle performance. As a result, this analysis always requires a trade-off between accuracy and speed, which necessitates a comprehensive understanding of the optimization area as well as significant analysis times.

There are significant epistemic uncertainties in the conceptual design phase due to a lack of information about the system. Because many of the vehicle design parameters are updated as the subsystem designs evolve in the preliminary design phase, the optimum control design may not be as beneficial as intended in subsequent design design phases. In fact, performing a trajectory optimization at the preliminary design phase, when only a few vehicles are evaluated, may be more efficient.

These challenges with trajectory optimization can be solved by trajectory engineers with sufficient computational resources and long analysis times to optimize the trajectories of various concepts. When time restrictions exist during the conceptual design process, a low-fidelity trajectory simulation, such as a 3 DOF simulation with a point-mass assumption, is frequently employed to speed up the analysis. Additionally, using a constant con-

troller design may be one way to conduct this study quickly. However, the effect of using a constant controller design on the performance evaluation of vehicles must be thoroughly examined. If employing a constant controller enables an acceptable design trade-off, it may be used to reduce the analysis's run-time requirements.

Trajectory Optimization Software

This section summarizes several of the most commonly used trajectory optimization software.

Program to Optimize Simulated Trajectories (POST)

The Program to Optimize Simulated Trajectories (POST) was originally written in FORTRAN in the 1970s for the purpose of optimizing the trajectory of the Space Shuttle. Since then, various versions with enhanced features have been developed. POST is capable of simulating and optimizing 3 DOF and 6 DOF trajectories for a variety of aerospace vehicles. POST utilizes the direct shooting method to integrate the trajectory in time [36].

Optimal Trajectories by Implicit Simulation (OTIS)

OTIS was developed by the Boeing Company in the 1980s and has since been updated. OTIS contains propulsion, weights, atmosphere, and aerodynamics models. 6 DOF simulations are performed for vehicle models. Although shooting is an option, OTIS solves nonlinear programming problems primarily through nonlinear programming and collocation [37].

AeroSpace Trajectory Optimization Software (ASTOS)

ASTOS was initially designed for trajectory optimization. It now offers modules for various analysis, simulation, and design capabilities throughout the project life cycle. ASTOS has capabilities for launch vehicle development that include performance analysis, multi-disciplinary and detailed design optimization, flexible multi-body dynamics and sloshing, 6 DOF closed-loop simulation, guidance, navigation, and control design [38].

Sparse Optimal Control Software (SOCS)

SOCS was developed by Boeing to solve optimal control problems. Trajectory optimization is one of the applications. Sparse Nonlinear Programming software, which is included with SOCS, makes use of sparse linear algebra technology to tackle very large optimization problems considerably more rapidly than traditional methods [39].

2.2.3 Aerodynamics Modeling

A launch vehicle is subjected to a variety of atmospheric conditions, which have a significant impact on its aerodynamic behavior and challenging to model because all subsonic, transonic, supersonic, and hypersonic flight regimes must be modelled.

The methods to perform the aerodynamic analysis were summarized below [40]:

- Data-sheet Methods:

  Because of their complexity, the Navier-Stokes equations are difficult to solve. Using experimental data to construct an aerodynamic coefficient database is one method. This method is effective for evaluating the performance of conventional concepts but may not allow for the assessment of aerodynamic trade-offs of advanced vehicles.

- Analytical Methods:

  Under certain assumptions, analytical formulas can be derived to estimate aerodynamic coefficients. An example of an analytical method is the lifting-line theory. While this method enables rapid, parametric, and straightforward analysis, it has some drawbacks. It cannot be employed, for example, with compressible or viscous flows. Corrective factors are introduced into analytical formulas in this case. Building empirical or semi-empirical relationships based on experimental data, observations, and correction factors is another method of creating analytical formulas. These formulas are widely employed during the early phases of design since they are computationally efficient.

Vehicle aerodynamics analysis can be conducted using a variety of available analytic models from the literature, each with varying levels of detail and accuracy. Furthermore, these models involve all flight regimes. With these analytic models, it is possible to quickly assess the drag and lift coefficients, the center of pressure, and normal forces for a body alone or a body with wings and aerodynamic control surfaces. Some aerodynamic modeling approaches can be found in [41], [42], [43], [44], [45].

- Computational Fluid Dynamics Methods:

  CFD methods are more complex than the previously mentioned methods since they require meshing and numerical resolutions. The main advantage of CFD methods is that they can overcome some limitations that other methods are subject to. CFD can handle advanced vehicles while allowing detailed trade-offs. However, they are computationally expensive.

Using empirical formulas at the conceptual design level and for design space exploration greatly expedite the analysis. When employing analytical methods, drag is often divided into multiple components, as summarized below. Various models for each of these components can be found in the literature. Each of these components is briefly summarized in the next section [40].

Drag decomposition;

- Friction and form drag
- Induced drag
- Interference drag
- Wave drag

1. Skin friction and form drag

The form drag occurs because of the surface pressure imbalance around a body which is integrated to calculate the form drag. This term is affected by the body shape, the angle of attack, and shocks. Skin friction occurs because of the shear stress acting in the drag direction. The skin friction drag depends on the smoothness of the surface and the size of the wetted area.

In the literature, two main methods are commonly used to estimate these components: the equivalent skin-friction method and the component buildup method. The first method assumes that the form drag is a small percentage of the skin friction. The component buildup method is more precise and estimates the drag coefficient of each component independently. Contrary to the equivalent skin-friction method, the component buildup method can enable geometry optimization and trade-off studies.

Induced drag

Wing-tip vortices result in an additional pressure drag component called induced drag. Prandtl's lifting line theory, the vortex lattice method, and the Weissinger nonlinear lifting line model are some methods used to estimate this component. Simplest methods models the induced drag as a function of lift coefficient and aspect ratio. Also, there are several empirical models available in the literature.

Interference drag

The total drag of combined bodies is greater than the sum of its components' drag. The interference drag is defined as pressure drag due to the mixing of flow fields around each component.

Wave drag

At supersonic speeds, shock waves form a pressure pattern with a significant pressure difference in the drag direction. The wave drag is generated by the integration of this pressure difference throughout the entire body. This drag coefficient is composed of two components: zero-lift wave drag and lift-induced wave drag. Preliminary supersonic drag

analyses are often based on linearized or modified linearized methods.

Aerodynamics Analysis Software

This section described several commonly used aerodynamics analysis software.

Aerodynamics Preliminary Analysis System

This software was created by Rockwell for NASA's Langley Research Center. At subsonic and supersonic speeds, the software is based on potential theory, whereas at hypersonic speeds it is based on impact theory. Although APAS is not very successful at transonic speeds, approximate transonic solutions can be produced by patching sonic and supersonic aerodynamics predictions. APAS is capable of doing rapid analysis on a broad variety of vehicle shapes [46]. As an illustration, APAS was utilized in [47] to analyze aerodynamics.

Missile DATCOM

Missile DATCOM which belongs to the US Air Force includes semi-empirical relationships and provides the users with the capability of aerodynamics modeling of different vehicle configurations easily. This software which was developed in the past to model missile aerodynamics contains some semi-empirical relationships. However, one significant limitation that should be mentioned is that DATCOM does not permit modeling boosters [48].

Missile DATCOM was utilized in several thesis studies and papers for conceptual design of launch vehicles such as [24], [49], [50], [51], [14], [30], [33], [34].

Some Property Software

In [52], The drag and lift coefficients were calculated using the ONERA code MISSILE. To estimate the aerodynamic forces and coefficients of various launch vehicle geometries, this software uses a simplified aerodynamics theory and an experimental database.

AeroDsn is yet another software program utilized in [53] and [54]. It is possessed by the United States Army and is used in the preliminary design of conventional missile designs.

Its primary function is to compute the aerodynamics of wings or tails, or both, added to a cylindrical-shaped body using a combination of theoretical and empirical data [55].

In [47], a property software; The HADES V15.0 platform which integrates several technical and economic modules within a system optimization loop was used. Propulsion, structure, aerodynamics, trajectory optimization, and cost are the primary disciplines covered in this platform.

Some Sizing and Synthesis Software Including Aerodynamics Analysis Capability

[56] presents an overview of some software programs for sizing and synthesis that include aerodynamics analysis capabilities. The Optimal Design Integration is one of these softwares (ODIN). ODIN was created in the 1970s as a software for sizing and synthesis of reusable launch vehicles. It encompasses a number of disciplines, including aerodynamics, thermodynamics, propulsion, weights, structure, aeroelasticity, economics, and stability. The software enables rapid problem formulation and automated exploration of the design space.

Aerospace Vehicle Interactive Design (AVID), like ODIN, is an integrated environment used for conceptual and preliminary design. Geometry, aerodynamics, propulsion, weight, performance, and economics are some of the disciplines covered. This program can assess a variety of vehicle concepts, including launch vehicles.

The Hypersonic Air Vehicle Optimization Code (HAVOC) performs aerodynamics analysis for a variety of vehicles, including launch vehicles. HAVOC consists of structural analysis, aerodynamics, and weight disciplinary models. FASTPASS (Flexible Analysis for Synthesis, Trajectory, and Performance for Advanced Space Systems) was developed recently to optimize vehicle design and mission requirements. Its objective is to automate the optimization process during vehicle sizing and performance assessment. Aerodynamics, propulsion, trajectory, structures, and weights are some of the disciplines covered [56].

2.2.4 Hybrid Rocket Propulsion Modeling

The three approaches for evaluating rocket engine performance were provided in [40] as follows:

- Single Parameter Approach

  The weight or engine performance is only dependent to a few parameters in this approach, such as the thrust required at sea level. The model is constructed using historical data and surrogate models. These methods are extremely quick, simple to build, and require only a few inputs. Nonetheless, their accuracy may be limited.

- Component-Based Approach

  In this method, the weight and characteristics of each component are estimated first and then integrated to estimate engine performance. In general, the computation time is significant.

- Cycle Parameters-Based Approach

  The main cycle parameters, such as the mass flow rate and the thrust required at sea level, are used in this method. In order to match the engine weight, it employs both historical data and correlation factors. This method offers a balance between the accuracy of the component-based method and the simplicity of the single parameter method.

Propulsion Analysis Software for Rocket Engines

Component-based software produces highly accurate results, but it is quite slow to run and computationally expensive in general. Cryogenic Rocket Combustion (CryoROC) is software that analyzes complex flows in cryogenic hydrogen/oxygen rocket engines' combustion chambers and nozzles. The Rocket Combustion Flow Analysis Module (ROCFLAM) is another code that analyzes flow phenomena in thrust chambers [40].

Some software programs for engine performance analysis, such as Rocket Propulsion Analysis (RPA), Cpropep, and Redtop, use the cycle parameters-based method. The main inputs of these software are propellants, combustion chamber pressure, and nozzle area ratio, and outputs are the optimal mixture ratio, exit speed, thrust coefficients, and specific impulse as a function of altitude. However, there are no software packages that satisfy all of the requirements for rocket engines [40].

2.2.5 Weight Modeling

Weight estimation is difficult in the early stages of design due to a lack of knowledge about a system and its subsystems. The Fixed-Fraction method, the Statistical Correlation method, and the Point Stress Analysis method are the three basic methods for weight estimation. However, none of these models are capable of modelling chemical rocket engines. Because hybrid rocket propulsion is a relatively new propulsion technology, physics-based modeling for weight and performance estimation is required. [40] developed a method for calculating the weight of a hybrid motor. A hybrid rocket motor was decomposed into its components, including a tank for the liquid oxidizer, a tank for the pressurization gas, a combustion chamber storing the solid fuel grain protected by internal insulation, and a nozzle assembly. After calculating the masses of each component using parametric equations, the overall mass of a hybrid motor was computed by summing the masses of all mass components. This method, however, relied on some many assumptions.

Another method is to use the Propellant Mass Fraction (PMF) variable to model weight. When there is a lack of knowledge about the the propulsion system during the conceptual design phase, this variable can represent weight at a high level. Using PMF is particularly advantageous for trade-off analyses in design. After selecting a feasible vehicle design from the design space, the associated PMF value for the propulsion system can be defined as a requirement. Similarly, the Inert Mass Fraction (IMF) can be utilized for the same

reason because it is defined as equal to 1-PMF.

$$PMF = \frac{m_p}{m_p + m_i} \tag{2.4}$$

$$IMF = \frac{m_i}{m_p + m_i} \tag{2.5}$$

In this equation;

PMF: Propellant Mass Fraction

IMF: Inert Mass Fraction

m_p: Usable Propellant Mass

m_i: Stage Inert Mass

2.3 Advanced Design Methods as Enablers for Rapid Launch Vehicle Conceptual Design

The launch vehicle conceptual design trade-off is challenging, especially when the design space is large and the multidisciplinary models and simulations are computationally expensive. Traditionally, the conceptual design approach is a point design process where design space is explored manually around only a few concepts [17]. When the design space is small and an organization's expertise and data are sufficient for designing the vehicle, the traditional approach may be useful. This approach, however, may not be practical when exploring a very large design space for an advanced concept. As a result, state-of-the-art methods in systems design, called "Advanced Design Methods" evolved, introducing some approaches from other disciplines such as operation research, biology, and control theory into aerospace system design [15],[17]. The next section discusses some advanced design methods that can be used to speed the design trade-off process.

DOE and surrogate models are two key enablers of advanced design methods. These aren't optimizers; instead, they break down difficult optimization problems into smaller

pieces that optimization methods can handle [21].

Design of Experiments (DOE)

DOE is typically used to sample a design space such that maximum information related to the design space can be extracted with a minimum effort [17]. Surrogate models can be created using the design points obtained using a DOE. There is usually a trade-off between the experimental expense and the design space covered in DOE applications [57].

Some commonly used DOE methods are classical techniques such as Central Composite Design, Box-Behnken Design, Full Factorial Design, and Fractional Factorial Design [21]. These designs generate points at the design space's corners and extremes. As a result, they could put computer codes at risk of crashing. Other techniques include more recent DOE techniques such as Quasi-Monte Carlo, Latin Hypercubes, and Sphere-Packing, which are referred to as Space Filling Designs. These designs generate more points in the design space's interior space, making them more suitable for computer coding. Several DOE types have been summarized briefly below [17].

Full Factorial Design

A full factorial design is the simplest type of DOE. The number of design points is equal to the product of the levels for each factor, and typically two or three level full factorial designs are used. The advantage of a full factorial design is that it is orthogonal; however, the disadvantage is that it produces an extremely large number of cases in more than a few dimensions. Additionally, this method cannot be used to study the interior of the design space.

Central Composite Design

A full-factorial design is augmented with a center point and two additional points for each factor, resulting in a total of five levels. Although this design necessitates a high number of design points, it is advantageous in some applications due to its ability to cover a large amount of design space. This design has the advantage of being orthogonal. The

disadvantage is that modeling and simulation codes may be unable to run at the design's extreme points [17].

Box-Behnken Design

Because these designs do not contain any corners, they are ideal for computer applications, as they prevent the code from crashing. The advantages of this design are that it is orthogonal and requires fewer cases than the DOE mentioned previously. The disadvantage is that the design space's corners are insufficiently covered [17].

Space Filling Design

For computer experiments, it is common to use space-filling designs that equally cover the design space. These DOE designs can be advantageous, particularly during the early phases of design, when the form of a surrogate model is unknown [58]. The advantages of this design are that it covers a greater number of interior points and requires fewer cases than the DOEs mentioned previously. However, these are not orthogonal designs [17].

Some of these DOE methods were illustrated in Figure 2.4 [17].

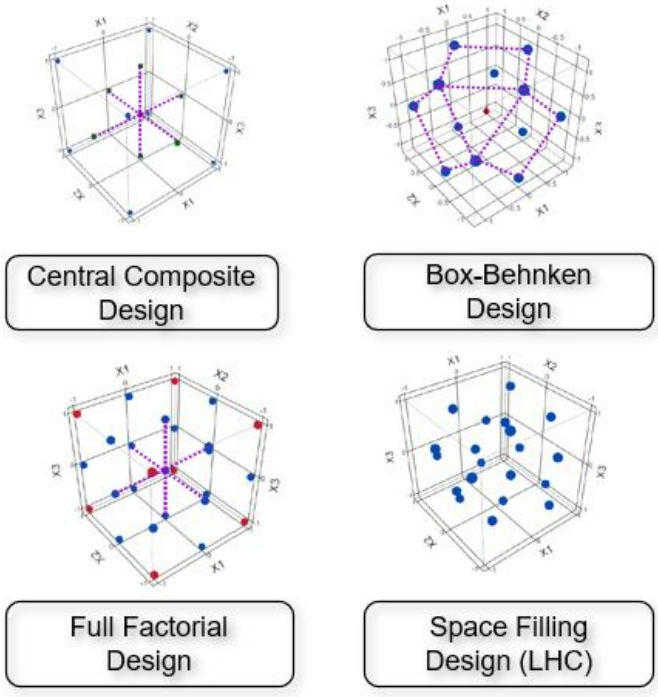

Figure 2.4: Some Types of Design of Experiments

Surrogate Modeling Methods

Surrogate models are approximations of complex models obtained through function fitting [15]. Surrogate modeling is used to accelerate analysis in aerospace engineering applications. The classification of surrogate models is illustrated in Figure 2.5 [17]. Several methods for surrogate modeling are summarized below.

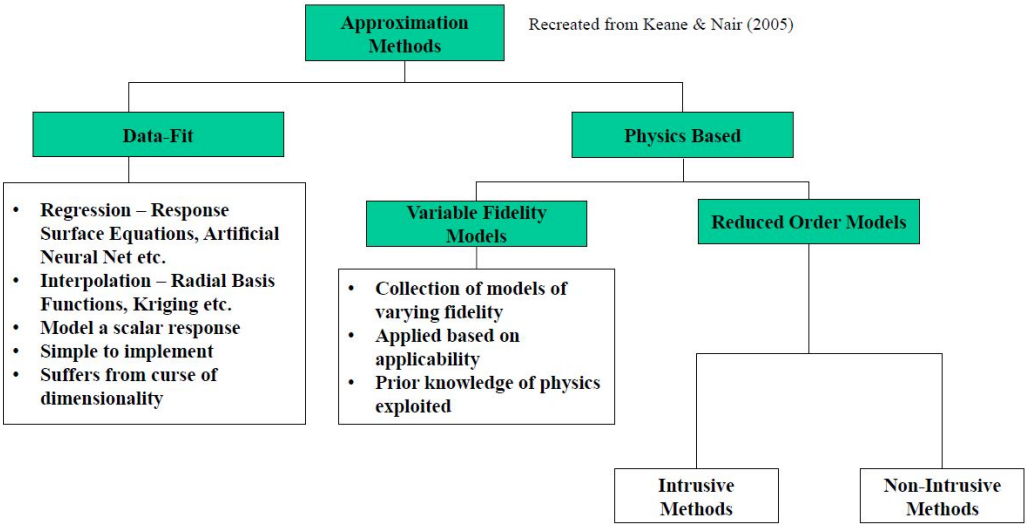

Figure 2.5: Taxonomy of Surrogate Modeling Methods

Response Surface Equations

Response Surface Equations (RSE) are obtained by using multiple linear regression methods which use variations of the least squares method to obtain n^{th} order polynomial fits for the responses. The structure of the equation is shown in Figure 2.6 where ϵ represents a normally distributed random error with mean zero and standard deviation σ, "x" represents the independent variables and "b" represents the regression coefficients.

$$y = b_0 + \sum_{i=1}^{k} b_i x_i + \sum_{i=1}^{k}\sum_{j=1}^{k} b_{ij} x_i x_j + \cdots + \varepsilon$$

Figure 2.6: Structure of the Response Surface Equation

Artificial Neural Networks

This method simply mimics the neurons in the brain. The input layer, hidden layer, and output layer of a feed-forward neural network model were illustrated in Figure 2.7 [21]. A node fits a model, for example, multiple linear regression, and then transmits the signal to a nonlinear or linear function. ANN is an extremely flexible method for dealing with highly nonlinear data. These models, on the other hand, are complex to interpret.

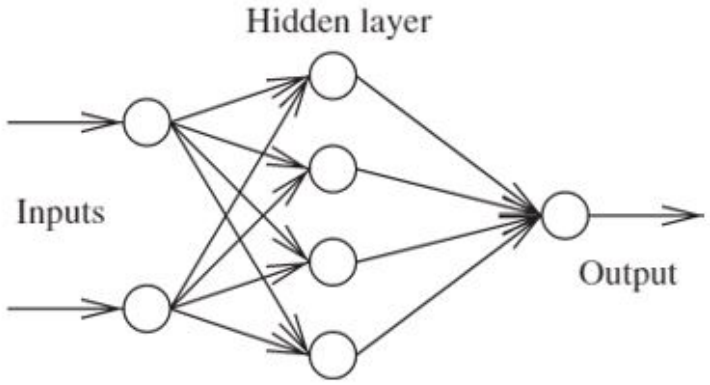

Figure 2.7: Sample Neural Diagram

The model was given with the following equation;

$$\hat{y}(x) = \sum_{i=1}^{m} \alpha_i \phi(a_i) \tag{2.6}$$

$$a_i = \sum_{j=1}^{p} w_{ij} x_j + \beta_j \tag{2.7}$$

where,

α, w, and β are unknown values that represent the weights and bias terms

$\phi(x)$: transfer or activation function such as tanh, linear or gaussian functions

Radial basis functions with various kernels (RBF)

RBF approximations are classified as generalized linear models. They differ from the RSE in terms of the basis functions they utilize. A radial basis function of the following

form is used in particular [21];

$$\hat{y}(x) = \sum_{i=1}^{n} \alpha_i K(||x - x^{(i)}||) \tag{2.8}$$

where,

$K(||x - x^{(i)}||)$ is a RBF,

α = [α_1 α_2 α_3 ... α_n] denotes a vector with undetermined weights

Linear splines, cubic splines, multi-quadratics, thin-plate splines, and Gaussian functions are all common choices for the RBF. In machine learning literature, the basis function K is also called a kernel. This method is frequently used to interpolate data, but it can also be formulated in a variety of ways and with secondary tuning parameters to perform regression [21].

Support vector machines (SVM)

Typically, SVM regression includes minimization of an ϵ-insensitive loss function;

$$\sum_{i=1}^{n} |y^{(i)} - \hat{y}(x^{(i)}, \alpha)|_\epsilon \tag{2.9}$$

where,

$$|y^{(i)} - \hat{y}(x^{(i)}, \alpha)|_\epsilon = \begin{cases} 0, & \text{if } |y^{(i)} - \hat{y}(x^{(i)}, \alpha)| < \epsilon \\ |y^{(i)} - \hat{y}(x^{(i)}, \alpha)| - \epsilon, & \text{otherwise} \end{cases} \tag{2.10}$$

ϵ is a parameter that is determined according to the level of error/noise expected in the outputs.

This technique enables the combination of multiple models with important data subsets (the so called support vectors). Multiple-dimensional problems involving massive amounts of data can be fairly efficiently solved [21].

Kriging and its derivatives

In general, this approach requires fine-tuning a large number of hyperparameters that impact the curvature and, potentially, the degree of regression. This technique can be computationally costly when dealing with big data sets with multiple dimensions.

Sensitivity Profiling

The sensitivity is a partial derivative of a response with respect to the design variables. Sensitivities are generally represented by using sensitivity profilers which show the relationships and trends of a parameter. They are used to visualize the design space and analyze how strongly a design variable affects a response dynamically. Figure 2.8 illustrates sensitivity profilers [15]. One advantage of surrogate modeling is that surrogate models can be used to obtain sensitivities to support the trade-off studies.

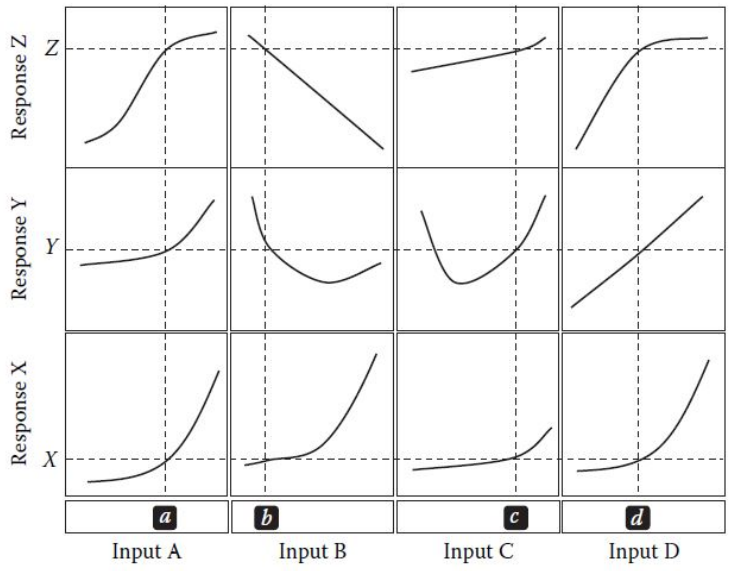

Figure 2.8: Sensitivity Profilers to Supoort Trade-Off Studies

2.4 Overview of the Recent Launch Vehicle Design Studies

2.4.1 Overview of the Design Space Exploration Studies

Design Space Exploration (DSE) methods allow a system designer to rapidly and accurately perform trade-off studies and analyze the feasibility of design space. This section examined some recent studies that were conducted to investigate the design space of a launch vehicle.

In [24], a methodology called RAPTOR was developed to explore the design space of launch vehicles. In this study, a physics-based approach using trajectory analysis was used. First, a control structure was selected to perform trajectory optimization. Next, a set of statistical methods were selected for performance evaluation where Some DOE and surrogate modeling methods were investigated. Sample applications that can be implemented using RAPTOR methodology were also stated, including design space exploration, system optimization, and payload contours. The DOE and surrogate modeling approach developed in RAPTOR may also be useful for the problem in this study. The study, however, only used continuous design variables, whereas the problem in this thesis includes discrete design variables such as the number of motors in each stage and the number of stages in the vehicle.

In [23], a methodology was developed to explore the architecture trades for launch vehicles. Using historical ideal ΔV data of heavy launch vehicles, an empirical modeling approach was employed. In this study, T/W was selected as the lone regressor. Moreover, probabilistic analysis was used for decision-making under uncertainty. A specific in-house high fidelity and multidisciplinary sizing environment were used for sizing the vehicles. Unless some historical data for small vehicles can be found, the empirical modeling approach developed in that study cannot be applied to the problem in this thesis.

In [18], the existing toolset was integrated and automated to enable a design space exploration of an Earth to orbit launch vehicle. The design space of an example problem

was then explored using RSE and DOE. After the surrogate models were obtained, k-fold cross-validation was implemented to check the goodness of fits. R^2, percent error of the surrogate model across the entire data set, actual-by-predicted, residual by predicted plots were also used to check the models. The sensitivity profilers were used to visualize the sensitivities and identify regions of interest. The number of engines, thrust per engine, engine ISP, oxidizer to fuel ratio, oxidizer tank cylinder length, max g, and max dynamic pressure were among the design variables. The payload delivered to orbit was the only response. An industrial software (POST v2) was used to optimize the trajectory.

In [35], a three-staged solid propulsion-powered vehicle with a payload capacity of 500 kg was investigated. The target orbit was a 500-kilometer circular orbit. To approximate and replace computationally expensive trajectory analysis, a feed-forward Neural Networks method was used. Latin Hypercube sampling was used to obtain the data points. The final velocity, height, and maximum normal overload were among the responses chosen. Grain shape parameters, flight trajectory parameters, and geometric parameters were included as design variables. A three-dimensional trajectory analysis was used in this study. The trajectory was optimized using the Particle Swarm Optimization (PSO) algorithm after the surrogate models were obtained, with the total gross weight of the vehicle being minimized.

2.4.2 Overview of the Hybrid-Powered Launch Vehicle Design Studies

In [59], a methodology for exploring design space was developed for the conceptual design of a vertically launched hybrid rocket. The study included the development of a swirling-oxidizer hybrid rocket engine with a single cylindrical grain port and the use of polypropylene as a fuel. Primary disciplines included propulsion, structural weight, trajectory, and aerodynamics. The vehicle's performance was estimated using a variety of responses, including flight altitude and gross weight. The study used a Multi-Objective Genetic Algorithm to solve the problem of multi-objective design. Two objective functions were considered: one that maximized flight altitude and another that minimized gross weight

where there was trade-off between these objectives. The rocket was assumed to have a point mass. The zero-lift aerodynamics analysis was based on the historical flight data of a similar rocket developed by Japan Aerospace Exploration Agency (JAXA). The design variables were mass flow oxidizer, fuel length, port radius of fuel, combustion time, combustion chamber pressure, and nozzle aperture ratio. To perform design trade-off studies, the design space was visualized using a scatter plot of non-dominated solutions.

In [60], a multi-island genetic algorithm (MIGA) was used to optimize a hybrid suborbital vehicle. The trajectory was evaluated using a 2 DOF trajectory simulation. Different gain types were explored, including star port, single circle port, wheel port, and multi-tube, in order to conduct a parametric analysis on the relationships between propellant combinations, design variables, and vehicle performance. Hydrogen peroxide and Hydroxyl-Terminated PolyButadiene (HTPB) propellant mixture was used in this study.

In [14], the smallest mass configurations of multistage hybrid rocket-propelled launch vehicles with various feed systems and propellant combinations were studied. A framework for multidisciplinary design and optimization studies of single-stage suborbital flight vehicles and two-stage-to-orbit flight vehicles powered by hybrid rocket motors has been developed. Different vehicle masses and feed system/propellant configurations were compared in terms of relative performance (payload fraction capability). A liquid oxygen and paraffin-wax-based launcher was observed to be the smallest feasible orbital launch vehicle.

In [12], the three-stage orbital vehicle concept of a private company was summarized. This small launch vehicle included eleven hybrid motors (seven motors in the first stage, and four in the second stage). The 75 kN hybrid motors used liquid oxygen and paraffin-based fuel. A cylindrical grain geometry with a single port was selected. To increase the payload capacity, a gas generator and turbo pump were used.

In [61], two phases of design informatics were used to create a single-stage launch vehicle powered by a hybrid motor: optimization and data mining. Evolutionary hybrid com-

putation, which combines a differential evaluation algorithm and a genetic algorithm, was used to perform multidisciplinary design optimization and data mining. A self-organizing map was used as a data mining method. Atmospheric effects were not taken into account during the trajectory analysis. Additionally, the disciplines of propulsion, weight, and aerodynamics were included. Aerodynamics was based on historical data of a similar rocket. Polypropylene was used as the solid fuel and liquid oxygen as the liquid oxidizer. The design variables included the initial mass flow of oxidizer, the fuel length, the initial radius of port, the combustion time, the initial pressure in combustion chamber, the aperture ratio of nozzle, and the elevation at launch time. As a result, design information was gathered regarding trade-offs and the behavior of design variables.

2.5 First Principles Approach vs Using Available Industrial Software in Conceptual Design Phase

In practice, the construction of a modeling and simulation environment is heavily reliant on the software and methodology that a designer is familiar with. If a system designer has reliable software to model any of these disciplines, it may be a time-efficient approach to utilize it because designing and validating one software from beginning can be a time-consuming procedure. However, there are some drawbacks of utilizing industrial software. First , some of these software have high fidelity and take a long time to execute. Furthermore, due to epistemic uncertainties resulting from a lack of knowledge about a system, it may not be very efficient to execute these computationally expensive software during the CDP. Next, specialized software in a company may be calibrated over time for specific missions or architectures. As a result, they may be insufficient for new missions or advanced vehicles. Finally, the inner workings of such software are mostly unknown [15]. As a result, understanding how the code works and the assumptions that this software employs may be difficult.

The first-principles approach is an alternative to using industrial software during the

CDP. First-principles are fundamental physics laws, fundamental theories, or relationships that are well known and acknowledged as correct by engineers. Using first principles provides the benefit of being aware of the assumptions to be employed, understanding how a code works, and making any adjustments to mission and vehicle architecture. With this approach, any fidelity level can be used to code an environment. A parametric and integrated environment can be built using a first-principles approach, which is advantageous for multidisciplinary problems.

2.6 Observations

- There are some problems with trajectory optimization, both in terms of processing cost and accuracy. Trajectory optimization becomes extremely expensive when a global optimization method is used. When a local optimization method is used, the solution may get stuck in a local optimum, resulting in an inaccurate evaluation of performance.

- By combining a low-fidelity trajectory simulation and a constant controller design, the conceptual design trade-off process can be accelerated.

- The problem stated in this thesis has a wide variability due to the architectural design variables. Additionally, this thesis requires a preconceptual, rapid turnaround study from an architecting perspective.

- Using legacy software has some drawbacks, such as long run-times due to high fidelity, code nontransparency, and inflexibility for new types of architectures and missions.

- Following a first principles approach can enable the construction of a parametric and integrated environment capable of modeling new types of missions and architectures.

- Sensitivity information is highly useful for exploring the design space and conducting trade-off analyses.
- DOE and Surrogate modeling are two important advanced design methods that can assist in speeding the design trade-off process in this study.

2.7 Overarching Hypothesis

Based on the observations, the following overarching hypothesis was stated. In the next chapter, the methods to test this overarching hypothesis were investigated and developed.

Overarching Hypothesis:

Following a first-principles approach for constructing a multidisciplinary M&S, using a constant controller design in trajectory analysis, and obtaining sensitivities will enable a rapid conceptual design trade-off study for a small LV with hybrid rocket propulsion.

CHAPTER 3
PROPOSED METHODOLOGY

The overarching hypothesis was stated as follows in the previous chapter:

> **Following a first-principles approach for constructing a multidisciplinary M&S, using a constant controller design in trajectory analysis, and obtaining sensitivities will enable a rapid conceptual design trade-off study for a small LV with hybrid rocket propulsion.**

The methods for achieving this overarching hypothesis were developed in this chapter. This hypothesis was broken down into three smaller problems, which were solved in the thesis's remaining sections. The three objectives goals of this chapter were stated as follows:

- Discussing which models to use in building the multidisciplinary M&S environment
- Investigating methods for obtaining sensitivities
- Investigating how to conduct a design trade-off study using a constant controller design in trajectory analysis

3.1 Construction of a Physics-Based Modeling and Simulation Environment

For this problem, propulsion, trajectory, aerodynamics, and weight were the primary disciplines to be modeled for some reasons. First, propulsion was an essential discipline in this problem since the feasibility of a launch vehicle design is highly dependent on the hybrid motor performance. Next, trajectory analysis was crucial for this study since it is the physics-based bridge between launch vehicle design and vehicle performance [24]. Since simple models such as Ideal Rocket Equation are not accurate enough to evaluate

the vehicle performance as discussed in the previous section, a physics-based trajectory analysis was required for this problem. Moreover, as the number of hybrid motors in each stage and the number of stages in a vehicle vary, the dimensions and flight characteristics of a vehicle substantially vary. Therefore, aerodynamics modeling was also crucial in this study. Finally, weight discipline is required for any launch vehicle design study. The weight discipline was represented at a very high level by using the PMF design variable. Other disciplines were regarded secondary for this study and thus not modeled in the environment.

The previous chapter stated that applying a first principles approach to this problem has numerous advantages. As a result, the following subsections discussed several first-principles approaches that have been proposed in the literature.

3.1.1 Review of Aerodynamics Modeling Approaches

There are various available analytic models in literature with varying levels of detail and accuracy. Also, these models include subsonic, transonic, supersonic, and hypersonic flight regimes. These models are based on theoretical (such as Slender-body theory), empirical and semi-empirical methods. It is possible to calculate the drag and lift coefficient, the center of pressure, and normal forces for body alone or bodies with wings and aerodynamic control surfaces with these analytic models. Some of these commonly used aerodynamic models can be found in [41], [42], [43], [44], [45].

A candidate model was identified through a literature search using an analytic model from a recent study [62]. This model was developed using a hybrid approach that incorporates components of the models presented in in [41], [44], [43]. The model calculates the drag coefficient for a SLV with various dimensions, body transitions, and fairing shapes. This model was validated in the same research by comparing the results to those of a CFD analysis (conducted with Ansys-Fluent), and the modeling error was found to be minor [62]. The main assumptions of this model can be summarized as follows;

- The angle of attack was kept zero by the attitude control system during all the phases of the mission profile,
- The vehicle did not have any control surfaces and possessed thrust vector capability,
- The vehicle did not have a wing which is the main source for lift generation. As a result, lift coefficient of the vehicle was assumed to be negligible,
- The main source of interference drag was assumed to be the integration of any boosters. As a result, for a launch vehicle without boosters, this component of drag was neglected.

Before determining whether to utilize this model, these assumptions must have been aligned with those of this thesis study. Therefore, these assumptions were discussed first. The angle of attack is typically maximum during a pitch over maneuver for a conventional launch vehicle with a typical ascent profile. This maximum angle of attack is typically small to minimize the vehicle's aerodynamic loads during atmospheric flight. Indeed, the angle of attack is close to zero for the majority of a launch vehicle's typical mission profile. As a result, the first assumption was reasonable. Following that, the vehicle concept used in this study was planned to be a vehicle without a wing, control surfaces, or boosters in order to keep the design as simple as possible in order to reduce any additional cost and complexity. As a result, the remaining assumptions of [62] were also evaluated to ensure that they were compatible with the overall design approach used in the thesis. If any of these assumptions were relaxed, an approach to aerodynamic modeling that is more rigorous would be used.

A sample vehicle design is illustrated in Figure 3.1, along with the steps for calculating the drag coefficient components. The main components of this vehicle were fairing, three stages, and three interstages. With this aerodynamics modeling approach, the individual drag coefficient for each component can be calculated by following the steps illustrated in

the same figure. Subsequently, the total drag coefficient for the vehicle can be calculated with Equation 3.1;

$$C_{D_{Launcher}} = \sum_{n=1}^{N} \frac{A_i C_{D_i}}{A_{ref}} \tag{3.1}$$

In this equation;

C_{D_i}: Individual component drag coefficient

A_{ref}: Reference area (maximum frontal area)

A_i: Local reference area

For each geometric component i, drag coefficient can be calculated by summing up skin friction drag coefficient, base drag coefficient, and body pressure drag coefficient as formulated in Equation 3.2:

$$C_{d_i} = C_{d_f} + C_{d_b} + C_{d_p} \tag{3.2}$$

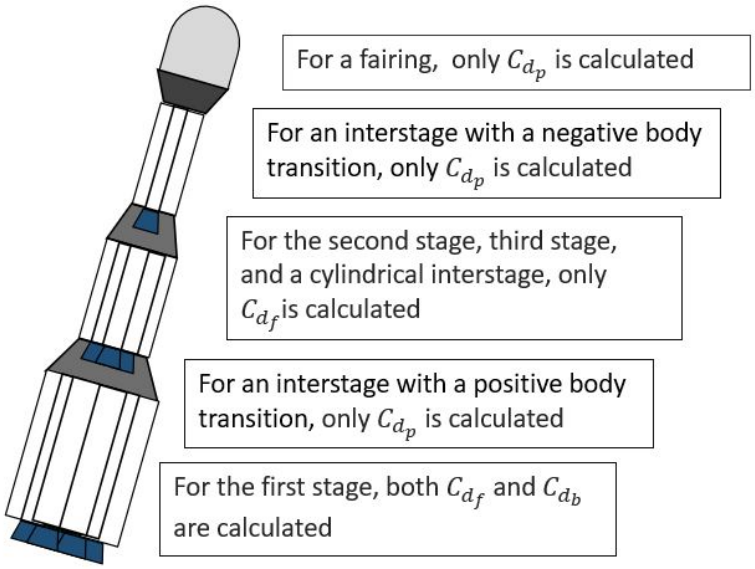

Figure 3.1: Drag Coefficient Modeling Steps

For many reasons, this model was considered advantageous for this thesis research. First, it allowed comparing different architectures since it models the drag coefficient for

every component of a launch vehicle separately. For instance, the drag coefficient of a two-stage or three-stage vehicle can be both calculated with this method.

The second benefit of this model is that it can be used to calculate the drag coefficient for a variety of fairing geometries, including conical, tangent ogive, secant ogive, L-D Haack, L-V Haack which were shown in Figure 3.2 [63]. As a result, this modeling method allowed for the selection of a fairing geometry with a low drag coefficient and a volume large enough to accommodate the payload.

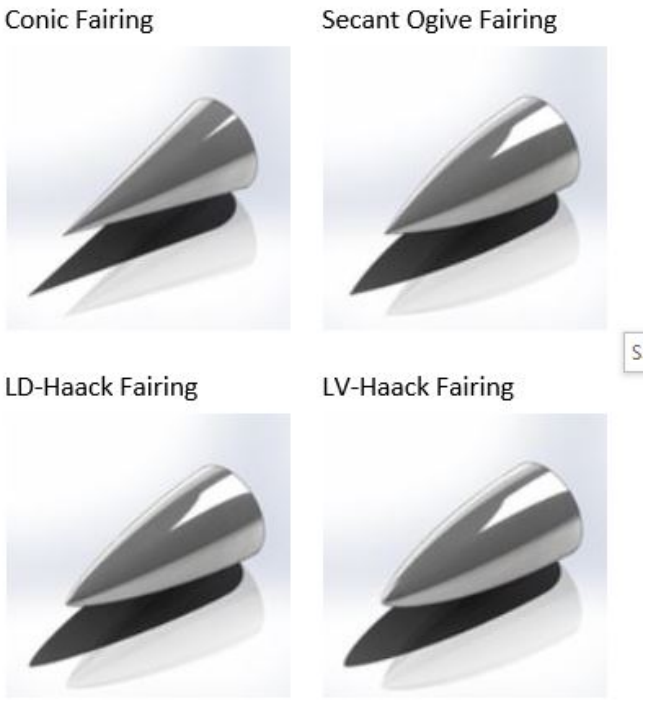

Figure 3.2: Fairing Shapes

Next, the model also calculates drag coefficient for interstages with various shapes such as cylindrical, positive and negative body transitions as shown in Figure 3.3. Since the number of motors was a design variable in this study, the diameters of stages would substantially vary for every vehicle design. As a result, an interstage may take on any of these forms. Having the capability to calculate the drag coefficient for each of these body transitions can help for a more accurate aerodynamics analysis for the vehicle. For this reason, this model was evaluated to be a suitable model for this study. The details of this

aerodynamics model were shared in Appendix A.

Figure 3.3: Interstage Shapes (Positive Transition, Negative Transition and Cylindirical respectively)

3.1.2 Review of Hybrid Propulsion Modeling Approaches

In this part, some hybrid propulsion modeling approaches were reviewed. The first candidate modeling approach was based on [40] where some surrogate models were developed by using a physics-based propulsion design software for evaluation of the performances of hybrid motors. Some examples of these surrogate models were shown in Figure 3.4 [40]. The surrogate models included commonly used fuels such as HTPB and Paraffin among others as well as various oxidizers. A wide range of values for the design variables was used such as Chamber Pressure = [2MPA, 12MPa] and Nozzle Area Expansion Ratio = [5, 200] to obtain these surrogate models. Although these models were shown to accurately approximate the actual performance results obtained using a physics-based tool for the predefined ranges in the same source; not all the assumptions used to produce these surrogate models were shared. As a result, the assumptions underlying these surrogate models cannot be checked for consistency with the problem's propulsion assumptions. Additionally, these models are incapable of providing a physical interpretation, which may be necessary during a vehicle design trade-off study.

Another model was presented in [7] with semi-empirical relationships derived from the hybrid combustion theory. Therefore, it used a first-principles approach for hybrid motor performance evaluation. This systematic approach can provide some insight into

$$
\begin{aligned}
&\text{O}_2/\text{HTPB:} \begin{cases} Isp_v = 277.33 + 2.17\log p_c + 18.49\log\epsilon \\ c^* = 1751.93 + 17.40\log p_c - 9.45\log\epsilon \\ O/F = 1.93 + 0.05\log p_c + 0.11\log\epsilon \end{cases} \\
&\text{O}_2/\text{Paraffin:} \begin{cases} Isp_v = 283.02 + 2.33\log p_c + 18.59\log\epsilon \\ c^* = 1787.97 + 16.72\log p_c - 9.54\log\epsilon \\ O/F = 2.24 + 0.05\log p_c + 0.12\log\epsilon \end{cases} \\
&\text{N}_2\text{O}/\text{HTPB:} \begin{cases} Isp_v = 251.96 + 1.09\log p_c + 13.57\log\epsilon \\ c^* = 1769.52 + 12.13\log p_c - 8.03\log\epsilon \\ O/F = 6.22 + 0.09\log p_c + 0.44\log\epsilon \end{cases}
\end{aligned}
$$

Figure 3.4: Some Examples of Surrogate Models

the physics of the problem during the trade-off studies of hybrid motor performance. In this analytic model, the simplified version of the fuel regression rate equation was used. Equation 3.3 combined the effects of axial combustion port location, blowing coefficient, fuel density, and gas viscosity in a parameter denoted by "a". The empirical relationships provided in the literature for various propellant combinations can be used to calculate a and n. Some values for these constants were shown in Table 3.1 [64].

The simplified form of the fuel regression rate equation was provided in Equation 3.3:

$$\dot{r} = a(G_0)^n \tag{3.3}$$

where,

G_0: Oxidizer mass velocity (i.e., the oxidizer mass flow rate divided by the combustion port cross-sectional area)

a and n: Empirically fitted constants

One important aspect of hybrid propulsion that should be taken into consideration in this study is that it has a dynamic behavior due to varying mixture ratios. The dynamic equations were derived only for circular ports in [7]. In this model, the oxidizer flow rate

Table 3.1: Empirically Fitted Constants for Various Fuels and Liquid Oxidizer

Fuel	a	n
Paraffin, SP1A	0.488	0.62
HTPB, (Thiokol)	0.146	0.681
HDPE	0.132	0.498
Paraffin, FR5560 + 13 % Nano Al	0.145	0.775
Paraffin, FR4550	0.427	0.748

was constant and fuel flow rate varied with time. This behavior dynamically alters the total mass flow rate where these dynamic equations were provided in Equation 3.4, Equation 3.5 and Equation 3.6.

Instantaneous fuel flow rate:

$$\dot{m}_f(t) = 2\pi N \rho_f L a \Big(\frac{\dot{m}_0}{\pi N}\Big)^n \Big\{ a(2n+1)\Big(\frac{\dot{m}_0}{\pi N}\Big)^n t + (R_i)^{2n+1} \Big\}^{\frac{1-2n}{1+2n}} \tag{3.4}$$

Instantaneous mixture ratio:

$$\frac{\dot{m}_0}{\dot{m}_f}(t) = \frac{1}{2\rho_f L a}\Big(\frac{\dot{m}_0}{\pi N}\Big)^{1-n} \Big\{ a(2n+1)\Big(\frac{\dot{m}_0}{\pi N}\Big)^n t + (R_i)^{2n+1} \Big\}^{\frac{2n-1}{2n+1}} \tag{3.5}$$

Total fuel consumed:

$$m_f(t) = \pi N \rho_f L \Big[\Big\{ a(2n+1)\Big(\frac{\dot{m}_0}{\pi N}\Big)^n t + (R_i)^{2n+1} \Big\}^{\frac{2}{2n+1}} - R_i^2 \Big] \tag{3.6}$$

where,

R_i: Initial port radius

N : Number of combustion ports

$\dot{m}_0$: Oxidizer flow rate

$\dot{m}_f$: Fuel flow rate

ρ_f : Density of the fuel

L : Length of the fuel grain

t : Time

a and n : Empirically fitted constants

For simplicity, an average fuel flow rate approximation was used instead of the dynamic flow rate model. With this approximation, the average flow rate was calculated by following the steps provided in Equation 3.7, Equation 3.8, Equation 3.9;

Since $\dot{m}_{ox}$ is constant;

$$m_{ox} = \dot{m}_{ox} t_b \tag{3.7}$$

$$m_{prop} = m_{ox} + m_{fuel} \tag{3.8}$$

$$\dot{m}_{ave} = \frac{m_{prop}}{t_b} \tag{3.9}$$

where,

t_b : Total burn time of the hybrid motor

$\dot{m}_{ave}$: Average propellant flow rate

Another assumption used in this model was a constant specific heat ratio during the combustion process which directly affects the thrust coefficient. As the masses or mole fractions of combustion reactants and products change, Cp (specific heat capacity) of the mixture is expected to vary, resulting in varying specific heat ratio. Similarly, fuel density in Equation 3.4, Equation 3.5, Equation 3.6 was assumed to be constant. In the CDP, these assumptions may be acceptable for simplicity although they may not yield a correct analysis in further design phases. The calculation steps of this model were shown in Figure 3.5. More details of this model were provided in Appendix B.

The requirements and outputs of the hybrid propulsion model fed to trajectory analysis and aerodynamics were summarized in Figure 3.6.

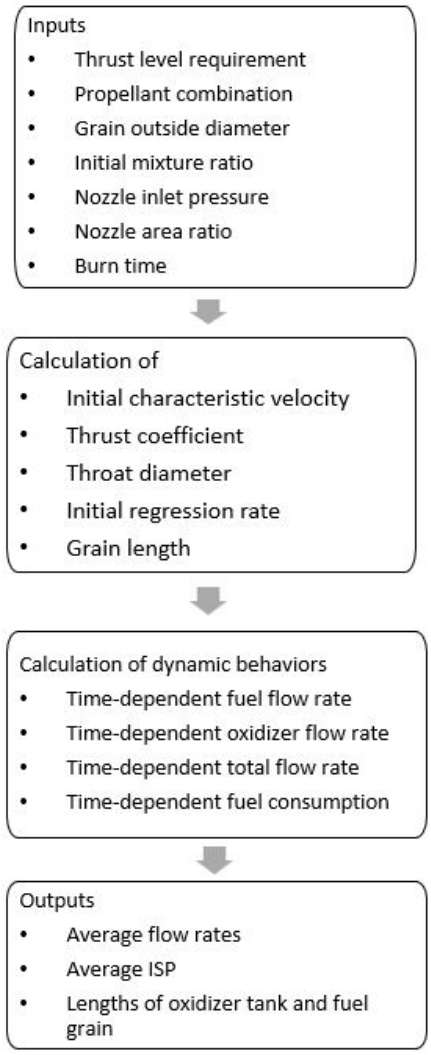

Figure 3.5: Hybrid Rocket Propulsion Modeling Steps

3.1.3 Review of Trajectory Analysis Tools

Trajectory analysis is composed of two elements: a trajectory simulation and a trajectory optimizer. It was stated in chapter 2 that using a low fidelity trajectory simulation with a constant controller design would speed up the trajectory analysis. Developing and validating a trajectory simulation is a time-consuming process that may not be necessary because people prefer to use industrial and reliable software. Roketsan (the sponsor company of these studies) owns a trajectory analysis software that includes both a simulation and an optimizer, which could be used in this study due to its availability. This software included

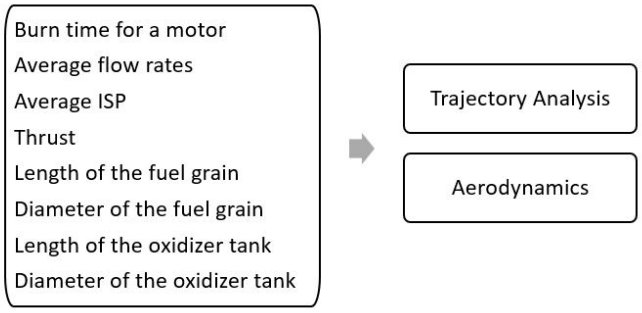

Figure 3.6: Outputs of Hybrid Propulsion Model

a 3 DOF trajectory simulation and a trajectory optimizer based on a genetic algorithm. This physics-based trajectory simulation used a first-principles approach that integrates equations of motion with the shooting method. Furthermore, it was not calibrated using historical data.

Following the selection of all methods and software, the physics-based modeling and simulation environment was built by integrating the aerodynamics model, the propulsion model, and the trajectory simulation. This environment's inputs and outputs were demonstrated in Figure 3.7.

3.2 Measures of Mission Performance Evaluation

The objective of this study was stated as "Develop a systematic methodology for conducting rapid conceptual design trade-off studies for an expendable small launch vehicle powered by hybrid rocket technology to determine the feasibility of an orbital launch from Earth to LEO." Therefore, a measure of $feasibility$ needs to be defined for this problem.

An orbital feasibility would necessitate an orbital injection with all orbital requirements met from the perspective of an orbital analyst. As a result, orbital injection necessitates detailed orbit design and analysis. However, the focus of this study was not on a detailed orbit design or analysis, but on developing a method to design some launch vehicles that could basically achieve the desired orbit. After reaching orbit, a small motor, such as a kick motor, can be used to locate the launch vehicle into a more desirable orbital position using

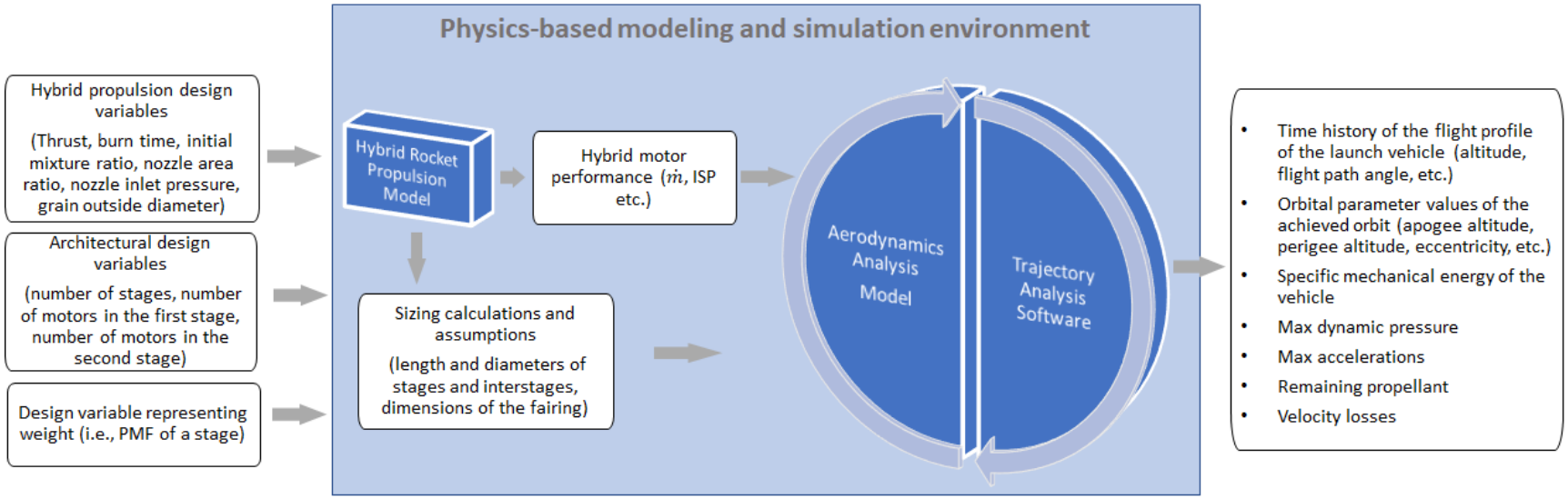

Figure 3.7: Summary of the Physics-Based Modeling and Simulation Environment

orbital maneuvers.

In orbital mechanics, an orbit can be defined by six classical orbital elements if inertial speed (V), altitude (h), and the zenith angle (γ) or flight path angle (ϕ) are known where these parameters can be calculated using trajectory analysis. These angles were defined in Figure 3.8 [65].

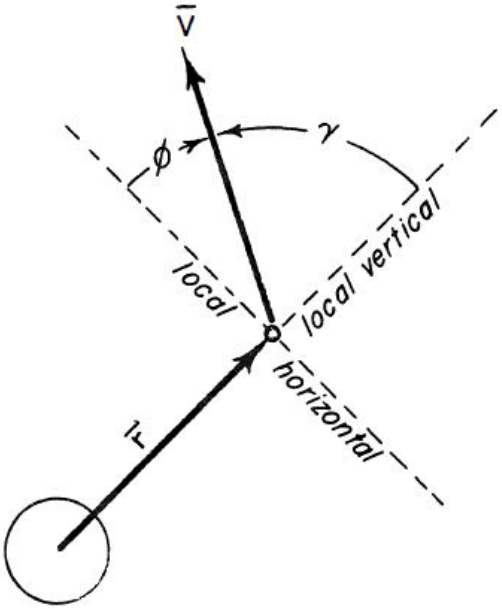

Figure 3.8: Flight Path Angle ϕ and Zenith Angle γ

The perigee and apogee altitudes of the reached orbits can be used to assess the feasibility of an orbital launch, as these parameters are generally high-level mission requirements. Specific mechanical energy can be another measure of feasibility. This energy is easily calculated by adding a vehicle's specific potential and specific kinetic energy. As a result, these measures may serve as a bridge between the mission feasibility evaluation and a more detailed orbital analysis, which will be carried out in later design phases. The altitude (h), speed (V), and flight path angle (ϕ) were used to calculate the apogee altitude, perigee altitude, and specific mechanical energy in the following equations [65].

The semi-major axis is calculated using the Vis-Viva equation with Equation 3.10:

$$V = \sqrt{\mu_{earth}(\frac{2}{r} - \frac{1}{a})} \tag{3.10}$$

The speed, position, and angle of the flight path are used to calculate angular momentum with Equation 3.11:

$$h = rVcos(\phi) \tag{3.11}$$

Angular momentum is used to calculate semilatus rectum with Equation 3.12;

$$p = \frac{h^2}{\mu_{earth}} \tag{3.12}$$

The semilatus rectum is used to calculate eccentricity with Equation 3.36;

$$p = a(1 - e^2) \tag{3.13}$$

The semi-major axis and eccentricity can be used to calculate apogee and perigee positions with Equation 3.14 and Equation 3.15;

$$r_a = a(1 + e) \tag{3.14}$$

$$r_p = a(1 - e) \tag{3.15}$$

Apogee and perigee altitudes can be calculated using the apogee and perigee positions with Equation 3.16 and Equation 3.17;

$$h_a = r_a - R_{Earth} \tag{3.16}$$

$$h_p = r_p - R_{Earth} \tag{3.17}$$

Finally, the specific mechanical energy of a vehicle can be calculated with Equation 3.18;

$$\epsilon = \frac{V^2}{2} - \frac{\mu_{Earth}}{r} \tag{3.18}$$

where,

r : Position in the inertial reference frame

V : Speed in the inertial reference frame

h : Specific angular momentum in the inertial reference frame

ϕ : Flight path angle

e : Eccentricity

a : Semi-major axis

p : Semilatus rectum

r_a : Apogee position

r_p : Perigee position

h_a : Apogee altitude

h_p : Perigee altitude

R_{Earth} : Radius of the Earth

μ_{Earth} : Gravitational parameter of the Earth

ϵ : Specific mechanical energy

Because the feasibility of an orbital launch is determined by vehicle performance as measured by h, V, and ϕ in these equations, the level of accuracy that trajectory analysis can provide in terms of these parameters is critical, as the accuracy in calculating these parameters is heavily influenced by the performance of a trajectory simulation (e.g. steady state errors of the controllers used in trajectory simulation, etc.).

3.3 Surrogate Modeling of the Modeling and Simulation Environment

The physics-based integrated environment in the previous section was built using an aerodynamics modeling approach, a hybrid rocket propulsion modeling approach, and trajectory analysis software. The following were some observations about the run time for this environment:

- The aerodynamics model was comprised of a number of semi-empirical relationships that could be evaluated quickly.
- The hybrid rocket propulsion model included a semi-empirical relationship as well as analytic models that can be quickly evaluated.
- The time required for a trajectory simulation was highly dependent on the software.

The time required to run a trajectory simulation is dependent on the complexity of the simulation, such as the degree of freedom involved, the complexity of the autopilots, etc. DOE and surrogate modeling methods were key enablers for speeding up analysis, as summarized in chapter 1. Surrogate models also allow obtaining the sensitivities easily. As a result, the surrogate modeling approach was a great fit for this problem, as it allows for faster analysis and provides a mechanism for obtaining sensitivity information.

Surrogate models are used to mimic a computationally expensive code. There are two steps to creating a surrogate model. First, some data are gathered using real code, with DOE methods widely used to obtain these data. The second step is to use these data to fit a regression model [21]. With this idea, the following research question was stated:

Research Question 1.
To approximate the modeling and simulation environment, which DOE method and surrogate modeling method should be used?

First, some DOE types were considered in order to obtain some sample data in the following section. Following that, some regression techniques were evaluated.

Some important factors to consider when selecting DOE were as follows [17];

- Number of design variables
- Run-times of analysis software
- Accuracy desired

For this study, the number of design variables was ten, as these variables were identified in the previous section. Due to the relatively long run-time of trajectory simulation compared to aerodynamics and propulsion models, the run-time of the code developed was expected to be medium. At some level, accuracy was desired, but very high accuracy is not usually the primary goal of conceptual studies. Based on these observations, Table 3.2 compared several DOE methods.

Table 3.2: Comparison of some DOE Methods

Criteria	Central Composite	Box-Behnken	Full Factorial	Space Filling
Includes interior points	◯	X	X	✓
Includes corner points	✓	✓	✓	◯
Orthogonality	✓	✓	✓	X
Number of runs required	medium	medium	high	medium

Classical DoE methods, such as Full factorial, Box-Behnken, and Central Composite, generate points at the extremes [17]. Because they can cover the interior space well, Space Filling DOE designs are better suited for computer codes. A space-filling DOE, on the other hand, typically does not adequately cover the corner points. A hybrid approach that combines two different DOE methods is also an option. As a result, a Space Filling DOE was combined with a DOE that covers the corner points.

There are numerous types of the space filling DOE, and seven different options to space filling design were considered, as listed below. Given that this problem involved some discrete variables (i.e., the number of motors and stages), the method chosen must be capable of dealing with them. Only the fast flexible filling design is capable of handling discrete variables with an any number of levels.

- Sphere-Packing Designs
- Latin Hypercube Designs
- Uniform Designs
- Minimum Potential Designs
- Maximum Entropy Designs
- Gaussian Process IMSE Optimal Designs
- Fast Flexible Filling Designs

In Fast Flexible Filling Design, the large number of randomly generated points is clustered into several clusters equal to the designer-specified number of runs using a Fast Ward algorithm. Several criteria are used to obtain the final design points [66].

To cover the corner points, a full factorial DOE can be used. However, if four or more levels are used with full factorial, the number of cases for ten design variables becomes unmanageable. As a result, a three-level full factorial DOE was combined with the Fast Flexible Filling DOE.

The second part was the selection of a surrogate modeling technique. Two very commonly used methods are RSE and ANN. These methods were expected to be suitable for this problem since they were used for similar problems [23],[24]. These methods were compared in Table 3.3.

Table 3.3: Comparison of Surrogate Modeling Techniques

Criteria	RSE	ANN
Suitability for highly nonlinear problems	X	✓
Number of points needed	low	high
Simplicity	✓	◯
Suitability to high-dimensions	X	✓

For a variety of reasons, the modeling and simulation code for this problem is extremely nonlinear. The nonlinearity is caused by a number of factors, including controller saturation, discontinuities or jumps during stage separation, and equations of motion that are inherently nonlinear. Additionally, some discrete design variables were incorporated, resulting in data with discontinuities. As a result, it was determined that ANN method was a better candidate for this problem due to its ability to deal with nonlinearities of this nature.

Based on this evaluation, the following hypothesis was stated:

Hypothesis 1.

A hybrid DOE composed of a Fast Flexible Filling & a Full Factorial DOE combined with Artificial Neural Networks will provide an effective method for approximating the M&S environment.

Some measures such as R-Squared, model fit error, model representation rrror, actual by predicted plot, residual by predicted plot were used in the next chapter to test the goodness of the fits obtained with the selected approach.

3.4 Specific Mechanical Energy Based Design Trade-Off Method

The overarching hypothesis stated that by employing a constant controller design, the trajectory analysis should speed up. However, if the trajectory is not optimized, a constant controller design will not result in a target orbit. For instance, in Figure 3.9, an optimized trajectory was plotted alongside a trajectory obtained using a constant controller design. In this case, the vehicle with the constant controller design reached an altitude of 280 km before continuing to fall back to earth rather than approaching the target orbit. This was expected because the vehicle with the constant controller design did not take the most efficient trajectory, whereas the vehicle with an optimized trajectory was able to reach the target orbit while minimizing energy losses. As a result, determining the actual performance of a vehicle with a constant controller was challenging.

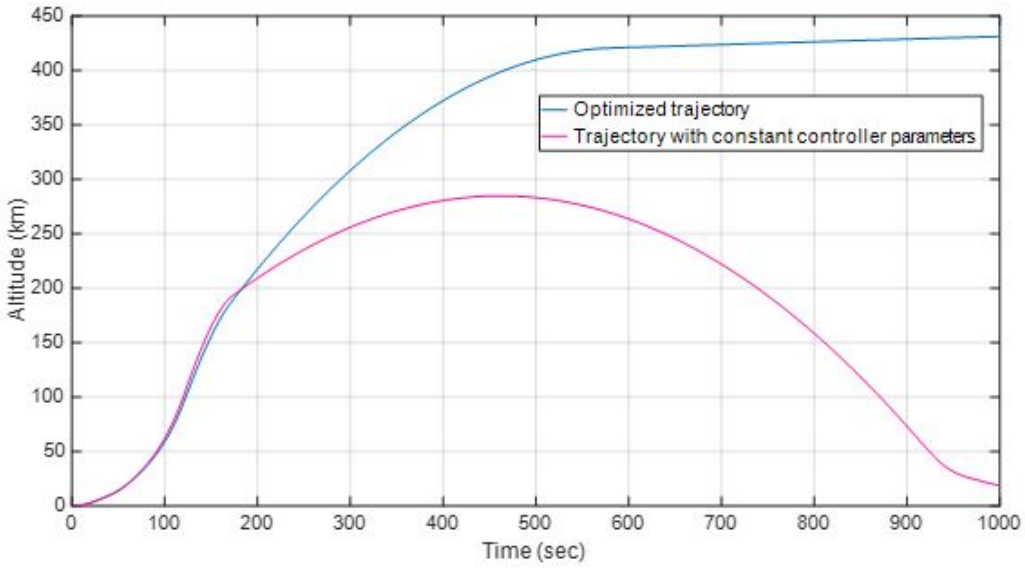

Figure 3.9: Optimized Trajectory and Unoptimized Trajectory

Since vehicle design trade-off studies are conducted based on an evaluation of the vehicle's performance, the following research question was posed in order to investigate how to conduct a trade-off study using a constant controller design.:

Research Question 2. Without performing trajectory optimization during the conceptual design phase, how can a trajectory-based vehicle design trade-off be performed?

As a starting point for the discussion, the specific mechanical energy for the optimized trajectory was plotted in Figure 3.10. This mission included a coast phase although some launch vehicles' mission profiles do not have a coast phase. The atmosphere was accepted to end at 100 km [67]. Therefore, drag was assumed to vanish above 100 km. Additionally, because thrust was not created during the coast phase and orbital motion, the specific mechanical energy, computed using Equation 3.19, was conserved throughout these phases, as illustrated in Figure 3.10. At the end of the restart phase, the vehicle achieved a specific mechanical energy that was exactly equal to the target orbit's specific energy requirement.

$$\epsilon = \frac{v^2}{2} - \frac{\mu}{r} = -\frac{\mu}{2a} \tag{3.19}$$

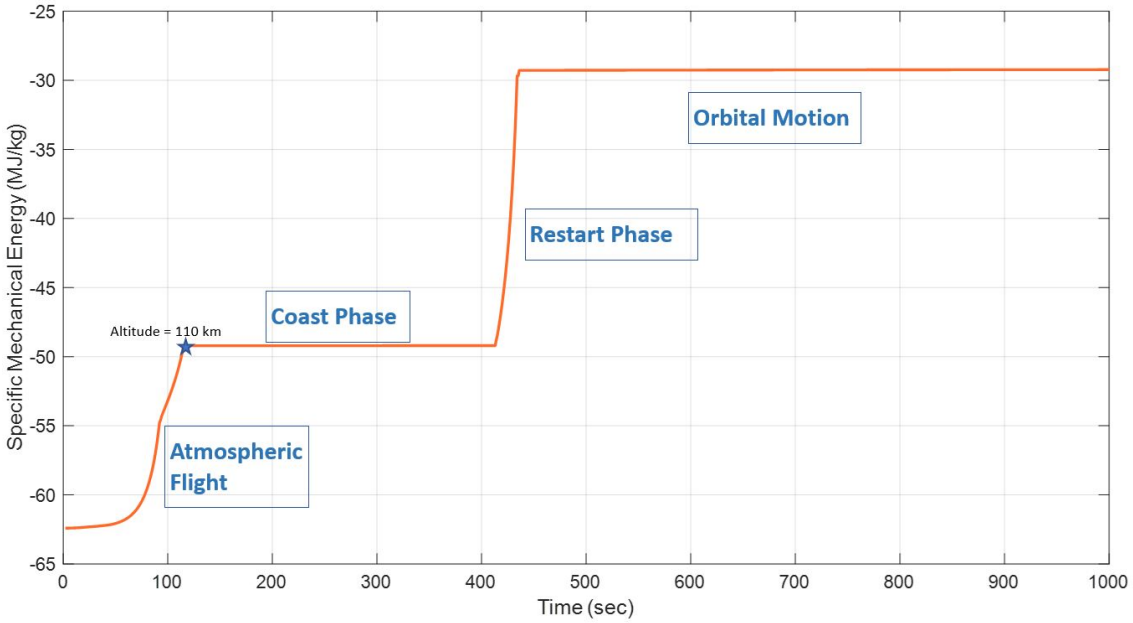

Figure 3.10: Specific Mechanical Energy Plot for the Optimized Trajectory

As a hypothetical situation, assume that a vehicle with a constant controller design consumes all its fuel at 100 km altitude and has a specific mechanical energy of ϵ_0 at this altitude, which is exactly equal to the specific mechanical energy requirement of the target orbit. If the trajectory of this vehicle was optimized, the energy losses would be reduced, therefore it is expected that this vehicle has a specific mechanical energy provided in Equation 3.20 when the fuel is consumed;

$$\hat{\epsilon} = \epsilon_0 + \delta_\epsilon \tag{3.20}$$

where;

$$\delta_\epsilon \geq 0 \tag{3.21}$$

This hypothetical situation demonstrates a critical observation. With some carefully optimized control variable settings, this vehicle will have a chance of reaching the target orbit, as its specific mechanical energy will be greater than the target orbit's specific mechanical energy requirement. Indeed, due to the extra energy δ_ϵ, the vehicle will have some propellant remaining when it reaches orbit. This discussion applies to any vehicle that reaches

an altitude greater than 100 kilometers and has a specific mechanical energy of ϵ_0 when it consumes all of its fuel.

Assume that such vehicles could be rapidly designed in the CDP. These vehicles can then be used as design candidates for further analysis and design. The following subsections examined the flight angle and maximum altitude constraints for these vehicles.

3.4.1 Flight Path Angle Constraint for Target Circular Orbits

The orbit that a vehicle attains when it has a specific mechanical energy ϵ_0 and has consumed all of its fuel above an altitude of 100 kilometers was named the "final orbit" and was illustrated in green ellipse in Figure 3.11. The target circular orbit was also shown with a blue circle in the same figure. By orbital mechanics, the final orbit must have an apogee altitude greater than the target altitude of the circular orbit in order to have the same specific mechanical energy requirement as the target circular orbit.

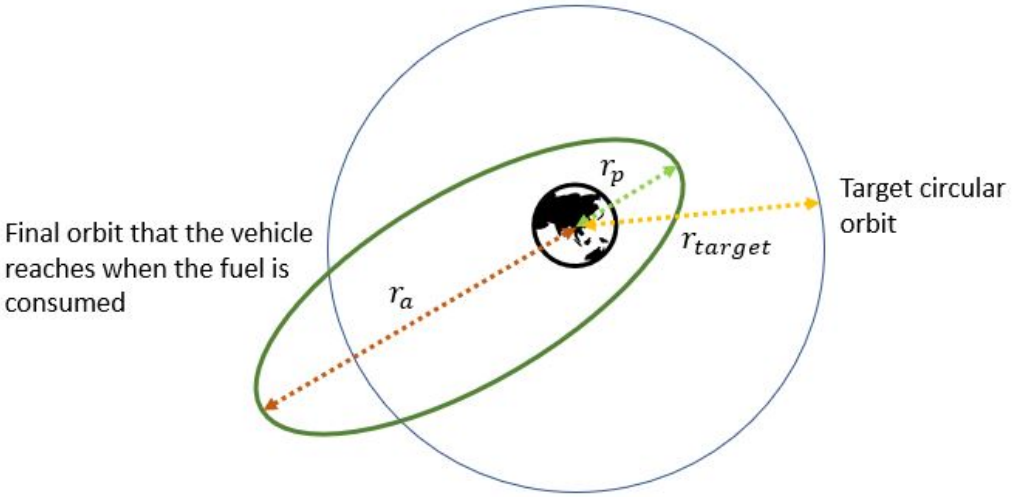

Figure 3.11: Final and Target Orbits

The vehicle must not only meet the specific mechanical energy requirement, but also a flight path angle, in order to reach the final orbit. As a result, investigating the flight path angle constraint for such a vehicle was critical. Depending on the flight path angle ϕ, eccentricity values of the final orbit can be calculated with Equation 3.22 where the

derivation of this equation was given in Appendix D. In Figure 3.12, eccentricity values e_{final} were plotted with respect to h_{final} for various flight path angle (ϕ_{final}) values. The circular orbit had a target altitude h_{target} of 400 km in this plot. The only way to obtain an eccentricity value of zero at h_{target} was to have a flight path angle zero as it was observed from this plot.

$$e_{final} = \sqrt{1 - \frac{(R_{Earth} + h_{final})(R_{Earth} + 2h_{target} - h_{final})}{(R_{Earth} + h_{target})^2} sin^2(90^\circ - \phi_{final})} \quad (3.22)$$

where,

ϕ_{final} : Flight path angle at the final orbit

R_{Earth} : Radius of the Earth

h_{final} : Altitude of the vehicle at the final orbit

h_{target} : Altitude of the vehicle at the target orbit

e_{final} : Eccentricity of the final orbit

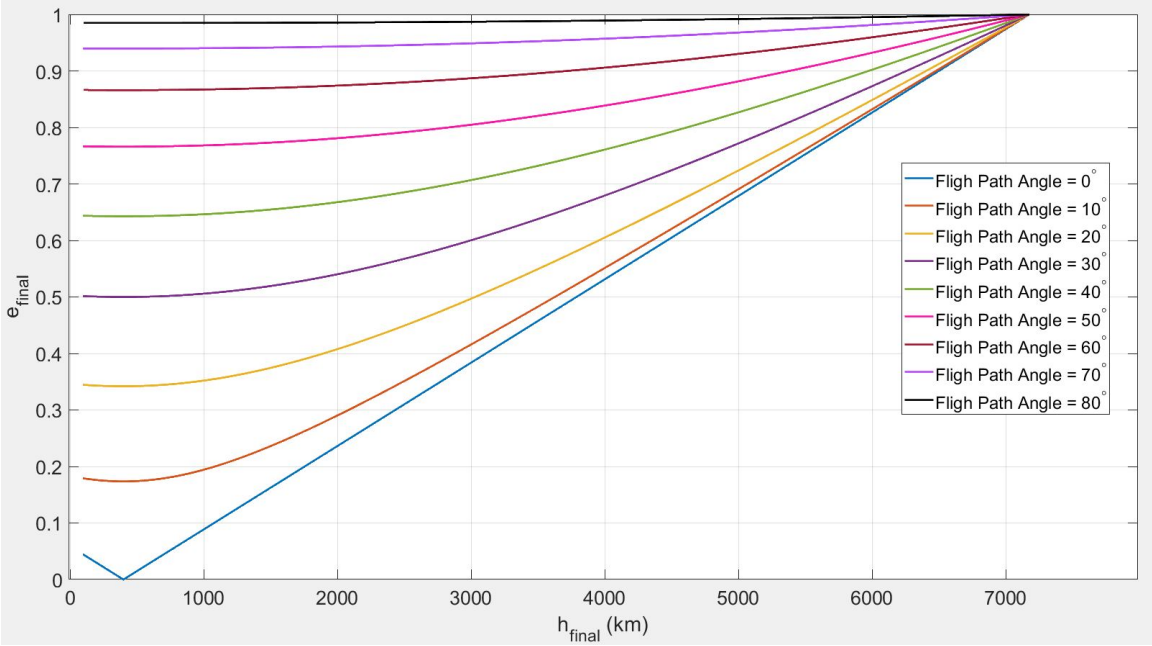

Figure 3.12: e_{final} vs h_{final}

The perigee and apogee altitudes can be calculated with Equation 3.23 and Equation 3.24 which were also derived in Appendix D. When the perigee and apogee altitudes for various flight path angles were plotted as shown in Figure 3.13 for a circular orbit of 400 km altitude, it was observed that the only way to obtain a closed circular orbit was to have flight path angle of zero. From this discussion, the conclusion was that the flight path angle when the fuel is consumed must be zero so that the final orbit and the target orbit have the same specific mechanical energy requirement.

$$h_{p,fin} = h_{targ} - \sqrt{(R_{Ear} + h_{targ})^2 - [(R_{Ear} + h_{fin})(R_{Ear} + 2h_{targ} - h_{fin})] sin^2(90^\circ - \phi_{fin})} \tag{3.23}$$

$$h_{a,fin} = h_{targ} + \sqrt{(R_{Ear} + h_{targ})^2 - [(R_{Ear} + h_{fin})(R_{Ear} + 2h_{targ} - h_{fin})] sin^2(90^\circ - \phi_{fin})} \tag{3.24}$$

where,

ϕ_{fin} : Flight path angle of the vehicle at the final orbit

R_{Ear} : Radius of the Earth

h_{fin} : Altitude of the vehicle at the final orbit

h_{targ} : Altitude of the vehicle at the target orbit

$h_{a,fin}$: Apogee altitude of the final orbit

$h_{p,fin}$: Perigee altitude of the final orbit

3.4.2 Maximum Altitude Constraint for Target Circular Orbits

The previous section stated that the vehicle must reach an altitude greater than 100 kilometers. As a result, 100 kilometers is the vehicle's minimum altitude requirement. This section also examined the maximum altitude requirement.

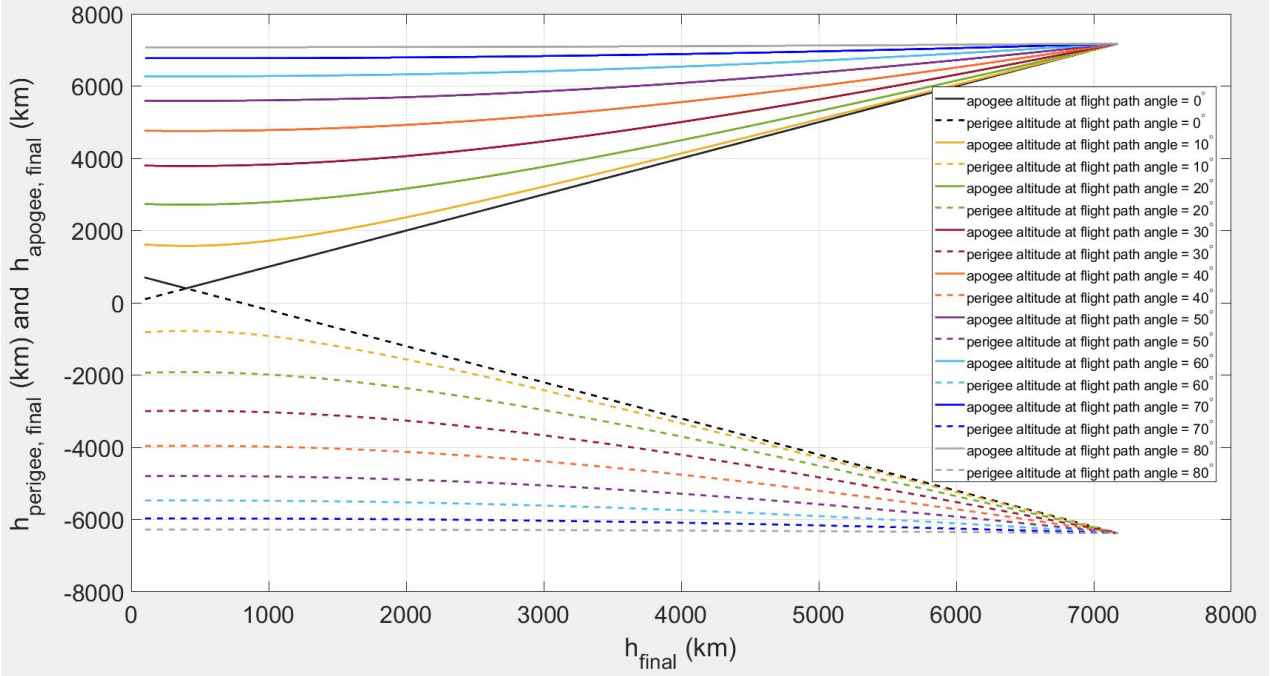

Figure 3.13: $h_{perigee,final}$ and $h_{apogee,final}$ vs h_{final}

The altitude at which V_{final} equals zero (and eccentricity equals one) can be calculated by equating $V_{final} = 0$ in Equation 3.25;

$$\epsilon = \frac{\mu_{Earth}}{2(R_{Earth} + h_{target})} = \frac{V^2}{2} - \frac{\mu_{Earth}}{R_{Earth} + h_{max,final}} = \frac{\mu_{Earth}}{R_{Earth} + h_{max,final}} \tag{3.25}$$

Using this equation, the maximum altitude was calculated as follows;

$$h_{max,final} = R_{Earth} + 2h_{target} \tag{3.26}$$

This is the maximum altitude which the vehicle should reach when the fuel is consumed. As a result, the vehicle should consume all fuel at an altitude between 100 km and $R_{earth} + 2h_{target}$. The speed of the vehicle at the final orbit can also be calculated with Equation 3.27. V_{final} was plotted in Figure 3.14 for the sample problem. The point which intersects the x axis illustrated the maximum altitude that this vehicle should reach. It was equal to h_{max} = 6378 km + 800 km = 7178 km for the sample problem where the target

orbit was a circular orbit with a 400 km altitude.

$$V_{final} = \sqrt{\mu_{Earth} \frac{R_{Earth} + 2h_{target} - h_{final}}{(R_{Earth} + 2h_{target})(R_{Earth} + h_{final})}} \tag{3.27}$$

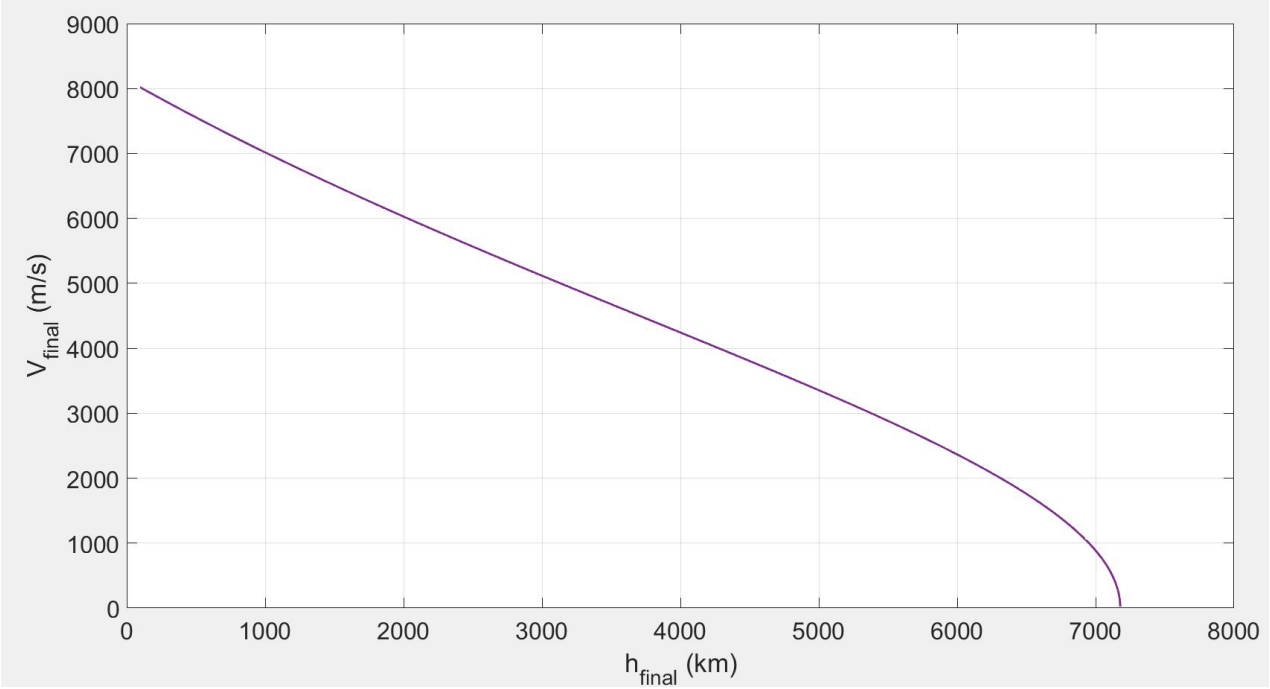

Figure 3.14: V_{final} vs h_{final}

3.4.3 Flight Path Angle and Maximum Altitude Constraints for Target Elliptical Orbits

The previous discussion was extended in this section to target elliptical orbits, where the flight path angle and maximum altitude constraints were investigated. For an elliptical orbit with a given h_p and h_a, the semi-major axis can be calculated with Equation 3.28.

$$a = R_{Earth} + 0.5(h_p + h_a) \tag{3.28}$$

The specific mechanical energy requirement of an elliptical orbit is equal to the specific mechanical energy requirement of a circular orbit with a semi-major axis a. Therefore, the equations Equation 3.22, Equation 3.23, Equation 3.24 that were derived in Appendix D

using the energy equation for circular orbits were valid for elliptical orbits as well. As a result, the zero path angle constraint was also valid for target elliptical orbits. In Figure 3.13, it was observed that any elliptic orbit can be obtained only with a flight path angle of zero.

The specific mechanical energy equation is used to calculate the semi-major axis which is given in Equation 3.30;

$$-\frac{\mu}{2a} = -\frac{\mu}{2(R_{earth} + h_{target})} = \frac{V_{final}^2}{2} - \frac{\mu}{(R_{earth} + h_{final})} \tag{3.29}$$

$$2a = 2(R_{earth} + h_{target}) \tag{3.30}$$

Equation 3.28 can then be used to replace semi-major axis parameter in Equation 3.30. Subsequently, Equation 3.31 is obtained;

$$h_a + h_p - h_{target} + R_{Earth} = 0 \tag{3.31}$$

Using this equation, three different scenarios were evaluated as follows;

1. If $100km \leq h_{final} \leq h_{target}$;

$$h_{final} = h_p \tag{3.32}$$

$$h_a = 2h_{target} - h_p = 2h_{target} - h_{final} \tag{3.33}$$

2. If $h_{final} = h_{target}$;

$$h_{final} = h_p = h_a = h_{target} \tag{3.34}$$

3. If $h_{target} < h_{final} < R_{Earth} + 2h_{target}$;

$$h_{final} = h_a \tag{3.35}$$

$$h_p = 2h_{target} - h_a \tag{3.36}$$

To summarize, for the target elliptical orbits, the vehicle should have a zero flight path angle and an altitude between 100 km and $h_{max} = h_a + h_p + R_{Earth} = R_{Earth} + 2h_{target}$.

3.4.4 Rapid Vehicle Design Using Specific Mechanical Energy

A rapid design trade-off method was developed in this section. The primary strategy was to fit surrogate models for final specific mechanical energy and final flight path angle, with data for fitting the surrogate models obtained by running the DOE cases in the integrated M&S environment. Subsequently, the sensitivity profilers obtained using these surrogate models can be used to design some vehicles which meet the constraints defined in the previous section.

To demonstrate the design trade-off approach, a scenario was created using the DOE and the cases were run in the M&S environment. The cases that reach an altitude of between 100 km and h_{max} when all the fuel was consumed were selected. The remaining cases were considered failed cases from this analysis's perspective, and thus were not used to fit surrogate models. A constant controller design was used for all cases. Some ANN models were fit using the data. The performance of these ANN models were discussed in the next chapter. Figure 3.15 shows the sensitivity profilers obtained using these ANN models for two responses; specific mechanical energy and flight path angle. A sample vehicle was designed by performing a trade-off study with these profilers. The selected design targeted the specific mechanical energy shown with a red box (ϵ_o = -29.4 MJ/kg for this orbit) and a zero-flight path angle shown in the blue box. As a result, this design was expected to have

a chance of reaching the target orbit, as discussed previously.

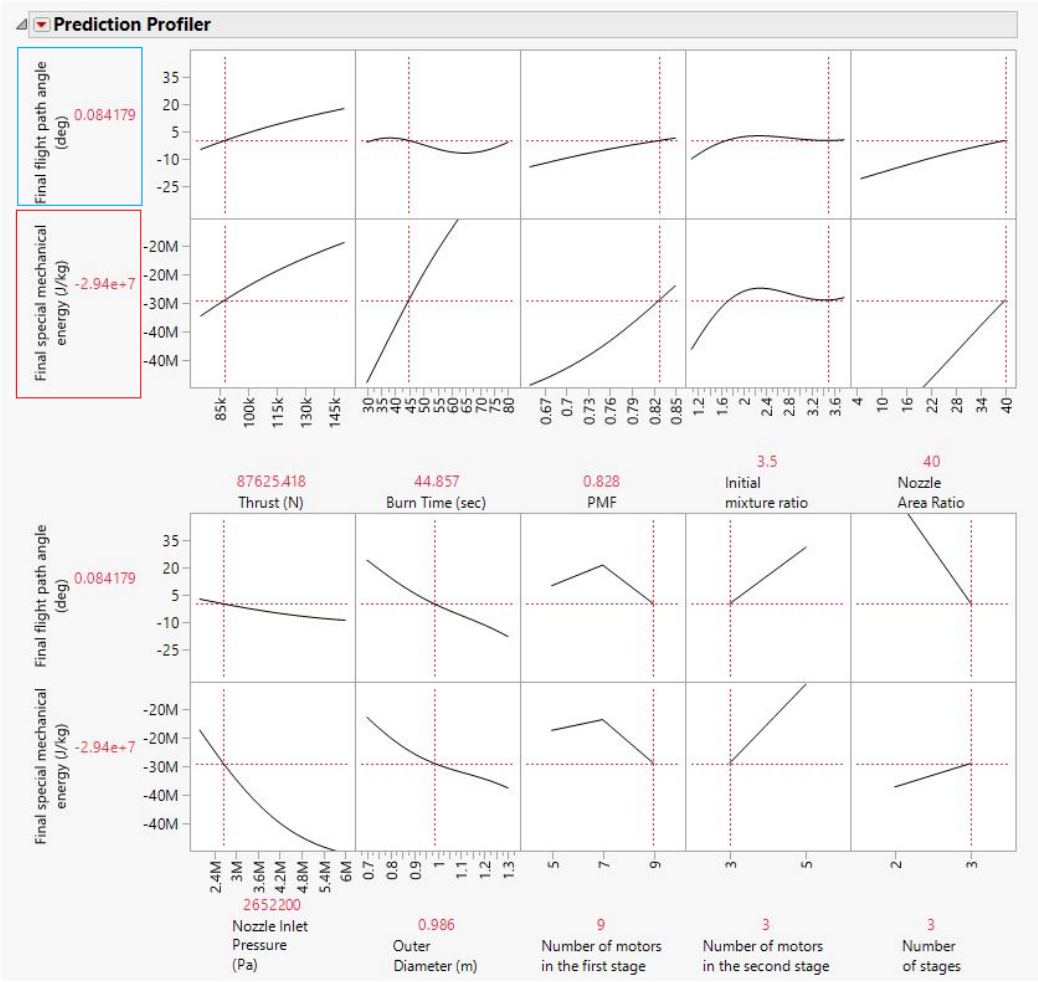

Figure 3.15: Vehicle Design Example Using Sensitivity Profilers

Because a surrogate model always has some training error, this vehicle cannot have a specific mechanical energy equal to the predicted energy if trajectory optimization is performed. As a result, the difference between the predicted specific mechanical energy value (-29.4 MJ/kg) and the "actual specific mechanical energy" value obtained through trajectory optimization had to be quantified.

The "actual specific mechanical energy" obtained through trajectory optimization was expressed in Equation 3.37. In this equation, $\delta_{training}$ represented the training error and δ_{opt} represented the specific mechanical energy savings to be obtained with trajectory optimization by minimizing energy losses. The former term, training error may result in an interval

[α,β] with unknown α and β such that; $\alpha, \beta \in R$. On the other hand, δ_{opt} would always be greater than zero due to energy savings. α value, in particular, would be of interest because it represents the lowest energy that this vehicle design can achieve. The closer the lowest energy is to the target energy ϵ_o, the closer the vehicle is to being a feasible design by making some minor design changes in subsequent design phases.

$$\epsilon = \epsilon_0 + \delta_{training} + \delta_{opt} \tag{3.37}$$

$$\delta_{opt} \geq 0 \tag{3.38}$$

$$\alpha \leq \delta_{training} \leq \beta \tag{3.39}$$

β, on the other hand, is of little interest to this study. For instance, a vehicle can be designed using the surrogate models for a circular orbit with 400 km altitude and it may end up reaching a circular orbit with 440 km altitude and -29.23 MJ/kg of specific mechanical energy when the trajectory optimization is conducted. This design is already feasible meeting and even exceeding the requirements. Such a vehicle can always be fine-tuned for a circular orbit with 400 km altitude with some propellant remaining. As a result, the lower bound on the training error is more critical for this study, and it will be estimated in the subsequent section.

3.4.5 Performance Estimation Using Prediction Interval Concept

One method to quantify the training error of ANN surrogate models was using prediction intervals. The prediction interval enables the prediction of a new observation with known probability using data from a sample [68]. A confidence interval, on the other hand, is a summary measure for a large population. Confidence intervals are used to estimate parameters such as a mean or a regression coefficient. A prediction interval is always wider than

a confidence interval. A distribution's prediction interval can be easily calculated using statistical analysis software.

After y % prediction interval [a,b] for the model fit error of specific mechanical energy is calculated, y % lower bound of the specific mechanical energy can be calculated as follows;

$$MFE_{\epsilon} = \frac{\epsilon_{min} - \epsilon_0}{\epsilon_{min}} = b \tag{3.40}$$

$$\epsilon_{min} - \epsilon_0 = b\epsilon_{min} \tag{3.41}$$

$$\epsilon_{min} = \frac{\epsilon_0}{1 - b} \tag{3.42}$$

where,

MFE_{ϵ} : Percentage model fit error of specific mechanical energy

ϵ : Actual specific mechanical energy

ϵ_0 : Predicted specific mechanical energy

ϵ_{min} : Lower bound of the actual specific mechanical energy with y % probability

y : Prediction interval coverage probability

b : Lower bound of y % prediction interval of model fit error of specific mechanical energy

The designer determines the value of the prediction interval coverage probability (y). As y approaches 1, the prediction interval widens as well. If a narrow prediction interval is desired, the y value must be small.

The steps involved in calculating $\epsilon_m in$ were summarized below:

1. Estimate the percentage model fit error of the specific mechanical energy prediction formula

2. Select a y value

3. Calculate y % prediction interval [a,b] for the percentage model fit error (a represents lower bound and b represents upper bound of the prediction interval)

4. Calculate ϵ_{min}, the lower bound for ϵ with;

$$\epsilon_{min} = \frac{\epsilon_0}{1-b} \tag{3.43}$$

   Note that the b value is used because the orbit's specific mechanical energy requirement is always negative.

5. Then estimate the lower bound of the actual specific mechanical energy of a vehicle with the following inequality;

$$\hat{\epsilon} \geq \epsilon_{min} \tag{3.44}$$

Following all of this discussion, the following hypothesis was stated:

Hypothesis 2.

A launch vehicle design that meets the following conditions will have a specific mechanical energy $\hat{\epsilon} \geq \frac{\epsilon_0}{1-b}$ at the target orbit with at least y % probability if its trajectory is optimized.

- **The surrogate models are fit by using the data of the vehicles reaching an altitude between 100 km and $R_{earth} + 2h_{target}$ when the fuel is consumed.**
- **The vehicle is designed using the surrogate models of ϵ and ϕ by targeting $\hat{\epsilon}_{final} = \epsilon_0$ and $\hat{\phi}_{final} = 0$.**

where,

ϵ : Actual specific mechanical energy

$\hat{\epsilon}$: Predicted specific mechanical energy

ϵ_0: The specific energy requirement of the target orbit

ϕ: Actual flight path angle

$\hat{\phi}$: Predicted flight path angle

ϕ_{final}: Actual flight path angle at the final orbit

h_{target} : Altitude of the target orbit

y : Prediction interval coverage probability

b : Lower bound of y % prediction interval of the model fit error of specific mechanical energy

R_{Earth} : Radius of the Earth

3.4.6 Discussions

The following is how this design-oriented analysis can be interpreted: If n vehicles are designed using this method, at least y percent of them should have a minimum final specific mechanical energy of $\frac{\epsilon_0}{1-b}$. This methodology can be very useful for rapid design trade-offs in conceptual design if a good combination of b and y can be found. There will always be a trade-off between b and y, and the system designer will choose these values.

A designer would like ϵ_{min} to be close to the target energy ϵ_0. Yet, if the ANN model is not well-fit, ϵ_{min} will diverge from the target energy. It should be noted that the hypothesis is highly dependent on the statistical performance of ANN models because it is dependent on b value. Therefore, the goodness of ANN models should be evaluated by examining model fit errors, model representation errors, R-Squared values, actual by predicted, and residual by predicted plots. Finally, note that the difference between ϵ_{min} and ϵ_0 is the accuracy cost of a rapid energy estimation without conducting a trajectory optimization.

As an illustration, if 1000 vehicles are designed using this methodology at a 20 % y value, at least 200 of these vehicles should have an actual energy value greater than the

lower energy bound ϵ_{min}, which is relatively close to the target energy ϵ_0. On the other hand, if 1000 vehicles are designed using this methodology at a 90 % y value, at least 900 of these vehicles should have an actual energy value greater than the lower energy bound that is relatively further away from the target energy in this case. Note that while these numbers may not be exact for a small sample size representing a population, they are theoretically expected to emerge as the sample size increases and converges to infinity.

A possible question is whether the upper bound on specific mechanical energy can be estimated similarly. For this discussion, it is required to return to Equation 3.37. The upper bound of the training error term provided in Equation 3.39 can be estimated using the prediction interval concept. However, δ_{opt} inequality is modeled only by a lower bound in this study as shown in Equation 3.38. To model an upper bound for this term, trajectory optimization must be performed to quantify the energy savings. As a result, since trajectory optimization was eliminated from the design process, it is impossible to estimate the upper bound for the specific mechanical energy using the methodology developed in this thesis.

Until this point, one implicit assumption has been made in this study: the steady-state error of specific mechanical energy obtained via trajectory simulation is assumed to be zero. This steady-state error is entirely dependent on the controller performance used in the trajectory simulation, particularly the controller used during the final launch phases. If the error is not negligible, it should be quantified and incorporated into the estimation. The quantification of such an error, on the other hand, is beyond the scope of this thesis. Because the controller performed well in the trajectory simulation used in this thesis, it was assumed that the steady-state error in specific mechanical energy was negligible.

Another possible question can be stated as follows: What if the surrogate models were fit by incorporating some cases where not all fuel is consumed between 100 km and $hmax$? In other words, what if these vehicles retained some propellant once they reached a minimum altitude of 100 kilometers? In this case, the vehicles are expected to have more energy than the required energy for the mission. The requirement that all fuel be consumed

in space was added to ensure that vehicle designs are not oversized. However, vehicles that still have some propellant may be used for surrogate modeling if desired, keeping in mind that they are already oversized for the required mission.

3.5 Summary of the Methodology

Conducting a trade-off study for launch vehicle design in the CDP is a time-consuming task when the design space is large. That is why, in this chapter, a rapid design trade-off methodology was developed that eliminated trajectory optimization from the design process through the use of constant controller design.

To begin, a multidisciplinary M&S environment comprised of four core disciplines was constructed: trajectory, aerodynamics, propulsion, and weight. Following that, several DOE and surrogate modeling approaches were investigated in order to obtain adequate surrogate models for any desired response. Finally, the specific mechanical energy-based design trade-off method which was summarized in Figure 3.16 was developed. The blue boxes in this process flow represented the steps at which a system designer make decisions.

In this chapter, two research questions and two hypotheses were stated:

Research Question 1.
To approximate the modeling and simulation environment, which DOE method and surrogate modeling method should be used?

Hypothesis 1.
A hybrid DOE composed of a Fast Flexible Filling & a Full Factorial DOE combined with Artificial Neural Networks will provide an effective method for approximating the M&S environment.

Research Question 2.

Without performing trajectory optimization during the conceptual design phase, how can a trajectory-based vehicle design trade-off be performed?

Hypothesis 2.

A launch vehicle design that meets the following conditions will have a specific mechanical energy $\hat{\epsilon} \geq \frac{\epsilon_0}{1-b}$ at the target orbit with at least y % probability if its trajectory is optimized.

- The surrogate models are fit by using the data of the vehicles reaching an altitude between 100 km and $R_{earth} + 2h_{target}$ when the fuel is consumed.
- The vehicle is designed using the surrogate models of ϵ and ϕ by targeting $\hat{\epsilon}_{final} = \epsilon_0$ and $\hat{\phi}_{final} = 0$.

In the next chapter, these hypotheses will be tested by planning out an extended design study. The results obtained by the implementation of this methodology will be compared to the actual data obtained by performing trajectory optimization.The outcomes of these tests will be thoroughly discussed in order to validate the methodology.

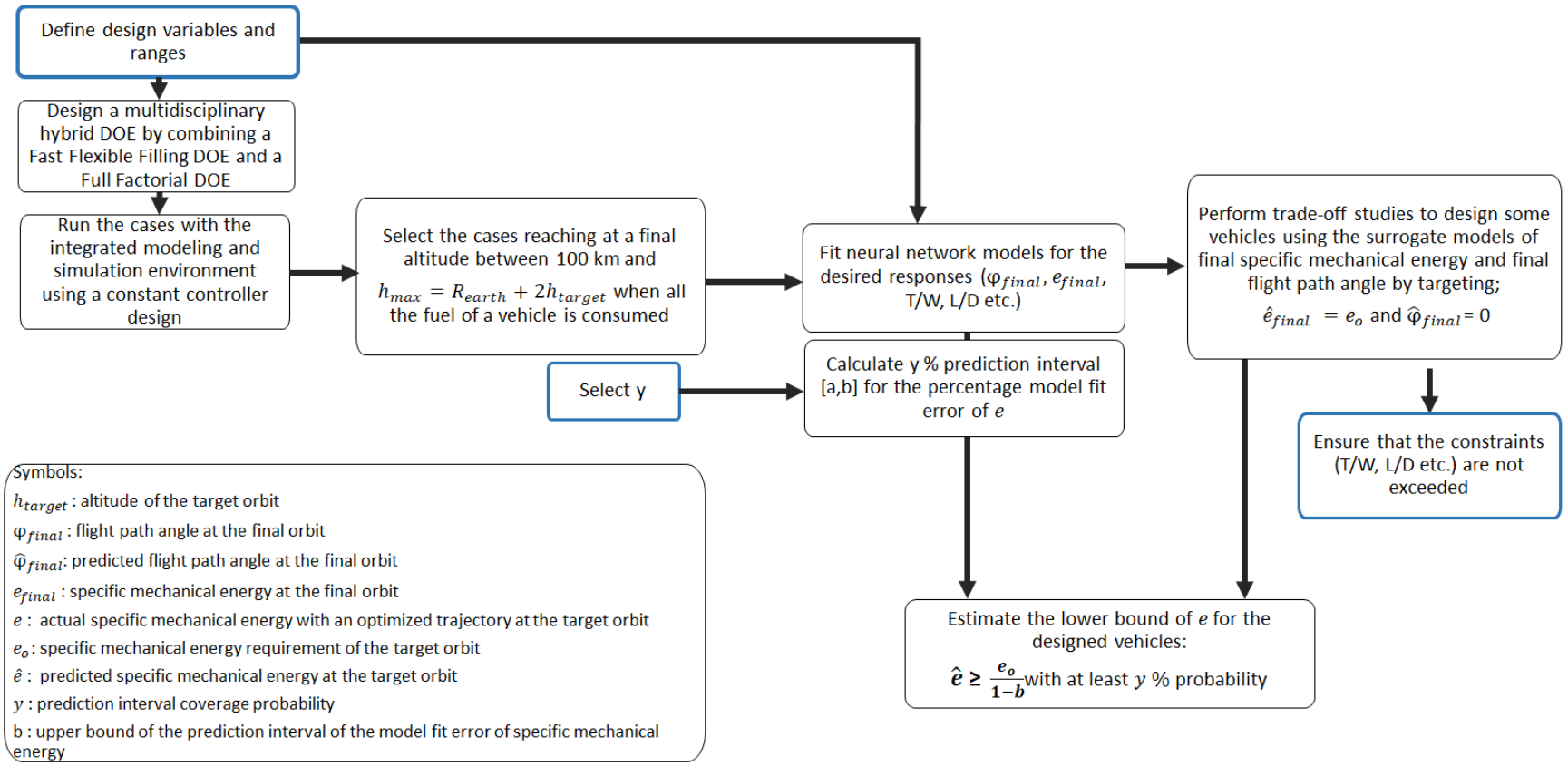

Figure 3.16: Specific Mechanical Energy-Based Design Trade-Off Methodology Process Flow

CHAPTER 4

RESULTS

4.1 Extended Design Study

An extended design study was presented in this section with some high-level requirements provided in Table 4.1. A circular low earth orbit with an altitude of 400 kilometers was selected as the target orbit. Max Length-to-Diameter Ratio (L/D) was selected as an aeroelasticity constraint while Thrust-to-Weight Ratio (T/W) was selected as a structural constraint. The Gross Lift-Off Weight of the vehicle was not included in this list since the weight of a small vehicle was not expected to exceed the launchpad structural limits where larger class vehicles such as Falcon 9 are launched from Cape Canaveral Launch Site. For the demonstration of the methodology, this list was selected but it can be extended to represent more requirements such as maximum acceleration, maximum dynamic pressure, or T/W constraints for each stage.

Table 4.1: High-Level Requirements

Target Orbit	400 km altitude, circular orbit
Payload Capacity	120 kg (12 X 10 kg nanosatellites)
Launch Site	Cape Canaveral, Florida
L/D of Vehicle	$L/D \leq 15$
T/W of Vehicle	$T/W \leq 2$

4.1.1 Current Design Strategies of Commercial Space Industry

This design study followed some current cost-effective design strategies implemented by the commercial space industry. For that purpose, some of the state of the art launch vehicles were examined in terms of their sizes, architectures, payload capacities, and engine performances [4]. Some information related to these vehicles were summarized as follows:

- Electron vehicle which was developed by Rocket Lab is a two-stage expendable vehicle. The first stage of Electron is powered by nine Rutherford engines, while the second stage is powered by one Rutherford engine. The Rutherford engine is a liquid engine with a thrust force of 22 kN and a propellant mixture of LOX and kerosene developed by the company. Electron has a payload capacity of 225 kg to LEO, a vehicle mass of 10500 kg, and an L/D ratio of 13.3. The vehicle does not contain any add-on boosters.

- Rocket Crafters is developing Intrepid-1, a two-stage small expendable launch vehicle powered by hybrid motors. The vehicle's first stage is expected to have four hybrid motors, each with 136 kN of thrust force, and the second stage will have four hybrid motors, each with 18 kN of thrust force. Intrepid-1 has a payload capacity of 500-750 kg to LEO, a vehicle mass of 45000 kg, and a length-to-diameter ratio of 10.7. There are no add-on boosters in this vehicle. The company has not released any information about the hybrid motor's design or performance.

- HyImpulse is developing a small expendable vehicle concept with hybrid rocket propulsion [12], [69]. This vehicle is expected to have seven hybrid motors in the first stage, each with a thrust force of 75 kN, four hybrid motors in the second stage, each with a thrust force of 100 kN, and four hybrid motors in the third stage, each with a thrust force of 25 kN. To reduce the motor's production costs, hybrid motors will use a simple, single-port cylindrical fuel grain. The payload capacity of this vehicle is 500 kilograms. The motors use LOX-Paraffin combination with some metal additives. The vehicle does not employ any add-on boosters.

The following observations were made based on this information:

- Developing a unique motor and designing a cluster of these motors in every stage is an up-to-date cost reduction strategy used by the commercial space industry. Merlin 1-D engine of SpaceX and Rutherford engine of Electron are the best examples

for this strategy. Additionally, this strategy aids in improving the repeatability and reliability of engine components.

- These state-of-the-art vehicle designs do not contain any boosters, wings, and control surfaces while they include a small number of stages for cost reduction and improved simplicity in design.

4.1.2 Initial Design Decisions and Assumptions

Each vehicle design process begins with a series of initial design decisions. Several design decisions were made in this section and were summarized in Table 4.2.

Historically, due to low regression rates, it was not possible to design a hybrid motor with a single port. Instead, multi-port motors were developed, which were complex and frequently included some unburned slivers, as illustrated in Figure 4.1 [22]. Following the development of paraffin-based fuels, it became possible to design single ports due to the increasing regression rates [70]. As a result, a Paraffin-LOX propellant combination and a single port were selected in this study. Because of the increasing simplicity of manufacturing, a cylindrical grain was chosen. Because of the observations made in the previous section, add-on boosters were not used on this vehicle in order to keep the design as simple as possible. Also, a LV-Haack fairing was selected since it can allow a large interior volume and relatively low drag coefficient [62]. A turbo-pump feed system was also chosen based on a study that concluded that a turbopump outperforms a pressure-fed system for a similar concept [12].

Table 4.2: Initial Design Decisions

Rocket propulsion type	Hybrid rocket propulsion only
Propellant combination	Paraffin-LOX
Feed system	Turbopump fed
Grain geometry	Cylindrical fuel grain
Number of combustion ports	Single
Use of boosters	No
Fairing type	LV-Haack nose cone

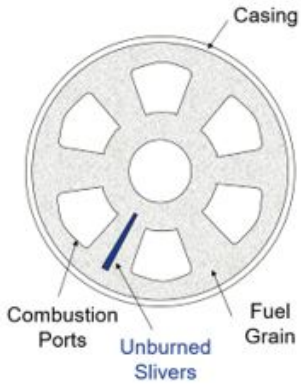

Figure 4.1: Multiport Design

4.1.3 Mission Profile

The mission profile was plotted in Figure 4.2 and it includes the following phases: lift-off, pitch over maneuver, gravity turn maneuver, first stage separation, second stage separation, fairing separation, a long coast phase in space, a short restart phase, and finally spacecraft separation. Notably, this vehicle is capable of restarting, since hybrid motors, like liquid engines, have this capability. If the vehicle is to be a two-stage vehicle rather than a three-stage vehicle, the mission profile can be modified to reflect this change.

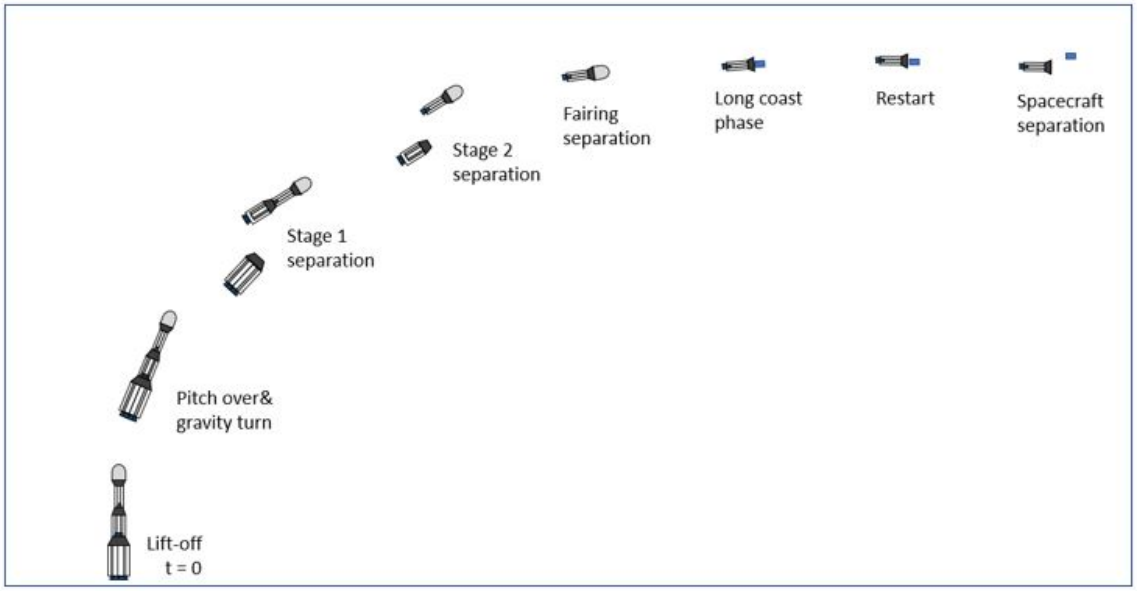

Figure 4.2: Mission Profile of the Launch Vehicle

4.1.4 Architectural Tradespace

The architectural tradespace of the vehicle in this study was defined by the number of stages and the number of motors within each stage. This vehicle can have two or three stages, each with a different number of motors, as shown in Figure 4.3. In the same figure, alternative motor cluster layouts were also sketched. The architectural trade tree was sketched in Figure 4.4.

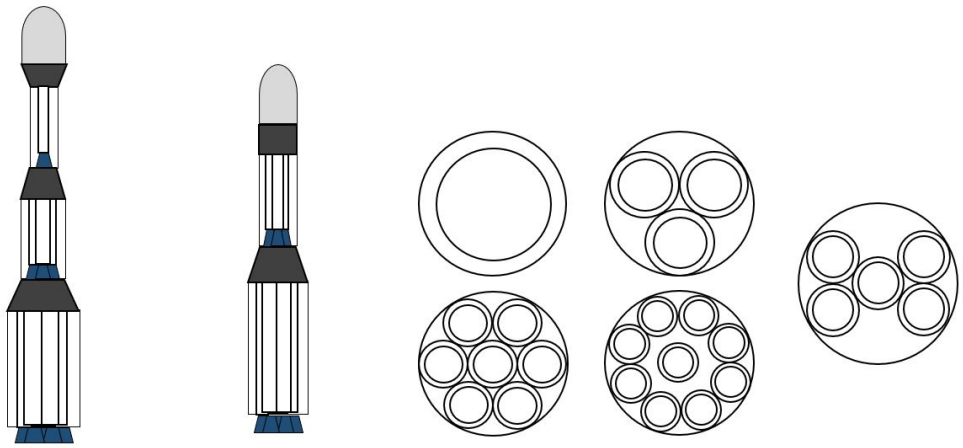

Figure 4.3: Architecture Alternatives for the Launch Vehicle

4.1.5 Hybrid Propulsion System Design Space

The design space for hybrid rocket propulsion was constructed using the design variables determined in the preceding chapter. The ranges for these design values were selected as illustrated in Table 4.3. Notably, all design variables were related to hybrid motor design, with the exception of the PMF variable, which was defined in this study for a stage (rather than a motor). For all stages, the PMF value was assumed to be identical.

4.1.6 Sizing Assumptions

Table 4.4 provided some assumptions related to the size and mass of several launch vehicle components. An interstage's fore and aft diameters were equal to the diameters of the

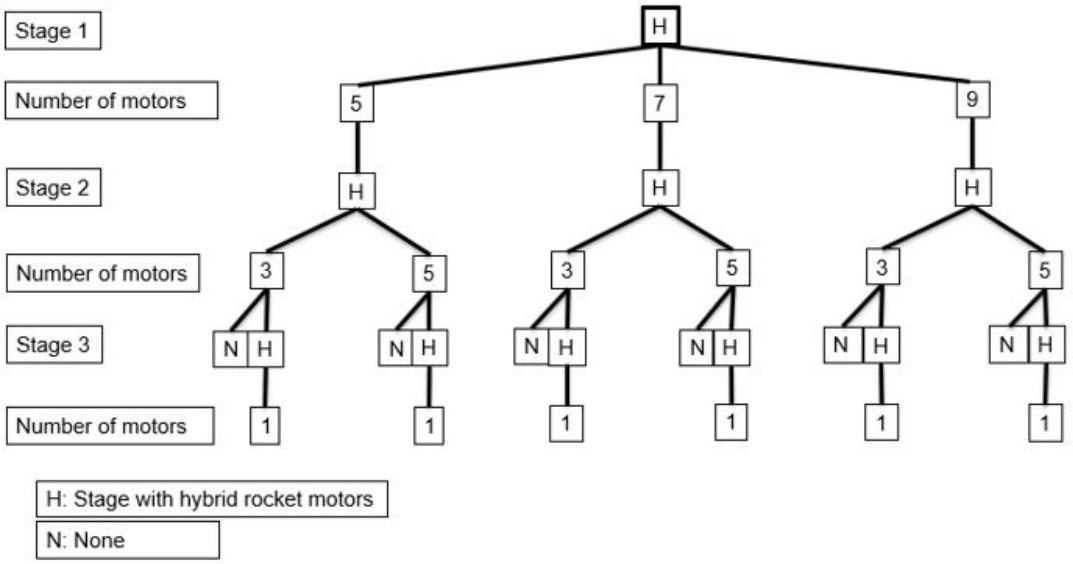

Figure 4.4: Architectural Tradespace

Table 4.3: Ranges of the Design Variables

Design Variable	Minimum	Maximum
Thrust of a hybrid motor (kN) (Sea level thrust)	75	150
Burn time of a hybrid motor (sec)	30	80
PMF of a stage	0.65	0.85
Initial mixture ratio	1.5	3.5
Nozzle area ratio	5	40
Nozzle inlet pressure (MPa)	2	6
Fuel grain outside diameter (m)	0.7	1.3

stages it connected.

The length of stages were also calculated. Figure 4.5 shows a sketch of the basic components of a hybrid rocket motor [71]. As seen from the picture, most of the length of a hybrid motor consists of fuel grain length and oxidizer tank length. Other components such as valves, pipes, gas tanks, and a nozzle occupy a smaller length compared to these large components. The length comprising the small components was assumed to be 20 % of the sum of the fuel grain length and the oxidizer tank length based on this observation.

Table 4.4: Sizing and Mass Assumptions

Component	Value
Fairing mass (kg)	50
Payload adapter mass (kg)	100
Length of interstage 1 (m)	0.8
Length of interstage 2 (m)	0.8
Length of interstage 3 (m)	0.8
Length of fairing (m)	3.5
Maximum diameter of fairing (m)	1.5

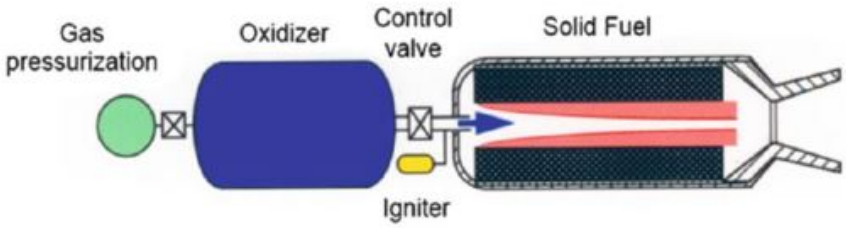

Figure 4.5: Basic Components of a Hybrid Rocket Motor

With this assumption, the length of a stage was calculated with Equation 4.1:

$$L_{stage} = (L_{oxidizertank} + L_{fuelgrain}) * 1.2 \tag{4.1}$$

The diameter of the fuel grain was a design variable in this study. Fuel grain length can be calculated using Equation 4.2 [7]. Also, the length of an oxidizer tank can be calculated using oxidizer mass, oxidizer density, and diameter of the oxidizer tank. The diameter of the oxidizer tank was taken to be equal to the diameter of grain. The tank was assumed to have a cylindrical shape.

Length of the fuel grain;

$$L = \frac{\dot{m}_f}{2\pi R_i \rho_f \dot{r}_i} \tag{4.2}$$

where

$\dot{m}_f$: Fuel flow rate

R_i: Initial port radius

ρ_f: Density of the fuel

$\dot{r}_i$: Initial regression rate

The diameters of stages were calculated by calculating the diameters of the motor clusters shown in Figure 4.3 using the circle geometry. First, the diameter of a hybrid motor was calculated by assuming a 10 % wall thickness for the casing;

$$D_{motor} = D_{fuelgrain} * 1.1 \tag{4.3}$$

For a 3-motor cluster:

$$D_{cluster} = D_{motor} * (2/\sqrt{3} + 1) \tag{4.4}$$

For a 5-motor or 7-motor cluster:

$$D_{cluster} = D_{motor} * 3 \tag{4.5}$$

For a 9-motor cluster:

$$D_{cluster} = D_{motor} * (1/sin(22.5^\circ) + 1) \tag{4.6}$$

The diameter of a stage was determined by assuming a 10 % wall thickness for casing once more;

$$D_{stage} = D_{cluster} * 1.1 \tag{4.7}$$

This concludes the vehicle's basic sizing calculations and assumptions. Not that sizing is not a primary focus of the study, but it is necessary to support the aerodynamics model.

4.2 Experiment 1. Approximation of the Modeling and Simulation Code by ANN Models

The purpose of this experiment was to test Hypothesis 1, which stated that a hybrid DOE composed of a Fast Flexible Filling DOE, a 3-level Full Factorial DOE, and ANN method would provide a good surrogate modeling approach for the M&S environment.

The first step in this experiment was to design a DOE by using the design variable ranges given in Table 4.3. Ten design variables shown in Table 4.5 were used to construct this DOE. To design the DOE, a statistical analysis software called JMP Pro was used. The DOE included 56245 cases in total (30000 cases with the Fast Flexible Filling DOE and 26245 cases with the 3-level full Factorial DOE). As seen from the table, three variables were discrete while the remaining variables were continuous.

Table 4.5: Types of Design Variables

Design variable	Type
Thrust per motor	Continuous
Burn time of a motor	Continuous
PMF of a stage	Continuous
Initial mixture ratio	Continuous
Nozzle area ratio	Continuous
Nozzle inlet pressure	Continuous
Fuel grain outside diameter	Continuous
Number of motors in the first stage	Discrete
Number of motors in the second stage	Discrete
Number of stages in the vehicle	Discrete

4.2.1 Reduction of the Design Space

Some of the cases created with the DOE were expected to be physically meaningless. To avoid crashing the code and wasting time running the cases, such cases needed to be removed from the design space before running them with the M&S environment. For this purpose, a separate script was written to evaluate and eliminate those cases.

The first category of such cases included infeasible hybrid motor designs, which were

defined as those involving motor designs with a negative initial port radius. These were found by employing the following approach:

The initial port radius of the fuel grain was calculated with Equation 4.8 [7].

$$R_i = \big(R_o^{2n+1} - a(2n+1)\big(\frac{\dot{m}_o}{\pi N}\big)^n t_b\big)^{\frac{1}{2n+1}} \tag{4.8}$$

where,

R_i: Initial port radius

R_o: Fuel grain outside radius

N : Number of combustion ports of radius R_i in the fuel grain (N = 1 in this problem)

$\dot{m}$: Total oxidizer flow rate

$\dot{m}_f$: Total fuel flow rate

$\dot{m}_o$: Oxidizer flow rate

a and n : Empirical constants for regression rate equation

t_b: Total burn time of the motor

To have a feasible motor design, R_i needs to be a positive value. Therefore, the cases that meet the following condition were considered infeasible and excluded. There were 8520 infeasible motor design cases in this problem.

$$R_o^{2n+1} \leq a(2n+1)\big(\frac{\dot{m}_o}{\pi N}\big)^n t_b \tag{4.9}$$

Additionally, in this study, it was desired that the nozzle exit area did not exceed the motor diameter. From a mechanical design perspective, it was decided to fit the nozzles into an interstage with any transition shape: positive, negative, or cylindrical. The cases which meet the condition in Equation 4.10 were evaluated as infeasible. 9847 of these infeasible cases were excluded from the design space in this problem.

$$D_{nozzle_{exit}} > D_{motor} \tag{4.10}$$

Nozzle exit diameter was calculated with the following steps [7]:

$$A_t = \frac{F}{C_F p_1}; \tag{4.11}$$

$$A_{nozzle_{exit}} = A_t \varepsilon; \tag{4.12}$$

$$D_{nozzle_{exit}} = \sqrt{\frac{4A_{nozzle_{exit}}}{\pi}}; \tag{4.13}$$

where,

F: Thrust of a motor

A_t: Nozzle throat area

C_F: Thrust coefficient

p_1: Nozzle inlet pressure

ε: Nozzle area ratio

Another group of cases that were regarded infeasible were those with a T/W ratio less than one at sea level, as such a vehicle cannot launch vertically. 751 of these infeasible cases were excluded from the design space. Table 4.6 summarizes the number of all these infeasible cases. Note that the sum of all rows does not add up to 56245 since there are some intersection sets between these infeasible groups. There were 40855 remaining cases after this initial infeasibility analysis.

Table 4.6: Infeasible Cases

Total number of cases	56245
Cases with infeasible motor design	8520
Cases with infeasible nozzle exit area	9847
Cases with infeasible T/W ratio	751
Remaining number of cases	40855

4.2.2 Constant Controller Design

To run 40855 cases with the physics-based environment, a constant controller was designed. The physical interpretation of this controller which was provided in Table 4.7 is as follows. During the pitch over maneuver, the vehicle was permitted to have a maximum angle of attack of 3°. Following the completion of the gravity turn maneuver and separation of the second stage, the upper stage was ignited and generated thrust until all fuel was consumed. The vehicle did not have a coast and restart phase. This vehicle had a zero final flight path angle command. However, because the trajectory was not optimized, it was expected that the majority of the cases would have non-zero final flight path angles. The trajectory simulation was stopped when the fuel of the upper stage was consumed.

Table 4.7: Constant Controller Design

Optimization control variable	Selected Value
u1 (max angle of attack in pitch over maneuver)	3°
u2 (ratio of restart time to the total burn time of the upper stage)	0
u3 (final flight path angle control command)	0°

A sample altitude profile was illustrated in Figure 4.6 and the thrust profile was provided in Figure 4.7 for a vehicle with this controller design. The vehicle had 7 hybrid motors with 103 kN thrust each in the first stage, 3 hybrid motors in the second stage, and one hybrid motor in the third stage, so the thrust levels were extremely high until the first stage separation. The simulation ended at t = 213 seconds, when the upper stage's fuel was consumed. As a side note, a successful case was defined as one in which the vehicle reaches at least 100 kilometers and h_max = 7178 kilometers of altitude when the fuel is consumed. As a result, the illustrated case was by definition one of the successful cases in this study.

The results were obtained by running 40855 cases, and it was observed that a large number of cases failed, with only 4959 cases meeting the success criterion. A scatter plot matrix shown in Figure C.1 was used to illustrate these design points. This situation

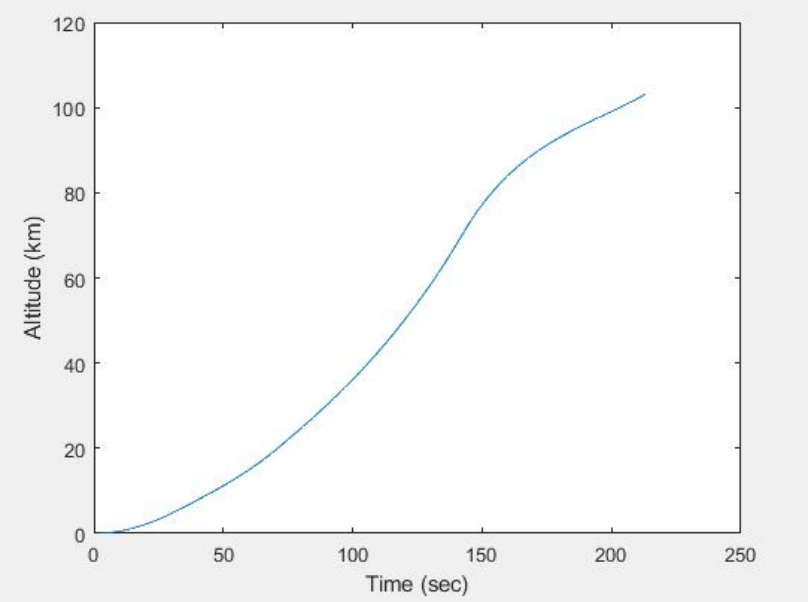

Figure 4.6: Altitude of the Vehicle

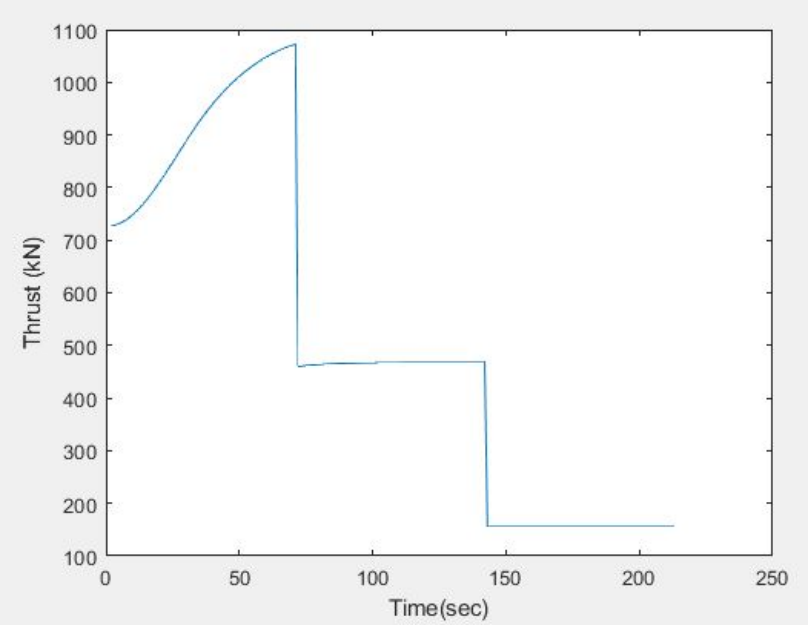

Figure 4.7: Thrust Profile of the Vehicle

exemplifies one of the difficulties inherent in launch vehicle design from the perspective of design space exploration. At times, even designing a feasible point can be a difficult task in the design of launch vehicles. Therefore, producing hundreds of feasible design points and performing some design trade-off may be difficult for a launch vehicle if such data

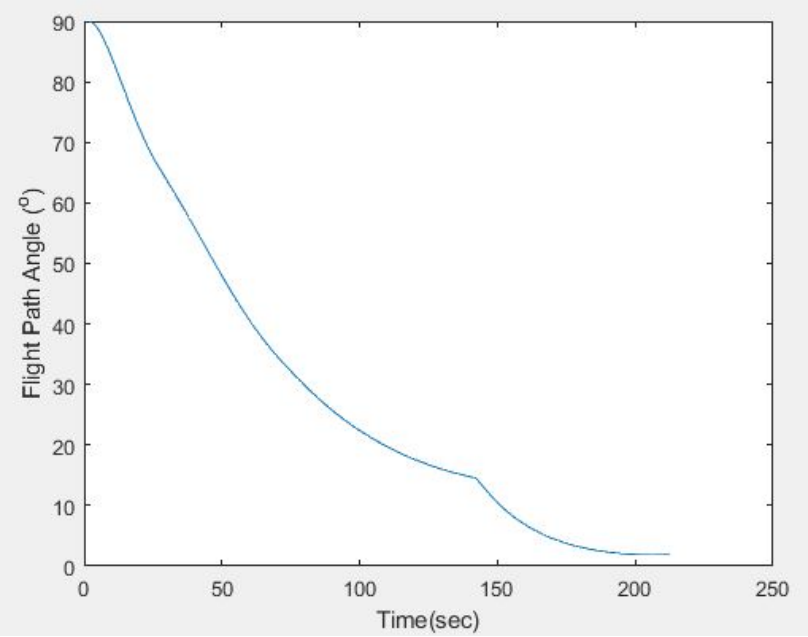

Figure 4.8: Flight Path Angle of the Vehicle

cannot be obtained. In such cases, the design variable ranges may be relaxed, or certain technologies may be integrated into the vehicle [17].

One possible question is how changing the controller design will affect the methodology's performance. Assume that a more complex controller design was selected for a launch vehicle. Remember, out of 40855 cases, only 4959 were successful for the previous controller. With a better controller, there is a chance that more vehicles will reach 100 km by following a better trajectory. Furthermore, there is a possibility that more vehicles will have a final flight path angle that is distributed about zero. This suggests that there should be a greater number of successful cases than 4959. With an increasing number of successful cases, better surrogate models may be constructed using ANN, allowing for more accurate predictions of the lower bound of specific mechanical energy. In conclusion, an improved controller design can increase the performance of the methodology presented in this thesis.

A designer who wants to employ an improved, more complex controller design can refer to [24]. In this study, a method for selecting the control structure for launch vehicles was developed. The method which is called "the OEPI method" was developed specifically

for the case when a small number of parameters is used to represent the control function, as is the case with launch vehicle trajectories. The method was demonstrated on three problems, including the optimal launch of the Delta IV Heavy. The OEPI method was applied to a set of representative launch vehicles, resulting in a single control structure that could be used for the design space.

4.2.3 Fitting Artificial Neural Network Models

Using the successful cases, artificial neural network models were fit using JMP Pro in this section. In this software, it is possible to choose a maximum of two layers and multiple nodes for an ANN model. To fit a good surrogate model, the number of nodes was fine-tuned. Two different scenarios were evaluated to investigate the ANN surrogate models' performances.

Scenario 1

First, an outlier analysis was conducted using the Multivariate Robust Outliers method that calculates Mahalanobis distance which is a measure of a sample point and a distribution [72]. This distance is dependent on the mean, standard deviation, and correlation estimates [73]. Extreme multivariate outliers were pointed out by finding the largest distance values which were shown in blue dots in Figure 4.9. Next, these outliers were excluded from the design space. Ten design variables and only two responses, the specific mechanical energy and final flight path angle, were included when this outlier analysis was conducted. There were 4031 remaining cases after this outlier analysis.

The neural network model was then fitted using 4031 cases. The R-Squared values for both training and validation were summarized in Figure 4.10. This analysis was repeated ten times to observe how R-squared varied. The results of the repeated analysis were shared in Table 4.8. Both the training and validation R-squared values indicated good fits since they were greater than 0.97. In this study, the k-fold validation method was used.

It is important to note that in order to obtain a good surrogate model, neural networks

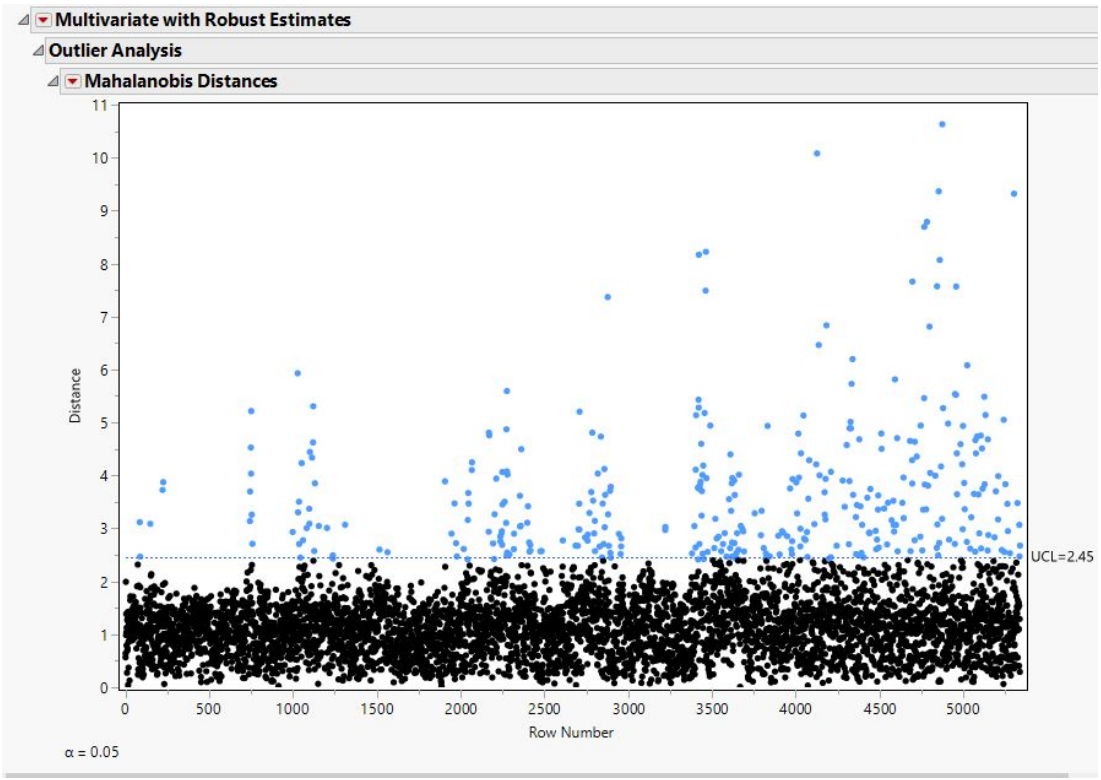

Figure 4.9: Outlier Analysis

typically require a large number of training points. This is especially true when many design variables are used and nonlinear input-output relationships exist. The time required to train an ANN model typically increases with the number of training points. More data are required to obtain a good model, especially when the model becomes complex with many nodes and layers. Running the code at many design points also takes time. As a result, for this study, a trade-off between the number of cases and the goodness of fits obtained with ANN method is always required.

Figure 4.11 illustrated the complex neural diagram of this model with three activation functions; tanH, linear and gaussian functions. Unfortunately, simpler models did not provide acceptable R-squared values. This diagram illustrated an important feature of neural network models: they are complex and difficult to interpret, but they are extremely flexible.

Other measures to test the goodness of fit of this model were the actual by predicted plot and residual by predicted plots as shown in Figure 4.12 and Figure 4.13. These plots

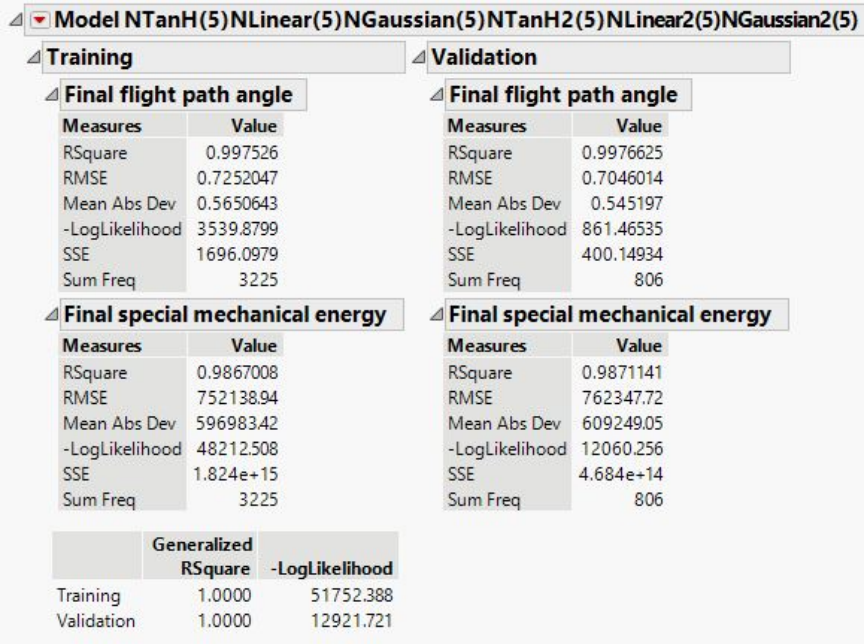

Figure 4.10: Training and Validation R-Squared Performance of a Neural Network Model

Table 4.8: R-Squared Values from Repeated Analysis for Scenario 1

Cases	Energy Training R^2	Energy Validation R^2	Flight Path Angle Training R^2	Flight Path Angle Validation R^2
1	0.983	0.983	0.994	0.995
2	0.983	0.983	0.994	0.994
3	0.989	0.990	0.994	0.994
4	0.990	0.991	0.995	0.994
5	0.977	0.975	0.993	0.994
6	0.988	0.988	0.997	0.997
7	0.989	0.991	0.994	0.994
8	0.989	0.989	0.994	0.994
9	0.976	0.975	0.994	0.993
10	0.978	0.979	0.997	0.997

were acceptable because they did not demonstrate a strong pattern or clustering of points.

The percentage model fit error distribution shown in Figure 4.14 was also obtained. This distribution resembled a normal distribution and had a mean of approximately 0. The prediction intervals for the MFE distributions were also calculated with JMP for 95 %, 80 %, and 50 % probabilities. For instance, the lower and upper bounds of the 95 % predictive interval were calculated as $[a, b] = [-3.67\%, 3.64\%]$

The sensitivity profilers obtained using these surrogate models were plotted in Figure 4.16. This plot was acceptable due to the absence of overfitting. It demonstrates the extent to which a design variable can affect the responses. Any relationship between design

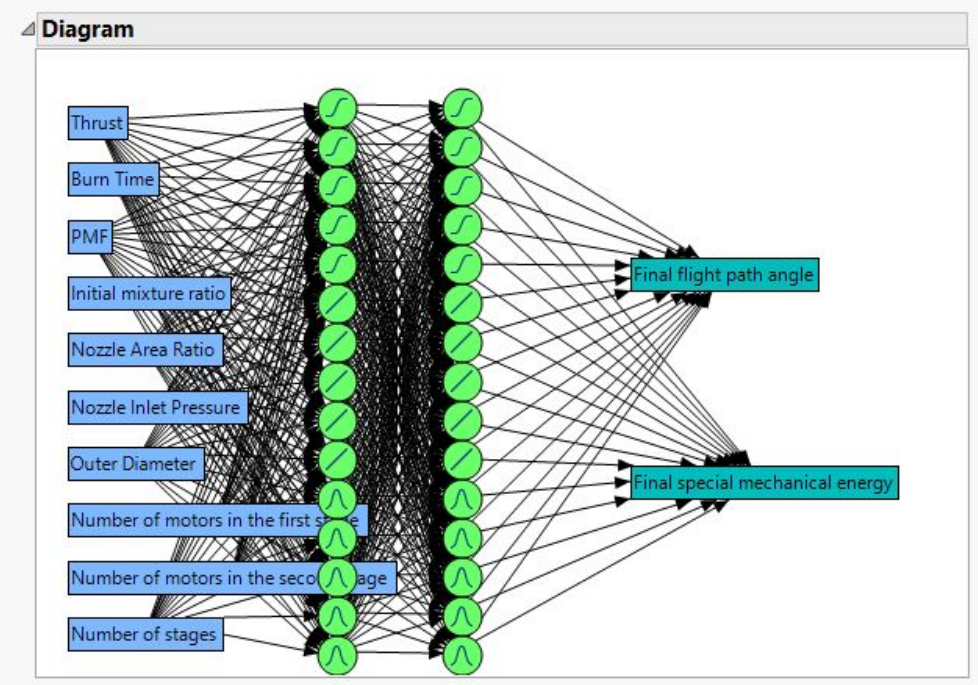

Figure 4.11: Neural Diagram for Scenario 1

variables and final specific mechanical energy and final flight path angle can be dynamically observed in this parametric environment, which greatly aids trade-off analysis.

Scenario 2

A more realistic design trade-off scenario was planned out in this part, where neural network models were fit for multiple responses. The responses can be any dependent variables of interest. As an illustration, final specific mechanical energy, final flight path angle, Thrust-to-Weight ratio, vehicle Length-to-Diameter ratio were selected as the responses. The complex neural diagram was shown in Figure 4.17 for this scenario.

The R-Squared values for a sample fit were shown in Figure 4.18. Most of the R-squared values were found to be around 0.99. This analysis was repeated ten times and the results were shown in Table 4.9. Overall, the R-Squared values indicated that the performance of the ANN surrogate models was acceptable.

The sensitivity profilers were provided in Figure 4.19 for this scenario. As an illustration, a designer may be interested in designing some vehicles with a specific range of

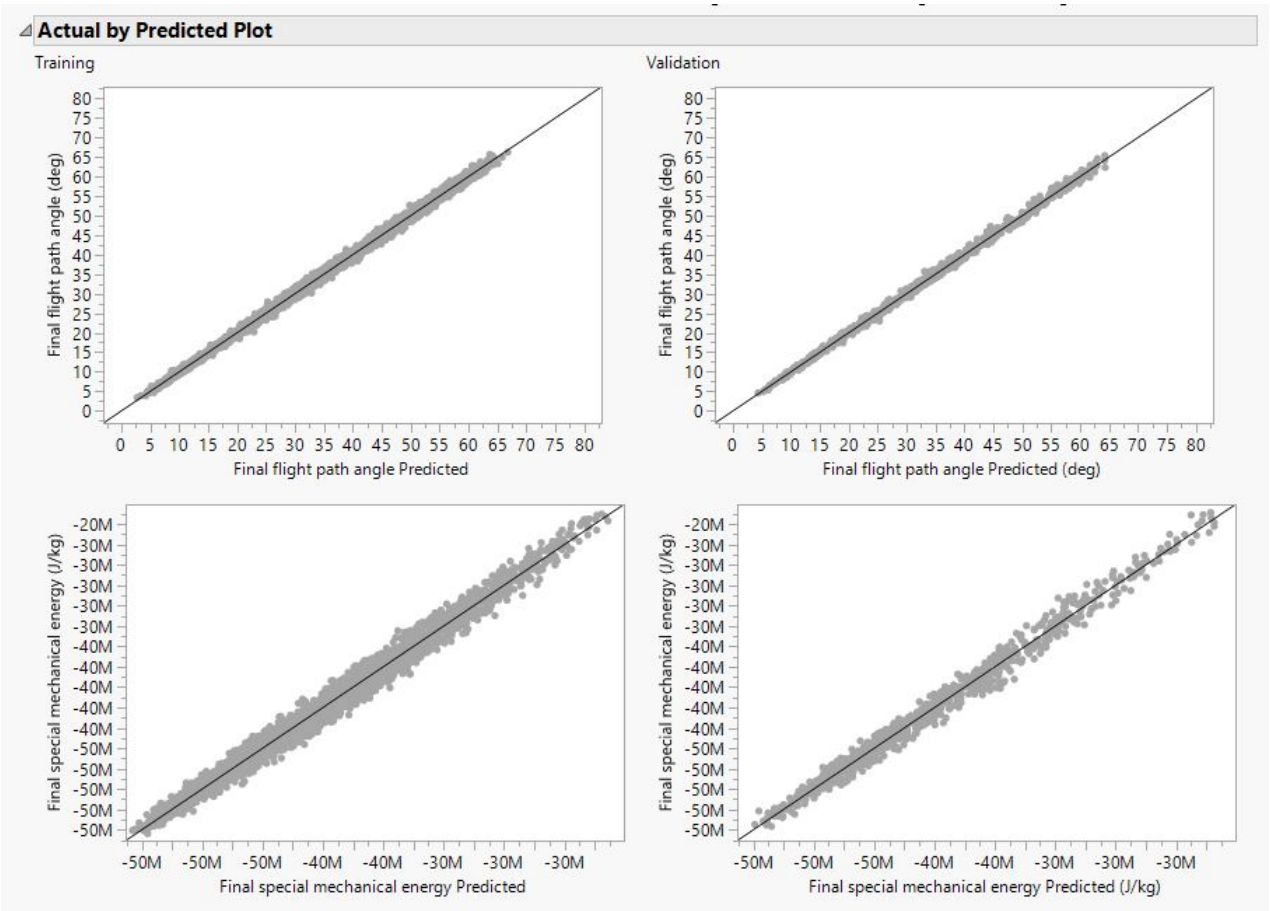

Figure 4.12: Actual by Predicted Plot for Scenario 1

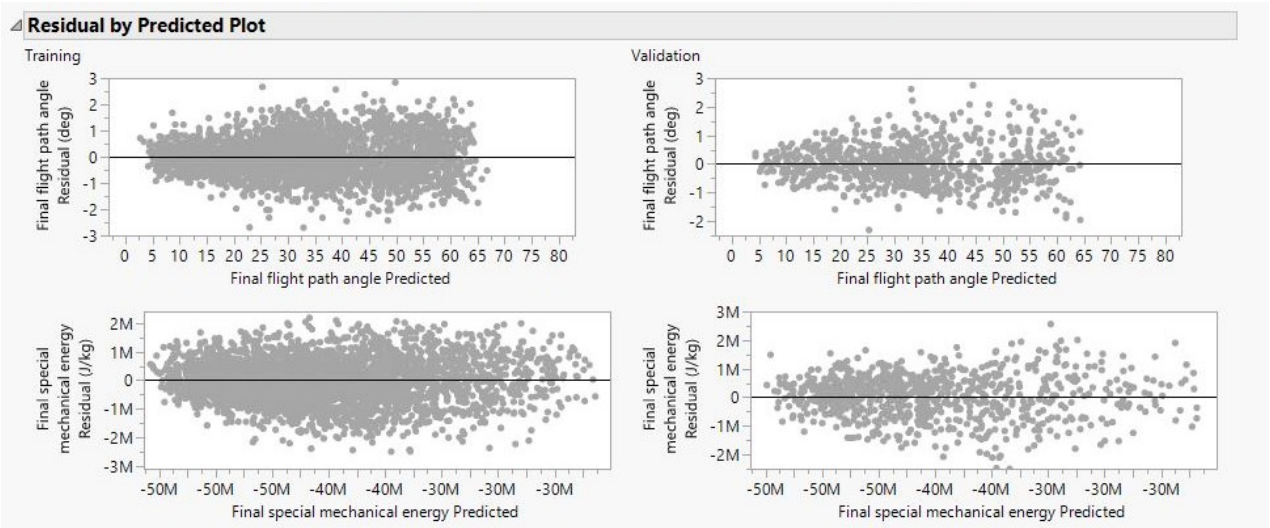

Figure 4.13: Residual by Predicted Plot for Scenario 1

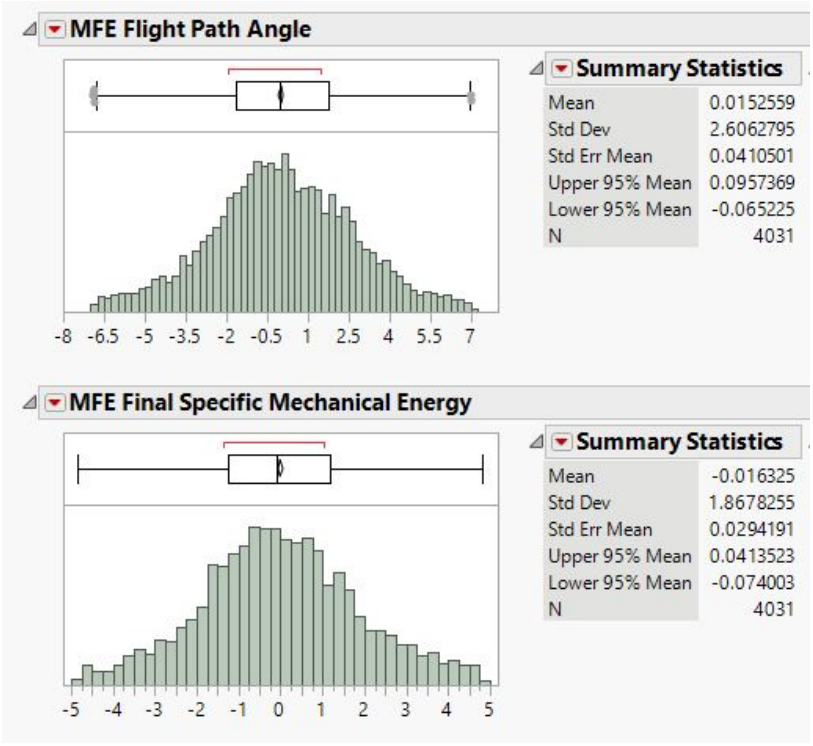

Figure 4.14: Percentage MFE of Specific Mechanical Energy for Scenario 1

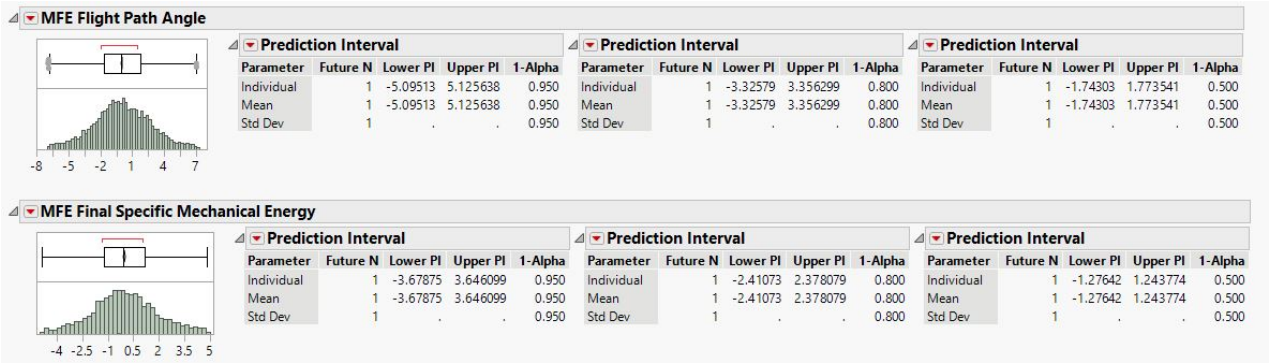

Figure 4.15: Prediction Intervals

Table 4.9: Repeated R-Squared Analysis for Scenario 2

Energy Training R^2	0.961	0.974	0.964	0.968	0.968	0.964	0.975	0.970	0.972	0.967
Energy Validation R^2	0.966	0.974	0.963	0.971	0.969	0.966	0.976	0.972	0.973	0.969
Flight Path Angle Training R^2	0.996	0.996	0.996	0.994	0.995	0.995	0.994	0.991	0.993	0.994
Flight Path Angle Validation R^2	0.996	0.996	0.995	0.994	0.995	0.995	0.994	0.991	0.993	0.994
T/W Training R^2	0.999	0.999	0.999	0.999	0.999	0.999	0.999	0.999	0.999	0.999
T/W Validation R^2	0.999	0.999	0.999	0.999	0.999	0.999	0.999	0.999	0.999	0.999
L/D Training R^2	0.999	0.999	0.999	0.999	0.999	0.999	0.999	0.999	0.999	0.999
L/D Validation R^2	0.999	0.999	0.999	0.999	0.999	0.999	0.999	0.999	0.999	0.999

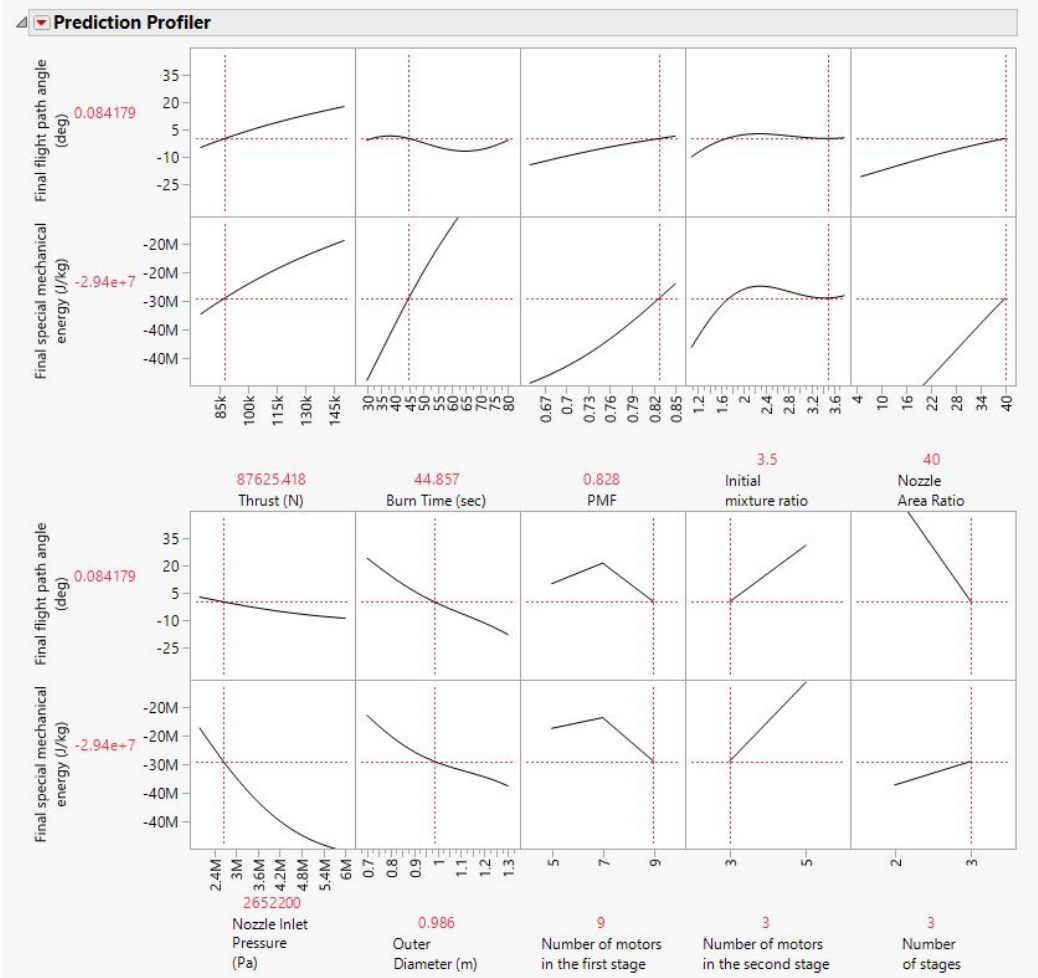

Figure 4.16: Sensitivity Profilers for Scenario 1

Thrust-to-Weight ratio. Using the sensitivity profilers shown in this figure, this designer can observe the dynamic behavior of other responses while conducting a trade-off study for Thrust-to-Weight ratio.

The actual by predicted plots and residual by predicted plots were also provided in Figure 4.20, Figure 4.21, Figure 4.22, and Figure 4.23. These plots also indicated good fits. As a result, Hypothesis 1 was validated.

4.3 Experiment 2: Specific Mechanical Energy-Based Design Trade-Off Study

In this experiment, some launch vehicles were designed using the proposed methodology. To validate the methodology, it was necessary to measure the actual performance of these

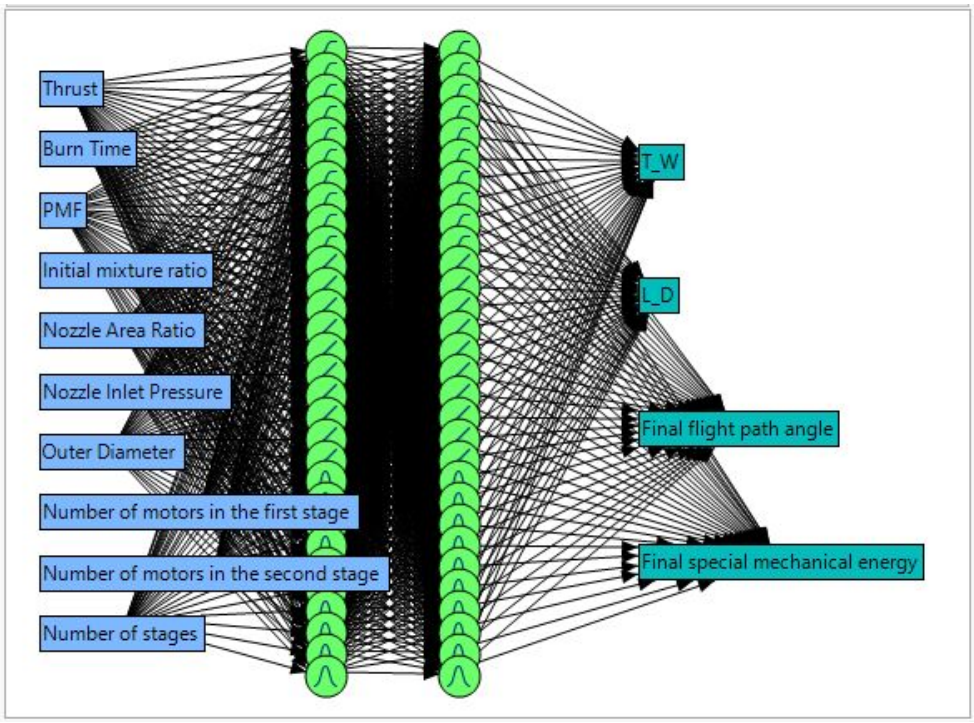

Figure 4.17: Neural Diagram with Two Layer and Multiple Nodes in Scenario 2

vehicles. To accomplish this, trajectory optimization was incorporated into the M&S environment in order to design the optimal controllers that provide the optimal trajectory. The actual performance of the vehicles was then compared to the predicted results.

4.3.1 Problem Setup with Trajectory Optimization

The latitude, longitude, and altitude of Kennedy Space Center was used in the trajectory simulation as an input:

LLA = $[28.6^\circ \ -80.7^\circ \ 10.0m]$;

The following weighted sum model was used as the objective function;

$$J = w_1\left|h_{a,target}+R_{Earth}-r_a\right|+w_2\left|h_{p,target}+R_{Earth}-r_p\right|+w_3\left|V_{target}-V\right|+w_4\left|\phi_{target}-\phi\right| \tag{4.14}$$

where,

$h_{a,target}$: Apogee altitude requirement of the target orbit

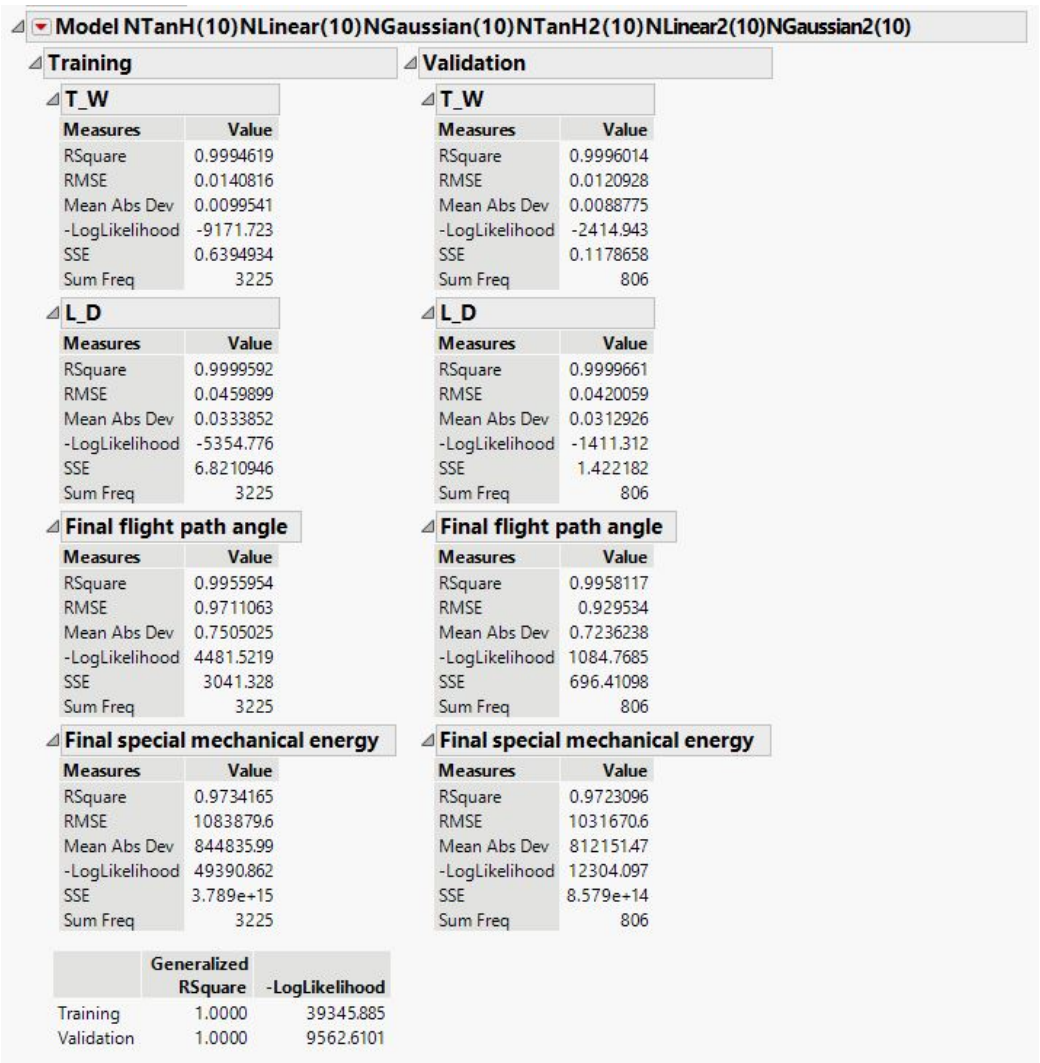

Model NTanH(10)NLinear(10)NGaussian(10)NTanH2(10)NLinear2(10)NGaussian2(10)

Training

T_W

Measures	Value
RSquare	0.9994619
RMSE	0.0140816
Mean Abs Dev	0.0099541
-LogLikelihood	-9171.723
SSE	0.6394934
Sum Freq	3225

L_D

Measures	Value
RSquare	0.9999592
RMSE	0.0459899
Mean Abs Dev	0.0333852
-LogLikelihood	-5354.776
SSE	6.8210946
Sum Freq	3225

Final flight path angle

Measures	Value
RSquare	0.9955954
RMSE	0.9711063
Mean Abs Dev	0.7505025
-LogLikelihood	4481.5219
SSE	3041.328
Sum Freq	3225

Final special mechanical energy

Measures	Value
RSquare	0.9734165
RMSE	1083879.6
Mean Abs Dev	844835.99
-LogLikelihood	49390.862
SSE	3.789e+15
Sum Freq	3225

Validation

T_W

Measures	Value
RSquare	0.9996014
RMSE	0.0120928
Mean Abs Dev	0.0088775
-LogLikelihood	-2414.943
SSE	0.1178658
Sum Freq	806

L_D

Measures	Value
RSquare	0.9999661
RMSE	0.0420059
Mean Abs Dev	0.0312926
-LogLikelihood	-1411.312
SSE	1.422182
Sum Freq	806

Final flight path angle

Measures	Value
RSquare	0.9958117
RMSE	0.929534
Mean Abs Dev	0.7236238
-LogLikelihood	1084.7685
SSE	696.41098
Sum Freq	806

Final special mechanical energy

Measures	Value
RSquare	0.9723096
RMSE	1031670.6
Mean Abs Dev	812151.47
-LogLikelihood	12304.097
SSE	8.579e+14
Sum Freq	806

	Generalized RSquare	-LogLikelihood
Training	1.0000	39345.885
Validation	1.0000	9562.6101

Figure 4.18: Training and Validation Performance of Neural Network Models

r_a: Actual apogee altitude

$h_{p,target}$: Perigee altitude requirement of the target orbit

r_p: Actual perigee altitude

V_{target}: Target speed

ϕ_{target}: Target flight path angle (at the target orbit)

ϕ: Actual flight path angle

R_{Earth}: Radius of the Earth

w_1, w_2, w_3, w_4: Weights

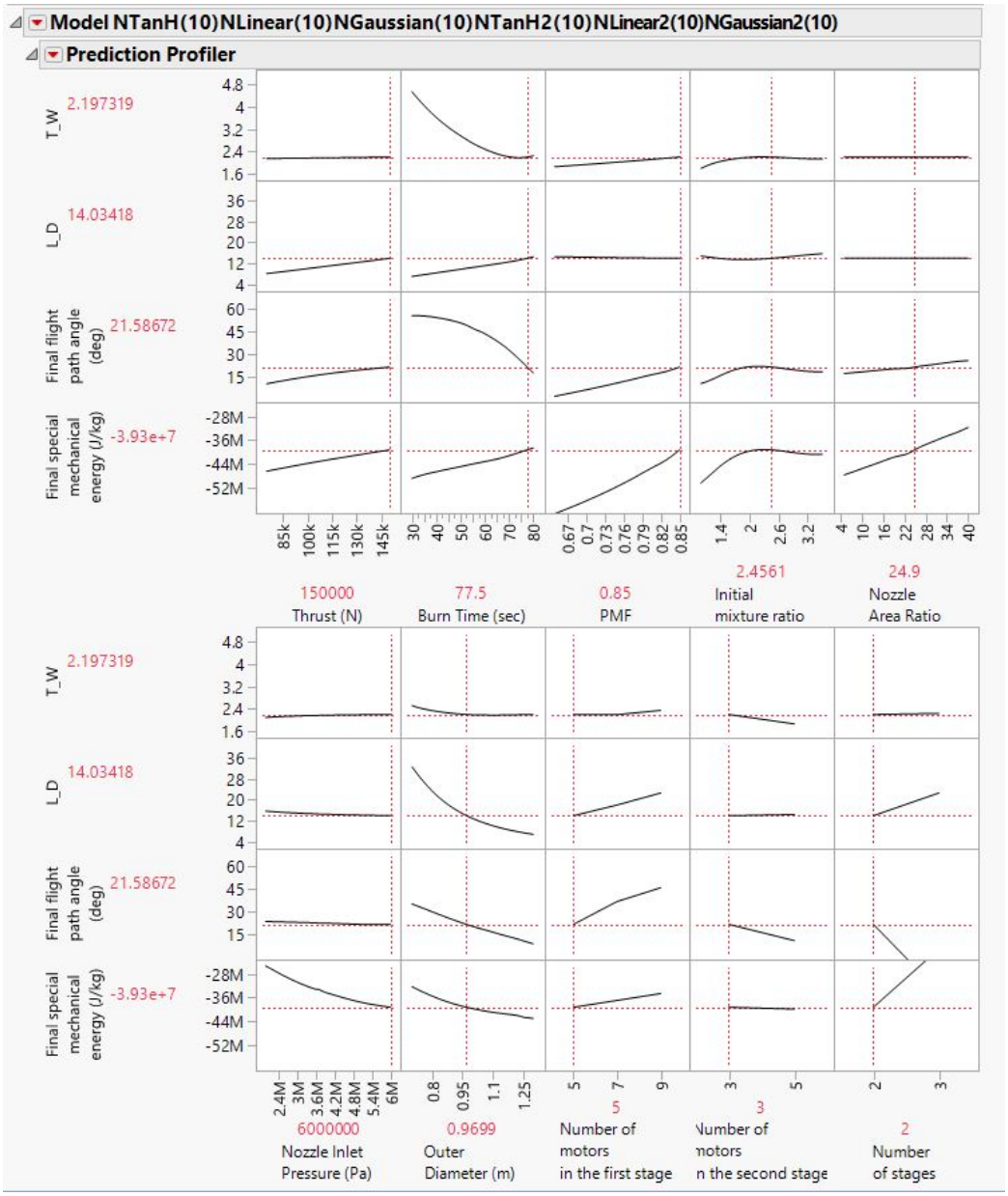

Figure 4.19: Sensitivity Profilers for Scenario 2

The control parameters were constrained as follows;

$$\alpha_{min} \leq \alpha \leq \alpha_{max} \tag{4.15}$$

$$t_{burn,upper} = t_{hybrid} \tag{4.16}$$

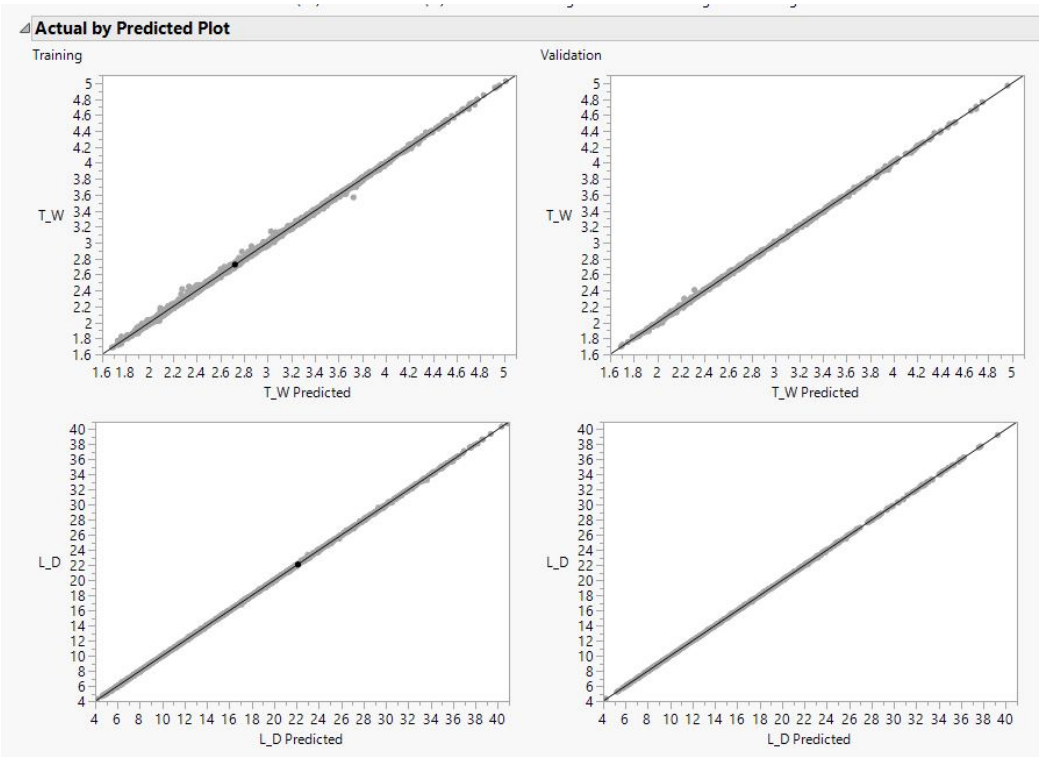

Figure 4.20: Actual by Predicted Plot for Scenario 2

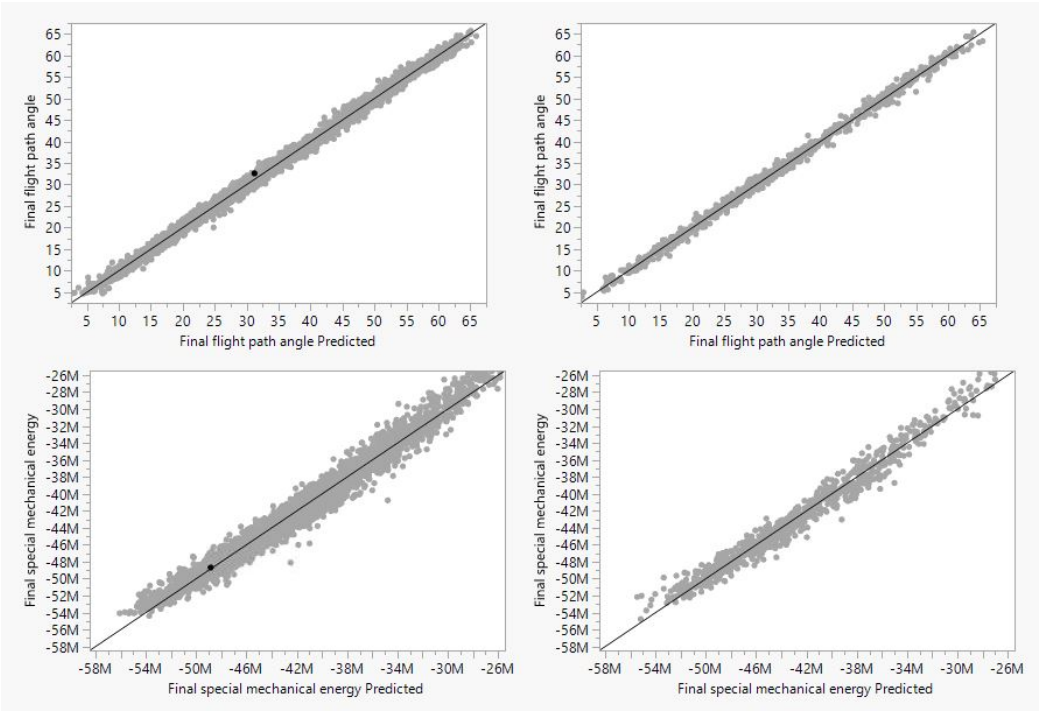

Figure 4.21: Actual by Predicted Plot for Scenario 2

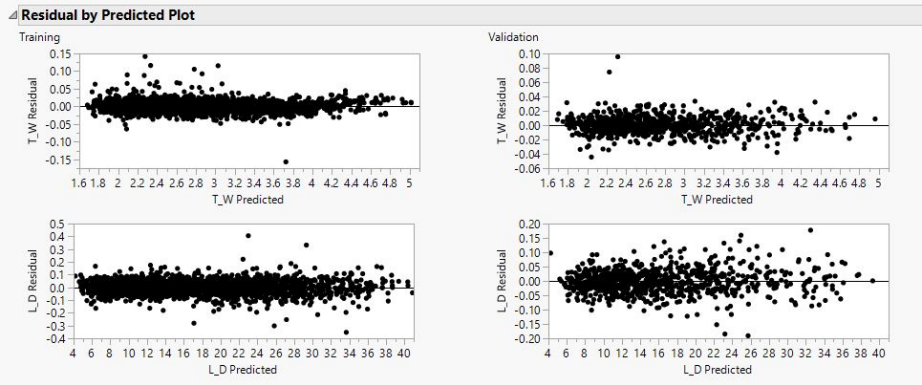

Figure 4.22: Residual by Predicted Plot for Scenario 2

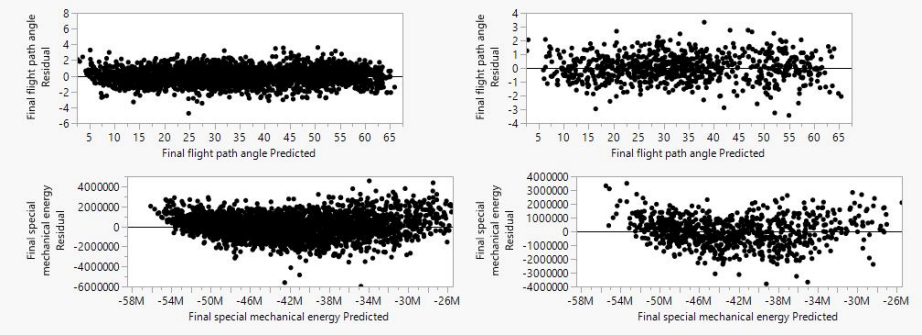

Figure 4.23: Residual by Predicted Plot for Scenario 2

$$\phi_{target} = 0 \tag{4.17}$$

$$r_{coast,min} \leq r_{coast} \leq r_{coast,max} \tag{4.18}$$

$$\phi_{coast,min} \leq \phi_{coast} \leq \phi_{coast,max} \tag{4.19}$$

where,

α_{min}: Minimum allowable angle of attack during the pitch-over maneuver

α_{max}: Maximum allowable angle of attack during the pitch-over maneuver

$t_{burn,upper}$: Burn time of the upper stage

t_{hybrid}: Burn time of a hybrid motor which is a design variable

ϕ_{target}: Target flight path angle

$r_{coast,min}$: Minimum ratio of the coast period to upper stage total burn time

$r_{coast,max}$: Maximum ratio of the coast period to upper stage total burn time

$\phi_{coast,min}$: Minimum allowable flight path angle at the end of the coast phase

$\phi_{coast,min}$: Maximum allowable flight path angle at the end of the coast phase

4.3.2 Validation of the Proposed Methodology

32 different vehicles were designed for a circular orbit of 400 km altitude using the proposed methodology. The values of the design variables associated with these vehicles were presented in Table 4.10.

A sample vehicle design process using a Contour Profiler was shown in Figure 4.24. This was the identical vehicle to Vehicle # 25 in Table 4.10. Constraints on the flight path angle and final specific mechanical energy were represented by solid red and blue lines in the plot. The shaded pink and blue regions denoted the infeasible regions, whereas the small white region denoted the feasible region defined by the responses' lower and upper limits. The black cross indicates the design point in the design space that has been selected. The factor table in this figure contains the values for the design variables associated with this design point. This process was repeated for each of the vehicles.

Next, the trajectories of the vehicles were optimized. It was observed that the actual specific mechanical energy values of most vehicles were very close to the predicted energy value which was -29.4 MJ/kg. The last column in the table shows the percentage prediction errors. It was observed that this error changes between [-3.96 %, 5.84 %]. As discussed in chapter 3, negative errors were considered significant because they revealed the worst designs that were unable to reach the target orbit.

The MFE distribution of specific mechanical energy was required to test Hypothesis 2. The MFE distribution provided in Scenario 1 was used to estimate the prediction interval's lower and upper bound values. For 95 % prediction interval, the lower and upper bounds

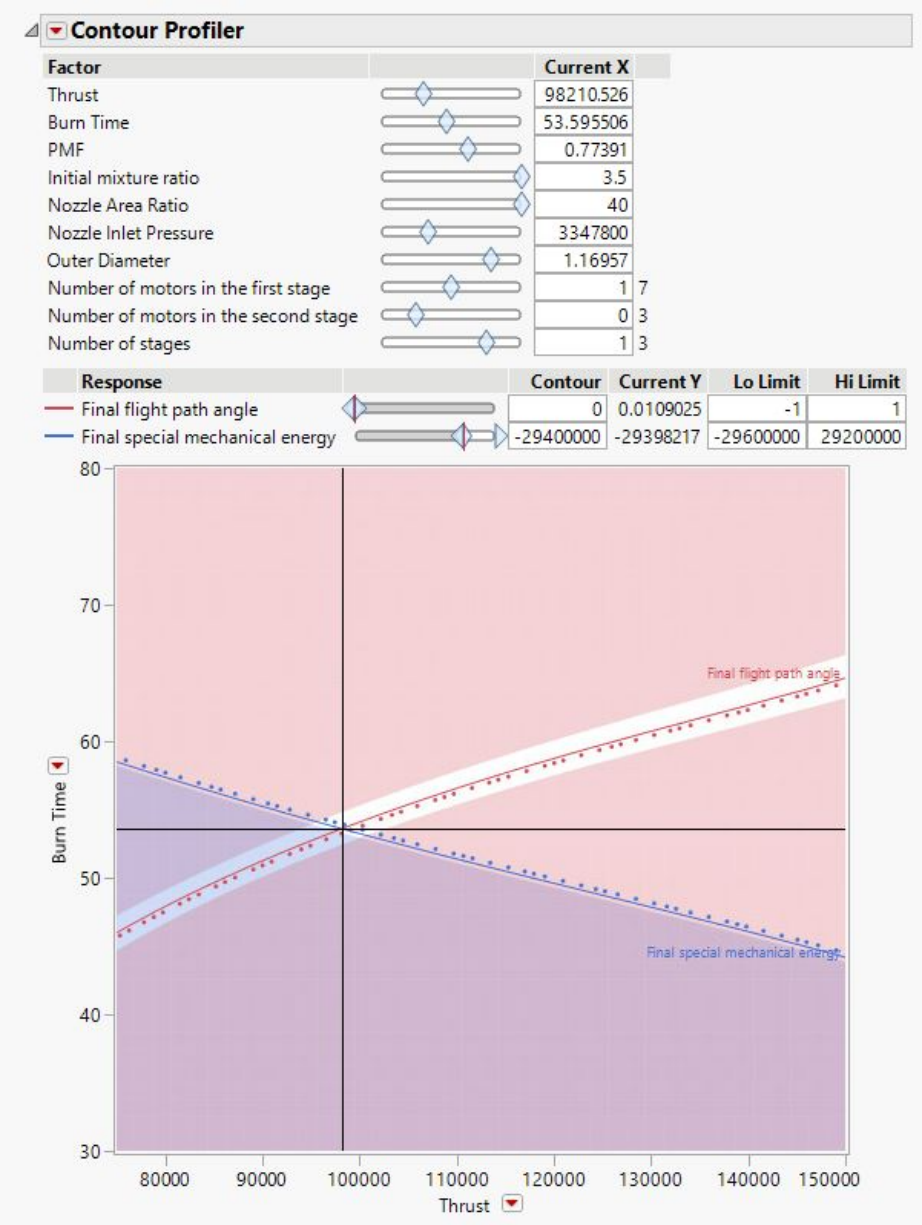

Figure 4.24: Sample Vehicle Design Using Contour Profiler

were calculated as [a,b]=[-3.67 %,3.64 %]

At least 30 of the vehicles (95 percent of all designs) were expected to have a specific mechanical energy greater than $\epsilon_{min} = \frac{-29.4}{1-3.64/100}$ = -30.5 MJ/kg, according to Hypothesis 2. The results indicated that 30 vehicles had a final specific mechanical energy value greater than this minimum value, thereby validating Hypothesis 2. Because the vehicle sample size is finite, some error is always expected between the predicted and actual number of

designs that satisfy the specific mechanical energy inequality. However, as the sample number increases and converges to infinity, it is theoretically expected that the difference between the actual and predicted number of designs that satisfy the specific mechanical energy inequality converges to zero.

An important observation was that the minimum specific mechanical energy prediction was dependent on the lower bound of the prediction interval of the model fit error. Therefore, having a lower boundary value close to zero will help to obtain good predictions.

For y = 50 %, at least 16 of the vehicles were expected to exceed the minimum energy level. There were 30 vehicles that satisfied the minimum specific mechanical energy prediction, $\epsilon_{min} = \frac{-29.4}{1-1.77/100} = -29.9MJ/kg$. Similarly, for y = 0.8, at least 25 of the vehicles were expected to exceed the minimum energy and 30 vehicles exceeded the minimum specific mechanical energy prediction, $\epsilon_{min} = \frac{-29.4}{1-3.35/100} = -30.4MJ/kg$. These results validated Hypothesis 2 since the resulting number of feasible designs exceeded the minimum number of designs expected. These results showed that even with a low y value, many feasible vehicle designs can be obtained, which would be very useful when putting this methodology into practice.

4.4 Sensitivity Analysis and Selection of Some Designs for Preliminary Design Phase

In this section, the methodology was used to demonstrate a design trade-off study that met the requirements specified in Table 4.1. Max L/D and max T/W were two constraints and they were included in the responses when fitting surrogate models. Other responses were selected as vehicle mass, ISP, ideal Delta-V, final speed, final flight path angle and, final specific mechanical energy. The R-Squared values for the obtained fits were shared in Figure C.2 and Figure C.3. A vehicle design process that meets both constraints, and the specific mechanical energy and flight path requirements was illustrated in Figure 4.25 using the contour profiler in JMP. The blue and green shaded regions represented the infeasible regions where the design points in these regions exceeded the L/D and T/W constraints.

This vehicle design could be chosen as a candidate for the preliminary design phase.

The sensitivity profilers were plotted in Figure 4.26. These profilers were extremely useful in determining which design variables had a significant effect on a response. For example, as expected, the specific mechanical energy of the vehicle depicted in this figure was highly dependent on the burn time and PMF. Likewise, the number of stages had a significant impact on the specific mechanical energy. The outer diameter, on the other hand, had a much smaller effect on the energy.

When the L/D ratio was examined, it was observed that burn time and outer diameter were the most important design variables affecting this response, whereas PMF and nozzle area ratio had no significant effect.

Vehicle mass profilers were also investigated to check if there was any unreasonable trend. Vehicle mass was observed to increase with increasing thrust, burn time, number of motors in the first stage and in the second stage as expected. Nozzle area ratio, nozzle inlet pressure, and outer diameter had small effect on the vehicle mass. Additionally, increasing the number of stages from two to three had a small effect on vehicle mass, which was unsurprising given that the third stage contained only one hybrid motor. This type of examination was extremely beneficial in identifying any bugs in the M&Scode.

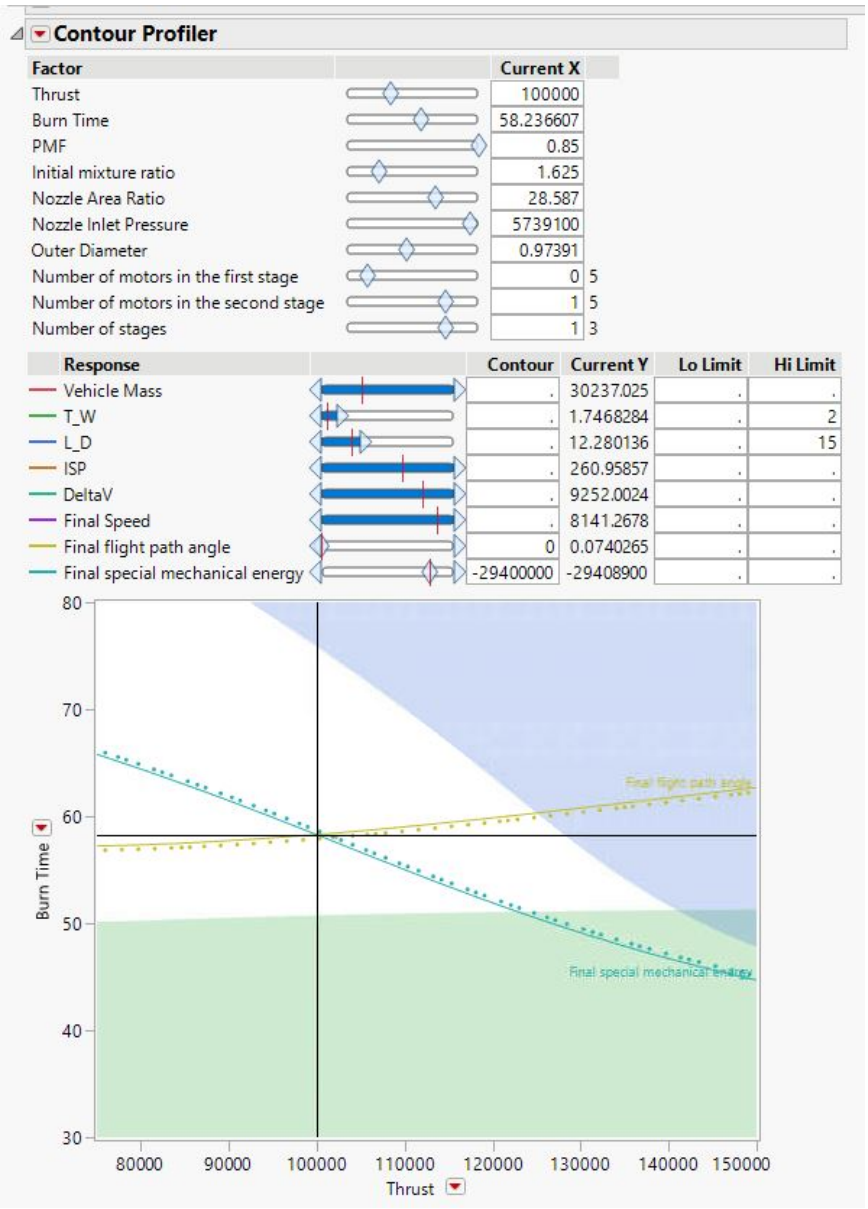

Figure 4.25: Vehicle Design Trade-Off Using a Contour Profiler

4.5 Summary of the Results

In this study, a methodology was developed to evaluate a large design space of a SLV which cannot be evaluated with simple performance models such as ideal rocket equation and a time-consuming trajectory optimization process for each point in the design space in the CDP.

The first hypothesis stated that combining a hybrid DOE composed of a Fast Flexible

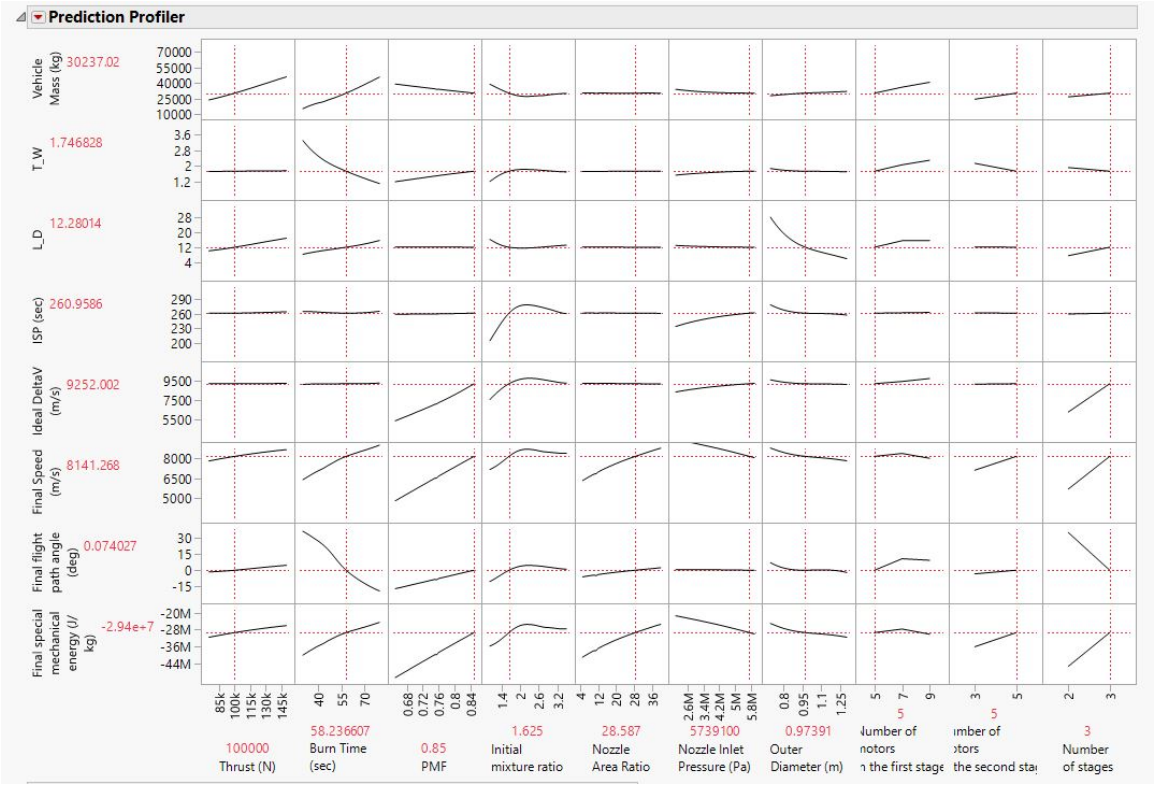

Figure 4.26: Vehicle Design Trade-Off Using Sensitivity Profilers

Filling and a Full Factorial DOE with Artificial Neural Networks would provide an effective method for approximating the M&S environment. The initial experiment was designed to evaluate this hypothesis using two separate scenarios. Both scenarios demonstrated that this approach to surrogate modeling is capable of accurately approximating the modeling and simulation code.

The second hypothesis stated that under certain conditions, the lower bound of a vehicle's actual final specific mechanical energy can be predicted. The second experiment was designed to test this hypothesis. The actual energies of the vehicles obtained through trajectory optimization were found to be very close to the predicted values. Thus, Experiment 2 validated the second hypothesis.

It was important to highlight the limitations of this methodology at this point. This methodology does not eliminate the need for trajectory optimization in any design phase, but it can assist in the design of feasible vehicle candidates without trajectory optimization

Table 4.10: Various Vehicles Designed in Experiment 2

Vehicle #	x1	x2	x3	x4	x5	x6	x7	x8	x9	x10	y1	y2	y3
1	87.6	44.8	0.82	3.5	40.0	2.6	0.98	9	3	3	-28.8	-29.4	2.08
2	82.1	62.2	0.79	2.4	5.0	2.2	0.98	7	5	3	-29.3	-29.4	0.29
3	91.4	63.2	0.79	2.4	24.7	4.2	0.98	9	5	3	-30.6	-29.4	-3.96
4	82.1	62.2	0.79	2.5	24.8	3.1	0.88	7	3	3	-29.2	-29.4	0.55
5	117.3	63.6	0.68	2.6	31.2	2.4	0.83	9	3	3	-30.7	-29.4	-4.10
6	136.1	60.9	0.68	2.3	31.2	2.4	1.05	7	3	3	-29.4	-29.4	-0.03
7	121.9	63.3	0.72	2.2	32.4	4.6	0.98	7	5	3	-29.4	-29.4	0.01
8	78.1	56.8	0.81	2.9	24.4	3.7	0.85	5	5	3	-29.6	-29.4	-0.74
9	85.6	61.5	0.79	2.6	20.5	2.4	0.96	7	3	3	-23.9	-29.4	0.02
10	129.6	56.6	0.81	3.5	32.7	3.7	1.25	7	3	3	-29.2	-29.4	0.55
11	113.3	53.3	0.83	3.5	32.7	3.7	1.06	5	3	3	-27.7	-29.4	5.84
12	75.0	55.0	0.78	2.2	37.7	3.6	0.86	5	3	3	-29.5	-29.4	-0.27
13	138.7	59.2	0.84	1.6	24.4	4.8	0.91	5	3	3	-29.3	-29.4	0.13
14	136.1	59.3	0.82	1.9	19.5	3.4	0.94	5	3	3	-29.3	-29.4	0.32
15	136.1	59.3	0.82	1.9	19.4	3.4	0.94	5	3	3	-29.4	-29.4	-0.002
16	139.9	56.4	0.77	2.6	17.5	2.6	0.94	5	5	3	-29.4	-29.4	0.01
17	116.5	54.4	0.71	2.0	28.5	2.6	1.02	5	5	3	-29.4	-29.4	-0.01
18	143.2	52.4	0.68	2.1	32.7	2.6	1.19	5	5	3	-29.4	-29.4	-0.003
19	94.0	59.1	0.68	2.1	32.7	2.6	1.19	7	5	3	-29.3	-29.4	0.23
20	93.8	62.3	0.70	2.5	32.7	3.3	0.83	7	5	3	-29.4	-29.4	0.03
21	106.5	62.4	0.71	2.6	27.4	2.9	0.86	7	5	3	-29.3	-29.4	0.28
22	81.4	67.1	0.72	2.6	27.4	3.0	0.82	9	5	3	-29.3	-29.4	0.34
23	81.5	67.3	0.77	2.5	25.9	4.0	0.99	9	5	3	-29.2	-29.4	0.49
24	97.6	68.5	0.77	2.5	22.9	4.0	0.99	9	5	3	-29.3	-29.4	0.43
25	98.2	53.6	0.77	3.5	40.0	3.3	1.16	7	3	3	-29.4	-29.4	-0.1
26	90.1	57.3	0.77	2.4	36.6	4.5	0.86	5	5	3	-28.7	-29.4	2.37
27	147.1	56.1	0.76	2.4	28.9	4.3	1.16	5	5	3	-29.3	-29.4	0.15
28	108.7	64.0	0.77	2.4	25.5	4.3	1.97	7	5	3	-29.1	-29.4	0.76
29	130.4	64.8	0.77	2.8	29.3	5.1	1.13	9	5	3	-29.3	-29.4	0.30
30	112.4	60.2	0.81	2.8	36.9	5.1	1.13	7	3	3	-29.3	-29.4	0.33
31	115.7	66.5	0.94	2.3	12.2	6.0	0.97	9	3	2	-29.3	-29.4	0.38
32	80.1	65.0	0.85	3.5	17.2	5.3	0.98	7	5	3	-29.5	-29.4	-0.19

x1: Thrust (kN)
x2: Burn Time (sec)
x3: PMF
x4: Initial Mixture Ratio
x5: Nozzle Area Ratio
x6: Nozzle Inlet Pressure (MPa)
x7: Grain Outside Diameter (m)
x8: Number of hybrid motors in the first stage
x9: Number of hybrid motors in the second stage
x10: Number of stages in the launch vehicle
y1: Actual Specific Mechanical Energy of the launch vehicle (MJ/kg)
y2: Predicted Specific Mechanical Energy of the launch vehicle (MJ/kg)
y3: Percentage Error for Specific Mechanical Energy prediction

in the CDP. These candidates can be evaluated and compared further during the preliminary design phase, when a smaller number of vehicles are traded off. These candidates can also provide system designers with some insight into where some feasible solutions accumulate in the design space. Furthermore, the sensitivity profilers can be used to determine which design variables have a strong or weak impact on the responses. Finally, using sensitivity profilers, system optimization can be performed to design the optimum vehicle in the design space while meeting design constraints and an objective function.

CHAPTER 5
CONCLUSION

Hybrid rocket propulsion is a promising technology candidate that provides cost and safety benefits for small launch vehicles. Although the space industry has developed hybrid-powered suborbital vehicles, no orbital launch vehicle with hybrid rocket propulsion has yet been operational. Because a small multistage launch vehicle with hybrid propulsion may be one possible design solution that can lower launch prices in the near future, commercial industry interest in these vehicles is increasing. Furthermore, a cost-cutting strategy currently employed by the commercial space industry was observed to be the development of a unique engine and the use of multiple of them in a launch vehicle. Following this trend, the vehicle concept investigated in this thesis was an expendable ground-launched vehicle with architectural variables such as the number of stages and the number of hybrid motors in each stage.

The design space exploration of such a launch vehicle would require very long times especially when traditional point design approaches are used. As the number of design variables increase, the design space exploration faces a combinatorial explosion. This situation poses a difficulty in performing a trade-off study for hundreds of vehicle design alternatives within the constraints of the conceptual design phase schedule. With this motivation, a methodology to conduct the rapid conceptual design trades of a SLV was presented in this thesis.

Small launch vehicles with hybrid rocket propulsion are relatively new concepts. Since there is not much historically available data of ground-launched small launch vehicles, empirical methods were not considered. Rather than that, a parametric and integrated Modeling and Simulation environment was developed for the purpose of generating and evaluating alternative vehicle designs. Following this physics-based approach, four critical

disciplines were modeled: trajectory, aerodynamics, propulsion, and weight. For aerodynamics and propulsion modeling, a first principles approach was used, and for trajectory analysis, a physics-based, transparent industrial software was used. However, this software, which simulates a 3 DOF trajectory, can be replaced with any other software in order to implement the methodology developed in this thesis.

The methodology consists of two steps. The first step was to implement a surrogate modeling approach in order to speed up the analysis with the M&S environment. To obtain good fits, various DOE and surrogate modeling techniques were investigated in this part. In particular, a hybrid DOE method that merges a Fast Flexible Filling DOE and a 3-Level Full Factorial DOE was selected to cover both the interior space and the extreme points. Next, the Artificial Neural Network method was selected to fit the approximation models since this nonlinear problem incorporates both continuous and discrete design variables. With Experiment 1, it was shown that these two methods together provide a good approach to approximate the modeling and simulation code.

In the second step, the specific mechanical energy-based design trade-off method was developed which was the main contribution of the thesis. Due to the elimination of trajectory optimization from the design trade-off process, no time was spent running a trajectory optimizer. This method used the prediction interval concept to predict the lower bound of the actual specific mechanical energy values of the vehicles which were designed by using surrogate models of the specific mechanical energy and flight path angle. Experiment 2, in which 32 different launch vehicles were designed using this methodology, demonstrated that feasible vehicle designs can be obtained rapidly. While this methodology cannot be used in place of trajectory optimization, it can assist a system designer in rapidly designing feasible vehicles that can proceed to the next design phase for further comparison, analysis, and design.

5.1 Future Work

The main assumption in this thesis was employing a constant controller design provide representative results for trajectories

The propellant used in this study was determined to be Paraffin-LOX. However, there are numerous fuel alternatives to Paraffin-LOX for hybrid motors. One possible future study is to include the type of fuel as a categorical design variable in the design space. In this way, various investigations can be performed about how fuel type affects vehicle performance. Similarly, another study may be to investigate state-of-the-art oxidizers. One such example is called Nytrox which is a mixture of liquid oxygen (O2) and nitrous oxide (NO2) where this class of oxidizers can combine the advantages of liquid oxygen (O2) and nitrous oxide (NO2) [74]. It may be worthwhile to investigate such oxidizers from the system design perspective.

Another future study may focus on modeling the performance of a hybrid motor in greater detail by removing some of the study's assumptions, such as a constant specific heat ratio, fuel density, and oxidizer density. In other words, it may be worthwhile to investigate whether higher-fidelity hybrid propulsion models can provide a benefit during the conceptual design phase. In this study, an average flow rate approximation was also used, despite the fact that the flow rate is dynamic in reality. As a result, the impact of using the dynamic flow rate equation on system design can be investigated.

The angle of attack was assumed to be zero throughout the flight in this study. However, angle of attack is not zero in reality, even if it is small in most launch vehicle flight regimes. As a result, modeling drag coefficients with angle of attack effects would be a significant contribution to this thesis, allowing for a more accurate drag model. Similarly, in this study, the lift coefficient was assumed to be zero. As a result, modeling lift coefficient may also be a useful contribution to this study.

The method developed in this thesis may be enhanced by employing a more sophisti-

cated controller design with significantly more control parameters. Additionally, quantifying the effects of using another controller design with a different level of complexity may be a significant contribution. A research of this kind could enable a designer to choose the level of complexity they desire for the controller depending on the computing cost and the accuracy of the results.

Appendices

APPENDIX A

AERODYNAMICS MODEL

The aerodynamics model provided in this appendix was based on [62]. Total drag for the launcher was calculated by separating it into N simple geometric components;

$$C_{D_{Launcher}} = \sum_{n=1}^{N} \frac{A_i C_{D_i}}{A_{ref}} \tag{A.1}$$

In this equation;

C_{D_i}: individual component drag coefficient

A_{ref}: Reference area (=maximum frontal area)

A_i: local reference area

For each geometric component i, drag coefficient was calculated by summing up skin friction drag coefficient, base drag coefficient, and body pressure drag coefficient as follows:

$$C_{d_i} = C_{d_f} + C_{d_b} + C_{d_p} \tag{A.2}$$

A.1 Skin Friction Drag Coefficient

Skin friction drag coefficient was calculated with following model:

$$C_{df} = \begin{cases} C_f(1 - 0.1M^2), & \text{if } M \leq 0.8 \\ \frac{C_f}{(1+0.15M^2)^{0.58}}, & \text{if } M > 0.8 \end{cases} \tag{A.3}$$

where skin friction coefficient C_f was calculated using the following equation;

$$C_f = \begin{cases} \frac{0.664}{\sqrt{Re}}, & \text{if } Re \leq 5.10^5 \\ \frac{0.455}{(\log_{10} Re)^{2.58}} - \frac{1700}{Re} & \text{if } 5.10^5 < Re \leq Re_{s.crit} \\ 0.032(\frac{R_s}{L})^{0.2}, & \text{if } Re > Re_{s.crit} \end{cases} \tag{A.4}$$

The surface number roughness critical number was defined as follows;

$$Re_{s.crit} = 51(\frac{R_s}{L})^{-1.039} \tag{A.5}$$

where;

L: Launcher length

Re: Reynolds number

R_s: Surface Roughness

A.2 Body Pressure Drag Coefficient

Several fairing shapes were presented and the mathematical models of body pressure drag coefficient were provided for these fairing shapes. The body pressure drag models can be found in [62].

A.2.1 Conical Fairing

The fairing pressure drag increases with increasing the joint angle ϕ which was shown in Figure A.1.

At low speeds, the pressure drag coefficient was modeled with the following equation:

$$C_{d_p,M=0} = 0.8sin^2(\varphi) \tag{A.6}$$

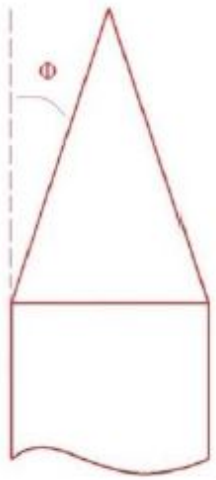

Figure A.1: Conical Fairing

When Mach number equals 1, the pressure drag coefficient was modeled with;

$$C_{d_p,M=1} = sin(\varphi) \tag{A.7}$$

At supersonic speeds, for Mach ¿ 1.3, the pressure drag coefficient was calculated with the following model;

$$C_{d_p,M>1.3} = 2.1sin^2(\varphi) + 0.5(\frac{sin(\varphi)}{\sqrt{M^2-1}}) \tag{A.8}$$

And the following model was used for Mach numbers lower than 1.3;

$$C_{d_p} = aM^b + C_{d_p,M=0} \tag{A.9}$$

where a and b were calculated using equations A.6, A.7, A.8, A.9 to fit a drag coefficient curve at these speeds.

A.2.2 Ogive Fairing

For subsonic speeds, the pressure drag coefficient was assumed to be zero, while in the transonic and supersonic regimes, the pressure drag coefficient was computed using the

conical fairing coefficient by correcting it with a factor K:

$$C_{d_p} = 0.72(K - 0.5)^2 + 0.82)C_{d,cone} \tag{A.10}$$

The shape parameter (K) of 1 corresponded to a tangent ogive. If 0¡ K ¡ 1, this corresponds to a secant ogive.

The L-D Haack series had small drag and the interior volume was relatively small. For a greater interior volume the L-V Haack series was preferred, although the drag increases.

Next, the model was expanded for different fairing fineness ratios. The fineness ratios was provided as follows:

$$f_N = \frac{L_{fairing}}{D_{fairing}} \tag{A.11}$$

The dimension used in this calculation was the fairing's base diameter. For a fairing with a fineness ratio of zero, measurements from a blunt cylinder with a pressure drag coefficient proportionate to the stagnation pressure were utilized.

$$C_{d_P,f_{N=0}} = 0.85\frac{q_s}{q} \tag{A.12}$$

$$\frac{q_s}{q} = \begin{cases} 1 + \frac{M^2}{4} + \frac{M^4}{40}, & \text{if } M \leq 1 \\ 1.84 - \frac{0.76}{M^2} + \frac{0.166}{M^4} + \frac{0.035}{M^6} & \text{if } M > 1 \end{cases} \tag{A.13}$$

After gathering data for two different fineness ratios (0 and 3), the following approach was used to estimate the pressure drag coefficient [75]:

$$C_{d_P} = \frac{a}{(f_N + 1)^b} \tag{A.14}$$

where a and b were calculated as follows;

$$a = C_{d_P, f_N=0} \tag{A.15}$$

$$b = \log_4(\frac{C_{d_P, f_N=0}}{C_{d_P, f_N=3}}) \tag{A.16}$$

Since the nose is blunted in most cases, the bluntness ratio B_r was defined as follows:

$$B_r = \frac{R_n}{R_f} \tag{A.17}$$

where;

R_N: Nose radius

R_f: Fairing base radius

The bluntness ratio was limited at 15 in this study.

To calculate the effect of tip bluntness, the following equations were used:

$$C_{d_P, blunt} = C_{d_P, sharp} F_{c,r} \tag{A.18}$$

$$F_{c,r} = 1 - 0.16B_r + 4.6(B_r)^2 \tag{A.19}$$

A.2.3 Body Transitions

Cylindrical Stages

For the cylindrical stages, the pressure drag coefficient was assumed to be zero.

Positive Body Transition

For positive transitions, a similar approach which was used to calculate the pressure drag coefficient for a conical fairing was used. More information can be found in [62].

Negative Body Transition

The pressure drag coefficient for a negative inter-stage was provided with the following equation:

$$C_{d_p} = \beta C_{d_b,aft} \frac{A_{fore}}{A_{aft}} \begin{cases} 1, & \text{if } \sigma \leq 1 \\ \frac{3-\sigma}{2} & \text{if } 1 < \sigma \leq 3 \\ 0, & \text{if } \sigma > 3 \end{cases} \tag{A.20}$$

$$\beta = \begin{cases} 0, & \text{if } M \leq 0.8 \\ 1, & \text{if } M > 0.8 \end{cases} \tag{A.21}$$

where;

σ: length to height ratio

Cd_{b_aft}: equivalent base drag coefficient for the aft part of the transition

$$\sigma = \frac{length}{d_{fore} - d_{aft}} \tag{A.22}$$

A.3 Base Drag Coefficient

The base drag was modeled using a hybrid approach based on the experimental data from in [75] and [76] in the same study. For subsonic speeds, the data were based on [75] while the data from [76] were used for supersonic speeds. A curve model was proposed for $0.8 < M < 1.5$. The model was multiplied with 1.2 for the transonic regime.

The model used to calculate the base drag coefficient was provided below. The experimental data were a function of only Mach number and base drag coefficient at any Mach

number was calculated by interpolation.

$$C_{d_b} = \begin{cases} \text{Subsonic experimental data from [75] ,} & \text{if } M \leq 0.8 \\ \text{Subsonic experimental data [75]*1.2} & \text{if } 0.8 < M < 1.5 \\ \text{Supersonic experimental data from [76] ,} & \text{if } 1.5 \leq M < 10 \\ \frac{0.13}{M} & \text{if } M \geq 10 \end{cases} \tag{A.23}$$

APPENDIX B

HYBRID PROPULSION MODEL

The hybrid propulsion model provided in this appendix was based on the model provided in [7].

The simplified form of the fuel regression rate equation was given as follows:

$$\dot{r} = a(G_0)^n \tag{B.1}$$

where,

G_0: the oxidizer mass velocity (i.e., the oxidizer mass flow rate divided by the combustion port cross-sectional area)

a and n: empirically fitted constants that can be found in the literature.

B.0.1 Dynamic Behaviour

Dynamic behavior in hybrid propulsion systems is important because mixture ratio always varies even during steady-state oxidizer flow.

$$\dot{m} = \dot{m}_0 + \dot{m}_f = \frac{p_1 A_t}{c^*} \tag{B.2}$$

The thrust was provided as follows;

$$F = \dot{m} I_s g_0 = (\dot{m}_0 + \dot{m}_f) I_s g_0 \tag{B.3}$$

For circular port geometries with inner radius R, the regression rate was restated as

follows;

$$\dot{r} = a\Big(\frac{\dot{m}}{\pi R^2}\Big)^n \tag{B.4}$$

The mass flow rate was given in the following equation;

$$\dot{m_f} = \rho_f A_b \dot{r} = 2\pi\rho_f R\dot{r} \tag{B.5}$$

Length of the fuel grain was given with;

$$L = \frac{\dot{m_f}/N}{2\pi R_i \rho_f \dot{r}_i} \tag{B.6}$$

where,

A_b: Combustion port surface area

L: Length of the fuel grain

Combining these two equations, the fuel production rate can be obtained as follows;

$$\dot{m_f} = 2(\pi)^{1-n}\rho_f L a \dot{m_0}^n R^{1-2n} \tag{B.7}$$

For a grain configured with N circular combustion ports, combustion port radius R(t) as a function of time and oxidizer flow rate was provided with the following equation:

$$R(t) = \Big\{a(2n+1)\Big(\frac{\dot{m}_0}{\pi N}\Big)^n t + (R_i)^{2n+1}\Big\}^{\frac{1}{2n+1}} \tag{B.8}$$

Instantaneous fuel flow rate was given with the following equation:

$$\dot{m_f}(t) = 2\pi N\rho_f L a\Big(\frac{\dot{m}_0}{\pi N}\Big)^n \Big\{a(2n+1)\Big(\frac{\dot{m}_0}{\pi N}\Big)^n t + (R_i)^{2n+1}\Big\}^{\frac{1-2n}{1+2n}} \tag{B.9}$$

Instantaneous mixture ratio was given with the following equation:

$$\frac{\dot{m}_0}{\dot{m}_f}(t) = \frac{1}{2\rho_f La}\Big(\frac{\dot{m}_0}{\pi N}\Big)^{1-n}\Big\{a(2n+1)\Big(\frac{\dot{m}_0}{\pi N}\Big)^{n}t + (R_i)^{2n+1}\Big\}^{\frac{2n-1}{2n+1}} \tag{B.10}$$

Total fuel consumed was given with the following equation:

$$m_f(t) = \pi N \rho_f L\Big[\Big\{a(2n+1)\Big(\frac{\dot{m}_0}{\pi N}\Big)^{n}t + (R_i)^{2n+1}\Big\}^{\frac{2}{2n+1}} - R_i^2\Big] \tag{B.11}$$

where,

R_i: the initial port radius

N : the number of combustion ports of radius R_i in the fuel grain

$\dot{m}$: the total oxidizer flow rate

$\dot{m}_f$: the total fuel flow rate

APPENDIX C

RESULTS OF THE STATISTICAL ANALYSIS

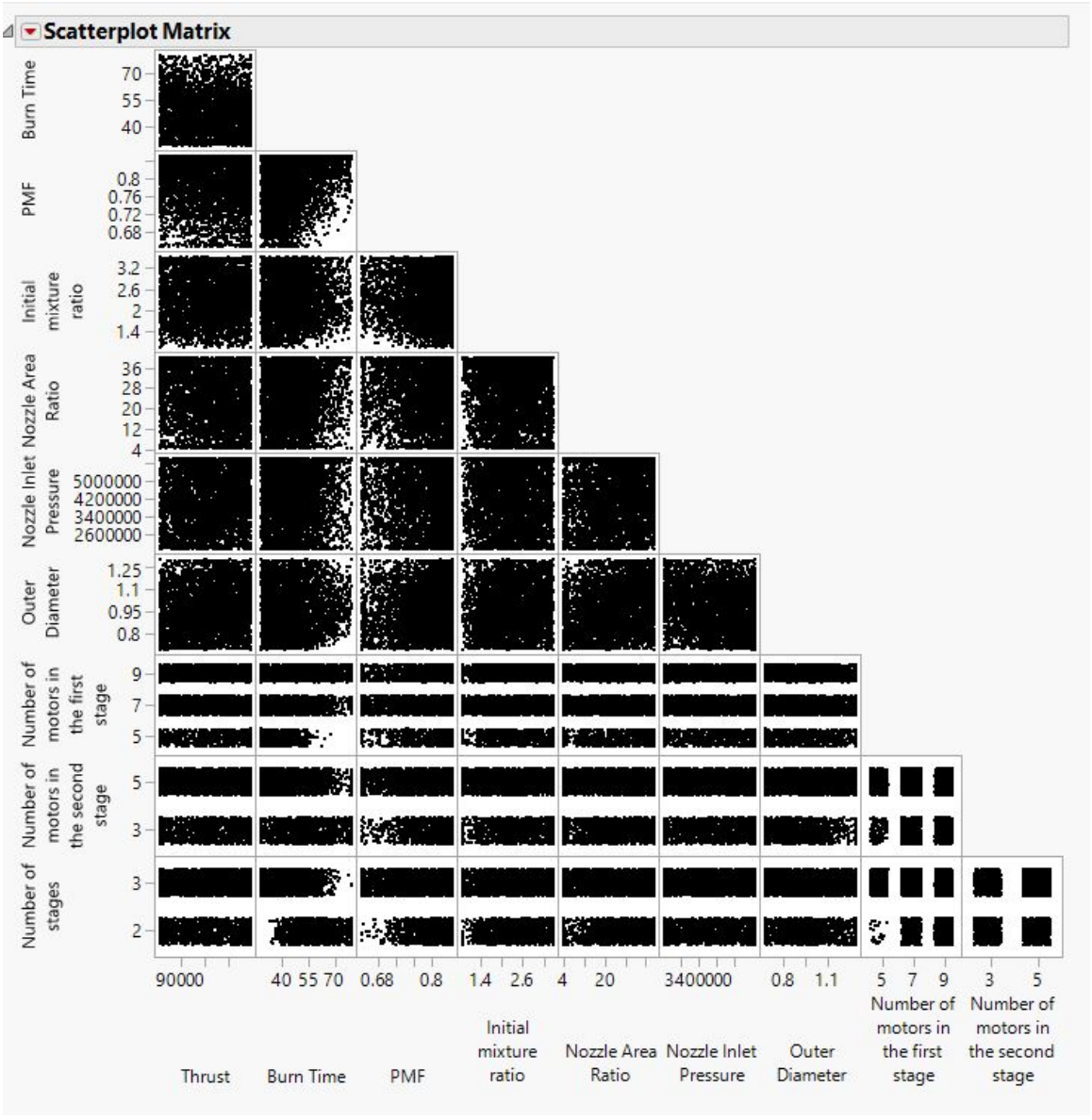

Figure C.1: Design Space Scatter-plot Matrix(4959 points)

Model NTanH(7) NLinear(7) NGaussian(7) NTanH2(7) NLinear2(7) NGaussian2(7)

Training

Vehicle Mass

Measures	Value
RSquare	0.9993245
RMSE	308.45379
Mean Abs Dev	208.51315
-LogLikelihood	23060.397
SSE	306838561
Sum Freq	3225

T_W

Measures	Value
RSquare	0.9996005
RMSE	0.012066
Mean Abs Dev	0.0087427
-LogLikelihood	-9669.924
SSE	0.4695217
Sum Freq	3225

L_D

Measures	Value
RSquare	0.9962745
RMSE	0.4369967
Mean Abs Dev	0.319704
-LogLikelihood	1906.3262
SSE	615.86574
Sum Freq	3225

ISP

Measures	Value
RSquare	0.9912452
RMSE	1.6546275
Mean Abs Dev	1.1140932
-LogLikelihood	6200.1091
SSE	8829.3801
Sum Freq	3225

DeltaV

Measures	Value
RSquare	0.9994388
RMSE	30.20954
Mean Abs Dev	21.463698
-LogLikelihood	15567.386
SSE	2943187.5
Sum Freq	3225

Validation

Vehicle Mass

Measures	Value
RSquare	0.9992445
RMSE	325.94499
Mean Abs Dev	215.50679
-LogLikelihood	5807.7677
SSE	85629550
Sum Freq	806

T_W

Measures	Value
RSquare	0.9996001
RMSE	0.0123327
Mean Abs Dev	0.0088453
-LogLikelihood	-2399.108
SSE	0.1225895
Sum Freq	806

L_D

Measures	Value
RSquare	0.9961476
RMSE	0.457295
Mean Abs Dev	0.3298756
-LogLikelihood	513.02865
SSE	168.54969
Sum Freq	806

ISP

Measures	Value
RSquare	0.9901315
RMSE	1.8141497
Mean Abs Dev	1.1312045
-LogLikelihood	1623.7317
SSE	2652.6582
Sum Freq	806

DeltaV

Measures	Value
RSquare	0.9994196
RMSE	31.22623
Mean Abs Dev	21.088303
-LogLikelihood	3917.3188
SSE	78591244
Sum Freq	806

Figure C.2: R-Squared Values for Training and Validation

Final Speed

Measures	Value
RSquare	0.9681878
RMSE	181.80203
Mean Abs Dev	140.96278
-LogLikelihood	21355.489
SSE	106592634
Sum Freq	3225

Final Speed

Measures	Value
RSquare	0.9666363
RMSE	183.82384
Mean Abs Dev	143.64486
-LogLikelihood	5346.1307
SSE	27235712
Sum Freq	806

Final flight path angle

Measures	Value
RSquare	0.98292
RMSE	1.9077084
Mean Abs Dev	1.4612118
-LogLikelihood	6659.113
SSE	11736.908
Sum Freq	3225

Final flight path angle

Measures	Value
RSquare	0.9826925
RMSE	1.9080589
Mean Abs Dev	1.475384
-LogLikelihood	1664.4101
SSE	2934.395
Sum Freq	806

Final special mechanical energy

Measures	Value
RSquare	0.9639594
RMSE	1251250.6
Mean Abs Dev	961103.41
-LogLikelihood	49853.961
SSE	5.049e+15
Sum Freq	3225

Final special mechanical energy

Measures	Value
RSquare	0.9628011
RMSE	1241246.6
Mean Abs Dev	965242.1
-LogLikelihood	12453.156
SSE	1.242e+15
Sum Freq	806

	Generalized RSquare	-LogLikelihood
Training	1.0000	114932.86
Validation	1.0000	28926.436

Figure C.3: R-Squared Values for Training and Validation

APPENDIX D

DERIVATIONS OF ORBITAL ANALYSIS EQUATIONS

Figure D.1 illustrated the "final orbit" which a vehicle reached when its fuel is consumed. The "target orbit" was also illustrated.

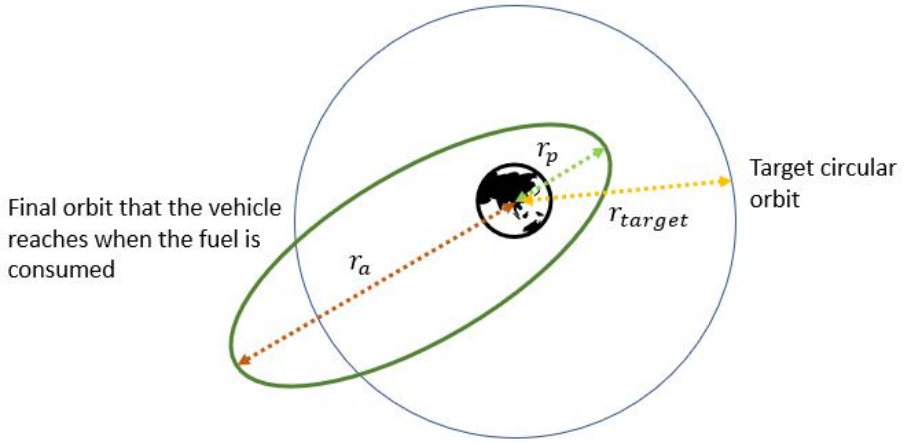

Figure D.1: Illustration of final orbit and target orbit

The semi-major axis was calculated with Equation D.1;

$$a = R_E + h_{targ} \tag{D.1}$$

where;

a : Semi-major axis of the target orbit

R_E : Radius of the Earth

h_{targ} : Altitude of the target orbit

The flight path angle of the vehicle in the final orbit was provided with Equation D.2

$$\phi_{fin} = \phi_{r=r_{fin}=R_E+h_{fin}} \tag{D.2}$$

where;

ϕ_{fin} : Flight path angle at the final orbit

r_{fin} : Position at the final orbit

h_{fin} : Altitude at the final orbit

The specific mechanical energy of the target orbit was calculated with Equation D.3;

$$\epsilon = -\frac{\mu_E}{2a} = \frac{V^2}{2} - \frac{\mu_E}{r} \tag{D.3}$$

where;

μ_E : Gravitational parameter of the the Earth

r : Position of the vehicle in the inertial frame

V : Speed of the vehicle in the inertial frame

The speed of the vehicle at the target orbit was derived by using Equation D.3 as shown in Equation D.4;

$$V = \sqrt{2(\frac{\mu_E}{r} - \frac{\mu_E}{2a})} = \sqrt{\frac{\mu_E}{ar}(2a - r)} \tag{D.4}$$

The altitude of the vehicle at the final orbit was derived by using Equation D.5;

$$h = rVsin(90^\circ - \phi_{fin}) = r\sqrt{\frac{\mu_E}{ar}(2a - r)}sin(90^\circ - \phi_{fin}) = \sqrt{\mu_E p} = \sqrt{\mu_E a(1 - e^2)} \tag{D.5}$$

The eccentricity of the final orbit was derived by using Equation D.5 as shown in Equation D.6;

$$e = \frac{\sqrt{a^2 - r(2a - r)sin^2(90^\circ - \phi_{fin})}}{a} \tag{D.6}$$

$$e(h_{fin}) = \frac{\sqrt{R_E^2 + 2R_E h_{targ} + h_{targ}^2 - (R_E + h_{fin})(2R_E + 2h_{targ} - R_E - h_{fin})sin^2(90^\circ - \phi_{fin})}}{R_E + h_{targ}} \tag{D.7}$$

$$e(h_{fin}) = \frac{\sqrt{(1 - sin^2(90^\circ - \phi_{fin}))(R_E + h_{targ})^2 + (h_{fin} - h_{targ})^2 sin^2(90^\circ - \phi_{fin})}}{R_E + h_{targ}} \tag{D.8}$$

$$e(h_{fin}) = \sqrt{1 - \frac{(R_E + h_{fin})(R_E + 2h_{targ} - h_{fin})}{(R_E + h_{targ})^2} sin^2(90^\circ - \phi_{fin})} \tag{D.9}$$

The perigee position was calculated using Equation D.10;

$$r_p = R_E + h_p = a(1 - e) = (R_E + h_{targ}) - (R_E + h_{targ})e \tag{D.10}$$

The perigee altitude of the final orbit was calculated using Equation D.11;

$$h_p = h_p(h_{fin}) = h_{targ} - (R_E + h_{targ})e \tag{D.11}$$

$$h_p = h_{targ} - \sqrt{(R_E + h_{targ})^2 - [(R_E + h_{fin})(R_E + 2h_{targ} - h_{fin})] sin^2(90^\circ - \phi_{fin})} \tag{D.12}$$

The apogee position was calculated using Equation D.13;

$$r_a = R_E + h_a = a(1 + e) = (R_E + h_{targ}) + (R_E + h_{targ})e \tag{D.13}$$

The apogee altitude of the final orbit was calculated using Equation D.14 and Equation D.15 ;

$$h_a = h_a(h_{fin}) = h_{targ} + (R_E + h_{targ})e \tag{D.14}$$

$$h_a = h_{targ} + \sqrt{(R_E + h_{targ})^2 - [(R_E + h_{fin})(R_E + 2h_{targ} - h_{fin})]sin^2(90^\circ - \phi_{fin})} \tag{D.15}$$

The speed at the final orbit was calculated using Equation D.16;

$$V = V(h_{fin}) = \sqrt{\frac{\mu_E}{ar}(2a - r)} = \sqrt{\mu_E \frac{R_E + 2h_{targ} - h_{fin}}{(R_E + h_{targ})(R_E + h_{fin})}} \tag{D.16}$$

The maximum altitude where the speed was equal to zero and eccentricity was equal to one was calculated using Equation D.17 and Equation D.18;

$$\epsilon = -\frac{\mu_E}{2(R_E + h_{targ})} = \frac{0^2}{2} - \frac{\mu_E}{(R_E + h_{fin})} \tag{D.17}$$

$$h_{fin(V_{fin}=0)} = R_E + 2h_{targ} \tag{D.18}$$

REFERENCES

[1] (2020). "Ucs satellite database," [Online]. Available: https://www.ucsusa.org/resources/satellite-database. (accessed: 10.01.2020).

[2] T. Wekerle, L. G. Trabasso, and L. Loures, "Status and trends of smallsats and their launch vehicles - an up to date review," *Journal of Aerospace Technology and Management*, vol. 9, no. 3, pp. 269–286, 2017.

[3] NASA. (2015). "Nasa technology roadmaps (launch propulsion systems)," [Online]. Available: https://www.nasa.gov/sites/default/files/atoms/files/2015_nasa_technology_roadmaps_ta_1_launch_propulsion_systems_final.pdf.

[4] FAA. (2018). "The annual compendium of commercial space transportation: 2018," [Online]. Available: https://www.faa.gov/about/office_org/headquarters_offices/ast/media/2018_ast_compendium.pdf.

[5] O. d. Weck, A. Siddiqi, M. Moraguez, A. Trujillo, G. Lordos, and M. Sarang. (2018). "Commercial space technology roadmap," [Online]. Available: https://www.nasa.gov/sites/default/files/atoms/files/commercial_space_technology_roadmap.pdf. (accessed: 10.01.2020).

[6] H. W. Jones, "The recent large reduction in space launch cost," *48th International Conference on Environmental Systems*, 2018.

[7] G. P. Sutton and O. Biblarz, *Rocket Propulsion Elements*. Wiley, 2016, ch. 16.

[8] P. Surmacz and G. Rarata, "Hybrid rocket propulsion development and application," 2009.

[9] J. M. Seitzman, "Lecture notes of rocket propulsion course (ae 6450)," 2019.

[10] M. A. Karabeyoglu, D. Altman, and K. J. Cantwell, "Combustion of liquefying hybrid propellants: Part 1,general theory," *Journal of Propulsion and Power*, vol. 18, no. 3, 2002, doi:10.2514/2.5975.

[11] M. A. Karabeyoglu and G. Z. et all, "Scale-up tests of high regression rate paraffin-based hybrid rocket fuels," *Journal of Propulsion and Power*, vol. 20, no. 6, 2004, doi:10.2514/1.3340.

[12] C. Schmierer, M. Kobald, K. Tomilin, U. Fischer, and S. Schlechtriema, "Low cost small-satellite access to space using hybrid rocket propulsion," *Acta Astronautica 159*, 2019, doi:10.1016/j.actaastro.2019.02.018.

[13] M. Kobal and U. Fischer, "Hybrid experimental rocket stuttgart a low-cost technology demonstrator," *Journal of Spacecraft and Rockets*, vol. 55, no. 2, 2018.

[14] T. L. Messinger, "Conceptual design and optimization of hybrid rockets," M.S. thesis, University of Calgary, 2021.

[15] C.E.Dickerson and D. Mavris, *Architectures and Principles of Systems Engineering*. Auerbach Publications, 2010.

[16] *Nasa systems Engineering Handbook*. NASA, 2016.

[17] D. Mavris, "Lecture notes of advanced design methods course (ae 6373)," 2019.

[18] L. F. Rowell and J. J. Korte, "Launch vehicle design and optimization methods and priority for the advanced engineering environment," *NASA-TM-2003-212654*, 2003.

[19] J. L. Sharma, "Stase: Set theory-influenced architecture space exploration," Ph.D. dissertation, Georgia Institute of Technology, 2014.

[20] D. J. Cloud and L. B. Rainey, *Applied Modeling and Simulation: An Integrated Approach to Development and Operation*. McGraw-Hill, 1998, ch. 7.

[21] A. K. Keane and P. B. Nair, *Computational Approaches for Aerospace Design*. WILEY, 2005.

[22] J. M. Seitzman, "Lecture notes of rocket propulsion course (ae 6550)," 2021.

[23] S. J. Edwards, "A methodology for risk-informed launch vehicle architecture selection," Ph.D. dissertation, Georgia Institute of Technology, 2017.

[24] M. J. Steffens, "Trajectory-based launch vehicle performance analysis for design-space exploration in conceptual design," Ph.D. dissertation, Georgia Institute of Technology, 2016.

[25] M. Steffens, "A combined global and local methodology for launch vehicle trajectory design-space exploration and optimization," M.S. thesis, Georgia Institute of Technology, 2014.

[26] A. Shirazia, J. Ceberiob, and J. A. Lozanoa, "Spacecraft trajectory optimization: A review of models, objectives, approaches and solutions," *Aerospace Science and Technology*, vol. 18, no. 3, p. 763, 2018.

[27] Y. Zheng, X. Fu, M. Xu, Q. Li, and M. Lin, "Ascent trajectory design of small-lift launch vehicle using hierarchical optimization," 2020, doi:10.1016/j.ast.2020.106285.

[28] P. F. Gath and A. J. Calise, "Optimization of launch vehicle ascent trajectories with path constraints and coast arcs," *JOURNAL OF GUIDANCE, CONTROL, AND DYNAMICS*, vol. 24, no. 2, 2001.

[29] A. J. Calise, S. Tandon, D. H. Young, and S. Kim, "Further improvements to a hybrid method for launch vehicle ascent trajectory optimization," 2000.

[30] F. M. Villanueva, H. Linshu, and X. Dajun, "Small solid propellant launch vehicle mixed design optimization approach," *J. Aerosp. Technol. Manag*, 2014.

[31] M. Balesdent, N. Bérend, P. Dépincé, and A. Chriette, "A survey of multidisciplinary design optimization methods in launch vehicle design," *Struct Multidisc Optim*, 2011, doi:10.1007/s00158-011-0701-4.

[32] L. Federici, A. Zavoliy, G. Colasurdoz, L. Mancinix, and A. Neri, "Integrated optimization of ascent trajectory and srm design of multistage launch vehicles," 2019.

[33] F. M. Villanueva, H. Linshu, A. F. Rafique, and T. Rahman, "Small launch vehicle trajectory profile optimization using hybrid algorithm," 2013.

[34] J. Roshanian, A. A. Bataleblu, and M. Ebrahimi, "Robust ascent trajectory design and optimization of a typical launch vehicle," 2018.

[35] M.-D. Qazi and H. Linshu, "Rapid trajectory optimization using computational intelligence for guidance and conceptual design of multistage space launch vehicles," 2005.

[36] G. L. Brauer, D. E. Cornick, and R. Stevenson, "Capabilities and applications of the program to optimize simulated trajectories (post)," 2977.

[37] D. Nelson. (2001). "Ae 8900 individual research project: Qualitative and quantitative assessment of optimal trajectories by implicit simulation (otis) and program to optimize simulated trajectories (post)," [Online]. Available: https://ssdl.gatech.edu/sites/default/files/ssdl-files/papers/mastersProjects/NelsonD-8900.pdf. (accessed: 07.18.2021).

[38] (2021). "Analysis, simulation and trajectory optimization software for space applications," [Online]. Available: https://www.astos.de/products/astos. (accessed: 06.24.2021).

[39] (2021). "Socs," [Online]. Available: https://swmath.org/software/7737. (accessed: 06.24.2021).

[40] C. P. Frank, "A design space exploration methodology to support decisions under evolving uncertainty in requirements ans its application to advanced vehicles," Ph.D. dissertation, Georgia Institute of Technology, 2016.

[41] J. N. Nielsen. (1988). "Missile aerodynamics," [Online]. Available: https://apps.dtic.mil/dtic/tr/fulltext/u2/a217480.pdf.

[42] L. Mason, L. Devan, F. G. Moore, and D. McMillan. (1981). "Aerodynamic design manual for tactical weapons," [Online]. Available: https://apps.dtic.mil/dtic/tr/fulltext/u2/a109180.pdf.

[43] E. L. Fleeman, *Tactical Missile Design*, ser. Education Series. AIAA, 2001.

[44] J. S. Barrowman. (1967). "The practical calculation of the aerodynamic characteristics of slender finned vehicles," [Online]. Available: https://ntrs.nasa.gov/citations/20010047838.

[45] A. Tewari, *Advanced Control of Aircraft, Spacecraft and Rockets*. Wiley, 2011.

[46] W. E. Hammond, *Design Methodologies for Space Transportation Systems*, ser. Education Series. AIAA, 2019, ch. 2.

[47] C. Dupont, A. Tromba, and S. Missonnier, "New strategy to preliminary design space launch vehicle based on a dedicated mdo platform," 2019.

[48] C. Rosema, J. Doyle, L. Auman, and M. Underwood, "Missile datcom user's manual 2011 revision final report," 2011.

[49] F. Castellini, "Multidisciplinary design optimization for expendable launch vehicles," M.S. thesis, Politecnico Di Milano, 2012.

[50] F. M. P. Morgado, "Coupled preliminary design and trajectory optimization of rockets using a multidisciplinary approach," M.S. thesis, Technico Lisboa, 2019.

[51] P. A. Ritter, "Optimization and design for heavy lift launch vehicles," M.S. thesis, University of Tennessee, Knoxville, 2012.

[52] L. Brevault, M. Balesdent, and A. Hebbal, "Multi-objective multidisciplinary design optimization approach for partially reusable launch vehicle design," *Journal of Spacecraft and Rockets*, vol. 57, no. 2, 2020, doi:doi.org/10.2514/1.A34601.

[53] D. J. Bayley, R. J. H. Jr, J. E. Burkhalter, and R. M. Jenkins, "Design optimization of a space launch vehicle using a genetic algorithm," *Journal of Spacecraft and Rockets*, vol. 45, no. 4, 2008, doi:10.2514/1.35318.

[54] D. J. Bayley and R. J. Hartfield, "Design optimization of space launch vehicles for minimum cost using a genetic algorithm," *Joint Propulsion Conference Exhibit*, 2007.

[55] G. A. Sanders, "Compuiter program for estimating stability derivatives of missile configurations -users manual," 1982.

[56] F. Villeneuve, "A method for concept and technology exploration of aerospace architectures," Ph.D. dissertation, Georgia Institute of Technology, 2007.

[57] P. O. de Weck and P. K. Willcox, "Multidisciplinary system design optimization course lecture notes," 2010.

[58] T. W. Simpson, J. D. Peplinski, P. N. Koch, and J. K. Allen, "Metamodels for computer-based engineering design: Survey and recommendations," 2001.

[59] Y. Kogusi, A. Oyama, K. Fujii, and M. Kanazaki, "Multidisciplinary and multi-objective design exploration methodology for conceptual design of a hybrid rocket," 2011, doi:10.2514/6.2011-1634.

[60] C. Guobiao, Z. Hao, R. Dalin, and T. Hui, "Optimal design of hybrid rocket motor powered vehicle for suborbital flight," 2011, doi:10.1016/j.ast.2011.12.014.

[61] K. Chiba, M. Kanazaki, M. Nakamiya, K. Kitagawa, and T. Shimada, "Conceptual design of single-stage launch vehicle with hybrid rocket engine for scientific observation using design informatics," *Journal of Space Engineering*, vol. 6, no. 1, 2013.

[62] A.-U. Onel, T.-P. Afilipoae, A.-M. Neculaescu, and M.-V. Pricop, "Drag coefficient modelling in the context of small launcher optimization," *INCAS Bulletin*, vol. 10, no. 4, pp. 103–116, 2018, doi:10.13111/2066-8201.2018.10.4.10.

[63] (2020). "Nose cone design," [Online]. Available: https://en.wikipedia.org/wiki/Nose_cone_design. (accessed: 03.12.2021).

[64] G. Zilliac and M. A. Karabeyoglu, "Hybrid rocket fuel regression rate data and modeling," *42nd AIAA/ASME/SAE/ASEE Joint Propulsion Conference Exhibit*, 2006.

[65] R. Bate, D. D. Mueller, and J. E. White, *Fundamentals of Astrodynamics*. Dover Publications, 1971.

[66] (2021). "Fast flexible filling designs," [Online]. Available: https://www.jmp.com/support/help/en/16.0/index.shtml#page/jmp/fast-flexible-filling-designs.shtml#ww146196. (accessed: 06.19.2021).

[67] (2021). "Karman line," [Online]. Available: https://en.wikipedia.org/wiki/K%C3%A1rm%C3%A1n_line. (accessed: 03.12.2021).

[68] (2021). "Prediction interval," [Online]. Available: https://www.sciencedirect.com/topics/mathematics/prediction-interval. (accessed: 06.20.2021).

[69] C. Schmierer, M. Kobald, K. Tomilin, U. Fischer, A. Petrarolo, and F. Hertel, "Advancing europe's hybrid rocket engine technology with paraffin and lox," *8th European Conference For Aeronautics And Aerospace Sciences (EUCASS)*, 2019.

[70] B. Cantwell, A. Karabeyoglu, and D. Altman, "Recent advances in hybrid propulsion," *International Journal of Energetic Materials and Chemical Propulsion*, vol. 9, no. 4, 2010.

[71] A. F. El-Sayed, *Fundamentals of Aircraft and Rocket Propulsion*. Springer, 2016.

[72] (2021). "Mahalanobis distance," [Online]. Available: https://www.mathworks.com/help/stats/mahal.html. (accessed: 03.12.2021).

[73] (2021). "Outlier analysis," [Online]. Available: https://www.jmp.com/support/help/en/15.2/index.shtml#page/jmp/outlier-analysis.shtml. (accessed: 03.13.2021).

[74] M. Karabeyoglu, "Nitrous oxide and oxygen mixtures (nytrox) as oxidizers for rocket propulsion applications," *Journal of Propulsion and Power*, 2014.

[75] W. Stoney, "Collection of zero-lift drag data on bodies of revolution from free-flight investigations," *NASA-TR-R-100*, 1961.

[76] C. S. James and R. C. Carros, "Experimental investigation of the zero-lift drag of a fin-stabilized body of fineness ratio 10 at mach numbers between 0.6 and 10," *NACA RMA53D02*, 1953.